AD-758 776

AZIMUTHAL AND DIURNAL PROPERTIES OF HF BACKSCATTER

R. P. McConville, et al

Avco Systems Division

Prepared for:

Rome Air Development Center

January 1973

DISTRIBUTED BY:

NTIS

National Technical Information Service
U. S. DEPARTMENT OF COMMERCE
5285 Port Royal Road, Springfield Va. 22151

AD 758776

RADC-TR-73-17
Final Technical Report
January 1973

AZIMUTHAL AND DIURNAL PROPERTIES OF HF BACKSCATTER

AVCO Corporation

Approved for public release;
distribution unlimited.

D D C
RECEIVED
APR 23 1973
B

Rome Air Development Center
Air Force Systems Command
Griffiss Air Force Base, New York

Reproduced by
NATIONAL TECHNICAL
INFORMATION SERVICE
U S Department of Commerce
Springfield VA 22151

173

Best
Available
Copy

AZIMUTHAL AND DIURNAL PROPERTIES OF HF BACKSCATTER

R. P. McConville
R. B. Penndorf
D. G. Detert
A. S. Weeks

AVCO Corporation

Approved for public release;
distribution unlimited.

FOREWORD

This Final Report describes work performed by AVCO Corporation, Systems Division, Wilmington, Massachusetts, under contract F30602-70-C-0083, Job Order Number 673A0112, for Rome Air Development Center, Griffiss Air Force Base, New York. Mr. Frank Antonik, OCSL, was the RADC Project Engineer.

This report has been reviewed by the RADC Information Office (OI) and is releasable to the National Technical Information Service (NTIS).

This technical report has been reviewed and is approved.

Approved: Frank Antonik
FRANK ANTONIK
Project Engineer

Approved: William T. Pope
WILLIAM T. POPE
Assistant Chief
Surveillance and
Control Division

FOR THE COMMANDER: Fred I. Diamond
FRED I. DIAMOND
Chief, Plans Office

UNCLASSIFIED

Security Classification

DOCUMENT CONTROL DATA - R & D

(Security classification of title, body of abstract and indexing annotation must be entered when the overall report is classified)

1. ORIGINATING ACTIVITY (Corporate author) AVCO Corporation Systems Division Wilmington, MA 01887	2a. REPORT SECURITY CLASSIFICATION UNCLASSIFIED 2b. GROUP N/A

3. REPORT TITLE

AZIMUTHAL AND DIURNAL PROPERTIES OF HF BACKSCATTER

4. DESCRIPTIVE NOTES (Type of report and inclusive dates)

Final Report

5. AUTHOR(S) (First name, middle initial, last name)

R.P. McConville, R.B. Penndorf, D.G. Detert, A.S. Weeks

6. REPORT DATE January 1973	7a. TOTAL NO. OF PAGES 160	7b. NO. OF REFS 20
8a. CONTRACT OR GRANT NO. F30602-70-C-0063 Job Order No. 673A0112	9a. ORIGINATOR'S REPORT NUMBER(S) None 9b. OTHER REPORT NO(S) (Any other numbers that may be assigned this report) RADC-TR-73-17	

10. DISTRIBUTION STATEMENT

Approved for public release; distribution unlimited.

11. SUPPLEMENTARY NOTES None Details of illustrations in this document may be better studied on microfiche.	12. SPONSORING MILITARY ACTIVITY Rome Air Development Center (OCSL) Griffiss Air Force Base, New York 13441

13. ABSTRACT

This report presents the results of several experiments related to the azimuthal and diurnal dependence of HF backscatter and terrestrial radio noise and the nature of earth backscatter from regions near the skip zone and from sea water. The first experiment consisted of stepped azimuth paroramic backscatter soundings over a diurnal cycle. The sounding waveform was linear FM/CW with an average transmitted power of 5 kW. The second experiment explored the details of the sunrise and sunset transition periods along a fixed azimuth, also instrumented with an oblique-incidence forward-scatter FM/CW ionosonde and a co-located broadband repeater. The third experiment collected an azimuthal sample of terrestrial radio noise in the guard frequency band of WWV during the silent period. The fourth experiment considered some characteristics of the leading edge of the backscatter region from the point of view of illumination control and frequency management.

DD FORM 1 NOV 65 1473

UNCLASSIFIED

Security Classification

UNCLASSIFIED

Security Classification

14 KEY WORDS	LINK A ROLE	LINK A WT	LINK B ROLE	LINK B WT	LINK C ROLE	LINK C WT
HF Propagation						
Backscatter						
FM/CW						

UNCLASSIFIED

Security Classification

ABSTRACT

This report presents the results of several experiments related to the azimuthal and diurnal dependence of HF backscatter and terrestrial radio noise and the nature of earth backscatter from regions near the skip zone and from sea water. The first experiment consisted of stepped azimuth panoramic backscatter soundings over a diurnal cycle. The sounding waveform was linear FM/CW with an average transmitted power of 5 kW. The second experiment explored the details of the sunrise and sunset transition periods along a fixed azimuth, also instrumented with an oblique-incidence forward-scatter FM/CW ionosonde and a co-located broadband repeater. The third experiment collected an azimuthal sample of terrestrial radio noise in the guard frequency band of WWV during the silent period. The fourth experiment considered some characteristics of the leading edge of the backscatter region from the point of view of illumination control and frequency management. The fifth experiment concerned the nature of sea clutter and its relationship and effect on an FM/CW OTH-B radar.

EVALUATION

This report describes the second phase of the work performed by the AVCO Corporation to investigate methods of determining and to provide useful data for those parameters peculiar to an HF backscatter system. These efforts are under the overall 673A program which is tasked with providing a technological base necessary for the design of OTH systems needed to satisfy a variety of Air Force operational requirements.

These studies have provided insight to the problems of backscatter propagation as a function of azimuthal, diurnal and seasonal variations. Further, they indicate the value of displaying vertical incidence traces on an oblique incidence ionogram that is used to select the correct operating frequency. This has been borne out by the experimental Ava/Dexter backscatter system.

The problem of ionospheric tilts was addressed in the context of tilts along the propagation path. A further effort has been initiated that will investigate a technique that will determine and provide corrections for ionospheric tilts in the transverse direction that produce lateral deviations of the ray path.

Frank Antonik

FRANK ANTONIK
Project Engineer

TABLE OF CONTENTS

1.0 INTRODUCTION 1

2.0 AZIMUTHAL VARIATION OF BACKSCATTER 4

2.1 Introduction 4
2.2 Discussion of the Data 7
2.3 Conclusions 14

3.0 SUNRISE/SUNSET TESTS 33

3.1 Introduction 33

3.1.1 Objective 33
3.1.2 Summary and Conclusions 34

3.2 Background Information 37

3.2.1 Leading Edge for Selected Critical Frequencies and Layer Heights 37
3.2.2 Mode Identification for the Leading Edge of Backscatter Traces 39
3.2.3 Test Configuration 42

3.3 Sunset Test 46

3.3.1 Ionospheric Variations During Test Period . . 46
3.3.2 Frequency Limits of Backscatter and Limits of Illuminated Ranges 51
3.3.3 Gradients of Leading Edge of Backscatter . . 56
3.3.4 Samples of Backscatter Records 65
3.3.5 Transponder Visibility 70

3.4 Sunrise Test 71

3.4.1 Ionospheric Variations During Test Period . . 71
3.4.2 Frequency Limits of Backscatter and Limits of Illuminated Ranges 75
3.4.3 Gradients of Leading Edge of Backscatter . . 80
3.4.4 Samples of Backscatter Records 83

TABLE OF CONTENTS (Cont'd)

3.5 Explanation of Test Results and Prediction of Backscatter 89

3.5.1 Non-Uniform Ionosphere 89
3.5.2 Sunset 95
3.5.3 Sunrise 97
3.5.4 Prediction 101

3.6 References 112

Appendices 113

A. Determination of Absolute Time Delay . 113
B. Methods to Obtain Leading Edge of Backscatter from Ionograms and NOAA predictions. 119

4.0 AZIMUTHAL DISTRIBUTION OF RADIO NOISE 121

4.1 Introduction. 121
4.2 Data Acquisition 121
4.3 Data Analysis 122
4.4 Summary 132

5.0 FURTHER ASPECTS OF THE BACKSCATTER ILLUMINATION CONTROL PROBLEM 113

5.1 Conversion of Time Delay to Ground Range. 113

5.1.1 Analysis of the Backscatter Ionogram Leading Edge. 116
5.1.2 The Effects of Ionospheric Model Heights on Leading Edge Simulations 117
5.1.3 Range/Time Delay Calculations for a Particular Backscatter Ionogram 124

5.2 Skip Region Measurements. 127
5.3 Backscatter and HF Repeater Echoes in the Skip Region 132
5.4 Conclusions. 137
5.5 References 159

LIST OF FIGURES

Figure No.		Page No.
2-1	Geomagnetic Indices K_{FR} and A_{FR} for the Experimental Period	15
2-2	Four-Quadrant Backscatter Ionograms, 2100-2130 UT	16
2-3	Four-Quadrant Backscatter Ionograms, 2200-2230 UT	17
2-4	Four-Quadrant Backscatter Ionograms, 2300-2330 UT	18
2-5	Four-Quadrant Backscatter Ionograms, 2335-0030 UT	19
2-6	Four-Quadrant Backscatter Ionograms, 0110-0140 UT	20
2-7	Four-Quadrant Backscatter Ionograms, 0300-0330 UT	21
2-8	Four-Quadrant Backscatter Ionograms, 0400-0430 UT	22
2-9	Four-Quadrant Backscatter Ionograms, 0500-0530 UT	23
2-10	Four-Quadrant Backscatter Ionograms, 0600-0630 UT	24
2-11	Four-Quadrant Backscatter Ionograms, 0700-0730 UT	25
2-12	Four-Quadrant Backscatter Ionograms, 0800-0830 UT	26
2-13	Four-Quadrant Backscatter Ionograms, 0900-0930 UT	27
2-14	Four-Quadrant Backscatter Ionograms, 1000-1030 UT	28
2-15	Four-Quadrant Backscatter Ionograms, 1100-1130 UT	29
2-16	Four-Quadrant Backscatter Ionograms, 1200-1230 UT	30
2-17	Four-Quadrant Backscatter Ionograms, 1300-1330 UT	31
2-18	Four-Quadrant Backscatter Ionograms, 1400-1430 UT	32

LIST OF FIGURES (Cont'd)

Figure No.		Page No.
3-1	Leading Edges in Backscatter Ionograms	38
3-2	Backscatter Ionogram in Winter	40
3-3	Backscatter Ionogram in Summer	41
3-4	Observed Temporal Variation of Ionospheric Parameters During Sunset Test Period	45
3-5	Observed Temporal Variation of Ionospheric Parameters Normalized to Solar Zenith Distance.	48
3-6	Observed Frequency and Time Delay Limits . . .	52
3-7	Frequency of Leading Edge for Selected Ground Ranges	54
3-8	Observed Gradients of Leading Edge	58
3-9	Backscatter Ionograms	60
3-10	Backscatter Ionograms	62
3-11	Samples of Backscatter Ionograms	66
3-12	Samples of Backscatter Ionograms	68
3-13	Samples of Backscatter Ionograms	69
3-14	Observed Temporal Variations of Ionospheric Parameters During Sunrise Test Period	72
3-15	Observed Frequency and Time Delay Limits . . .	76
3-16	Frequency of Leading Edge for Selected Ground Ranges	79
3-17	Samples of Backscatter Ionograms	84
3-18	Tracings of Backscatter Ionograms	86

LIST OF FIGURES (Cont'd)

Figure No.		Page No.
3-19	Overlapping Leading Edges for 1EGS and 1FGS Modes	90
3-20	Maps of True Height of F2 Layer Maximum and Constant Electron Density During Sunrise. . . .	92
3-21	Calculated Backscatter Ionograms for a Linear Horizontal Gradient in foF2.	93
3-22	Calculated Backscatter Ionograms for Changes in Horizontal Gradient in foF2.	97
3-23	True Height Electron Density Profile During Sunrise	98
3-24	True Height Electron Density Profile During Sunrise	100
3-25	Comparison Between Observed and Predicted Backscatter Ionograms During Sunset Test Period . .	104/109
4-1	Data Collection System	123
4-2	Sector Average Amplitude	124
4-3	Frequency of Occurrence of Thunderstorms Throughout the World for November	125
4-4a	Hourly Distribution, 1645 11 December 1970-1545 12 December 1970.	126
4-4b	Hourly Distribution, 1645 12 December 1970-0745 13 December 1970.	127
4-5	Sector Hourly Amplitude	129
4-6	Comparison of Radio Noise Levels and Propagation Factors	131

LIST OF FIGURES (Concl'd)

Figure No.		Page No.
5-1	Ground Range vs. Time Delay for One-Hop Ground Backscatter	134
5-2	Calculated Minimum Ground Range as a Function of Layer Maximum Height	139
5-3	Calculated Minimum Group Path (and Associated Ground Range) as a Function of Layer Maximum Height	140
5-4	Uncertainty in Ground Range and Group Path as a Function of Uncertainty in Layer Maximum Height	141
5-5	Reflectrix Analysis of FM/CW Backscatter Ionogram Leading Edge	145
5-6	Signal Strength Levels in the Skip Zone, Received on Cross-Polarized Antennas	149
5-7	Signal Strength Levels Received in the Skip Zone with Cross-Polarized Antenna System	150
5-8	Range-Time-Intensity Records of University of Illinois HF Repeater Echo for 18 and 19 February 1971 during Late Morning Local Time	154
5-9	Range-Time-Intensity Record of U.I. HF Repeater Echo 1442-1533 UT, 19 February Showing TID's and MUF Failure Effects	156

LIST OF TABLES

Table No.		Page No.
II-1	Schedule of Antenna Position (Transmitting) . . .	5
II-2	Schedule of Antenna Positions (Receiving)	5
II-3	Sunrise and Sunset Times	10
III-1	Theoretical Gradient Γ of Leading Edge for Backscatter	59
III-2	Observed Gradients Γ During Sunset	61
III-3	Observed Average Gradients Γ During Sunset . .	64
III-4	Observed Average Gradients Γ During Sunrise .	81
V-1	Calculation of Uncertainties in Range Introduced by Uncertainties in Layer Maximum Height . . .	143

1.0 INTRODUCTION AND SUMMARY

This report presents the results of five experiments which relate to the properties of backscatter data. In particular, most backscatter ionogram data have been obtained previously with antennas which are fixed in azimuth, and while defining the characteristics of backscatter propagation in that azimuth, give little in the way of insight into the azimuthal properties of propagation effects. It is not unusual to explain anomalies in the backscatter as resulting from antenna sidelobe effects.

The availability of receiving antennas which could be steered in azimuth, at the RADC Stockbridge field site, and a Wullenweber receiving antenna at the University of Illinois prompted the experimental program reported herein. The sounding instrumentation was of the linear FM/CW type, permitting high resolution backscatter soundings with high signal-to-noise ratios to be obtained. Additional instrumentation of a broadband repeater, and an oblique incidence FM/CW transmitter at the University of Illinois was utilized for a detailed study of sunrise and sunset effects on backscatter returns. In this instance, the receiver site was the RADC Dexter site, to which all receiving operations were transferred during the Fall of 1970. All backscatter sounding transmissions were from the RADC Ava test site.

The first experiment reported in Chapter 2, consisted of a series of stepped azimuth backscatter soundings covering a total of 24 hours in the

late summer of 1970. A circularly disposed antenna array (CDAA) or a rotatable log-periodic array was utilized for reception, and a rotatable log-periodic array for transmission. Indexing of the antenna beam positions was accomplished manually on a pre-arranged schedule such that, at least, one backscatter sounding was obtained on each receiving antenna to a cardinal compass direction during each hour. Although the interpretation of this data is somewhat mitigated by a malfunction in the receiver pre-selection filters, the results are still rather interesting. The stepped-azimuth data exhibited clearly defined azimuthal variations depending primarily on the diurnal phase associated with each azimuth. Specific auroral related phenomena were observed to the North, and sometimes to the West, but not in the other cardinal directions. The antenna sidelobes were not found to have a noticeable effect on the results obtained.

Due to the observation of rather rapid changes in the pattern of backscatter during the transition from day to night and particularly from night to day, a specific experimental procedure was devised to permit more frequent observations and correlation with ancillary data such as a repeater, oblique incidence forward scatter transmissions, and vertical incidence ionograms. This necessitated observing on only one azimuth, that from the Dexter field site to the University of Illinois. A diurnal cycle was observed and the experiment and detailed data analysis and interpretation presented in Chapter 3. Comparisons were made between the backscatter ionograms predicted from various vertical incidence ionograms, the

oblique incidence forward-scatter ionograms, and the repeater ionogram. The best correlation was obtained for ionospheric data which was relevant to the point of reflection for propagation to a given range. Changes in the slope of the backscatter ionogram as a function of frequency could be interpreted as resulting from changes in the ionospheric properties as a function of range along the propagation path.

The third experiment was a passive measurement of the azimuthal properties of terrestrial radio noise as a function of azimuth. The Wullenweber receiving array at the University of Illinois was configured to automatically step in azimuth during the WWV silent period and the radio noise amplitude observed in the internationally protected guard bands. The experimental results clearly exhibit an azimuthal dependence, which changes as a function of time. Certain rather anomalous results have been explained as a direct consequence of the receiving frequency being above the MUF (4000) to the principal thunderstorm areas which are thought to be the source of terrestrial radio noise. Although only a rather limited data sample was obtained, the results suggest that the azimuthal properties of terrestrial radio noise should not be ignored in system citing criteria, and also that the construction of a model for the azimuthal and temporal dependence of the noise power should be feasible, based on ionospheric propagation factors, and the location and source strengths of major thunderstorm regions.

The fourth experiment reported in Chapter 5 combined a study of the variation of group path and ground range to the leading edge of the backscatter with variation in the height of the ionospheric layer maximum with studies of the leading edge of the backscatter region from wideband backscatter ionograms, variation of the MUF on a fixed and point forward oblique path, and comparison of HF repeater echoes with ground backscatter variations during ionospheric changes. The general result of the effort is that focusing effects, in confirmation of theory, do occur near the leading edge of the backscatter but that propagation is too complicated and variable to be effectively predicted by ionospheric models or to be routinely utilized by OTH-B surveillance radars.

2.0 AZIMUTHAL VARIATION OF BACKSCATTER

2.1 INTRODUCTION

During the latter part of August and early September, 1970, an experiment was conducted to survey the variation of wideband ground backscatter returns (backscatter ionograms) with azimuth, particularly during the sunrise and sunset periods. The experiment was planned in the context of the antenna systems available at the RADC Ava (transmitting) and Stockbridge (receiving) test sites. At both sites, rotatable log-periodic beam arrays, covering the frequency range 6-30 MHz, were available; and, in addition, a CDAA (circularly disposed antenna array) was available at Stockbridge. The nominal azimuthal beamwidth of the log-periodic antennas is 60° and that of the CDAA 30°. In view of the relatively wide azimuthal beamwidth of the antennas which could be scanned over 360°, and the lack of an automatic means of synchronized scanning of the antennas, soundings were conducted only in the four cardinal directions, such that at least two backscatter ionograms were obtained in each direction every hour.

The sounding transmissions were of the linear FM/CW type with a positive sense sweep rate of 250 kHz/sec over the frequency range 6.5-28 MHz. An average power of 5 kW was achieved, and one sounding transmission performed every 5 minutes.

The transmitting antenna was indexed in accordance with a typical hourly schedule given in Table II-1, and the receiving antennas in accordance with a typical schedule given in Table II-2. It was the intention of the

TABLE II-1

Schedule of Antenna Position (Transmitting)

Time	Azimuth
1200	0°
1205	0
1210	270
1215	270
1220	180
1225	180
1230	90
1235	90
1240	0
1245	0
1250	0
1255	0
1300	0

TABLE II-2

Schedule of Antenna Positions (Receiving)

Time	LPA Azimuth	CDDA Azimuth (6-12 MHz)
1200	----	0°
1205	0°	----
1210	----	270
1215	270	----
1220	----	180
1225	180	----
1230	----	90
1235	90	----
1240		0
1245		0
1250		0
1255		0
1300		0

experiment to provide a comparison between the ionograms obtained with two different receiving antennas, however, equipment malfunction, described later, rendered such comparisons impossible and only the data obtained on the receiving CDAA are presented.

Figure 2-1 shows the geomagnetic indices for the time period during which this experiment was conducted, viz. 2100-0300 UT on 31 August-1 September 1970 and 0400 to 1400 UT on 2 September 1970. The daily A_{FR} (Fredricksburg) and 3-hour K_{FR} reveal that the time period during which the data were taken experienced magnetic activity at the highest levels that had obtained in the several preceding months. Consequently, the data presented cannot be considered as typical of the period, but it is not possible to compare the data with other days and so only some subjective comments can be made. It is likely that the extensive occurrence of sporadic E returns, the low values of foF2 experienced at night, and the relatively strong manifestations of auroral activity observed to the north are associated with the enhanced magnetic activity.

Unfortunately, a malfunction in the electronic circuitry associated with the actuation of the receiver preselection filters occurred, causing signal drop-out, and receiver sensitivity changes, but was not recognized until near the end of the second data run. This has resulted in relatively poor quality data, but the data which is presented in Figures 2-2 through 2-18 is extremely significant since clearly defined differences in propagation conditions as a function of azimuth, as well as time of day, are observed.

One immediate result of the data sequence was a comparison of the auroral (north) region records with the records from the three mode nearly normal mid-latitude records. It is seen that the differences in propagation conditions observed in the cardinal directions is a result of the ionospheric characteristics within the antenna beamwidth and not a consequence of antenna sidelobe returns.

2.2 DISCUSSION OF THE DATA

The figures 2-2 through 2-18 each contain a set of ionograms taken in the four cardinal directions, with a displayed range interval of 20 msec and a range resolution of 40 μsec. Particularly interesting results are evident when data taken 12 hours apart are made (East-West set of data) e.g., 2210 and 2230 with 1010 and 1030. The data exhibit substantially different MUF, with the higher MUF corresponding to propagation into the daylight regime.

It is clear that the backscatter soundings exhibit sufficiently different characteristics in the cardinal directions during any hour to exclude the serious possibility that the subtle features of the individual ionograms are the result of antenna sidelobe effects. Some of the ionograms may, however, exhibit the effects of gradients in the electron density in azimuth within the antenna 3 dB points. In addition, the sporadic-E effect may not always fill the beam, although there are cases where it clearly appears to do so.

A brief description of the sounding data for each hour follows:

2100-2130 UT

Beginning at 21 UT, we see the closest approximation to the normal quiet time concentric ionosphere, at approximately 4 p.m. local solar zenith time at the receiver site. The vertical incidence foF2 is approximately 8.25 MHz. Due to the lower frequency limit of the sounding foF1 is not observed, but its manifestation appears in the backscatter ionogram, particularly to the West at 2110 UT as a trailing edge focusing effect in the F-region backscatter. This feature is commonly observed from the spring through early fall on mid-latitude daytime ionograms and is a consequence of the gradient in electron density between the F1 and F2 layers. A fragment of the combination mode 1F/2F is observed at the lower frequencies (arising from the 3rd vertical incidence F-region return). The soundings to the East, South, and West are very similar in form, although details of the actual backscatter returns are determined by the distribution of surface scattering features and also the small scale structure of the ionosphere in each sector. Some traveling wave type effects can be seen at the longer ranges to the East. The backscatter to the North is generally weaker, and appears to be limited to a maximum time delay of 13 msec.

2200-2230 UT

The ionograms observed to the East, West, and South are fundamentally similar to those of the previous hour, except that the slant range to the skip focusing region at any frequency has increased, as a consequence of the decrease in the F-region maximum electron density. A strong

sporadic E return to the North is seen to be blanketing up to about 13 MHz, and partially reflecting up to about 18 MHz. Since the receiver is AGC controlled, this strong return is likely to have reduced the gain of the receiver, suppressing the ground backscatter return at the lower frequencies.

2300-2330 UT

A sharp reduction in the F-region electron density to the East is manifest by the convex nature of the groundscatter leading edge in the ionogram at 2330 UT, although the characteristics at close ranges are similar to those to the South and the West. This result is expected, as the longer ranges to the East are well into the sunset region, and should thus experience lower MUF values. The sporadic E to the North is no longer blanketing and appears to extend to 23 MHz. The West and South are still reflecting from a daylight ionosphere. Table II-3 shows that by 2300 and 2330 UT sunset effects have begun to affect propagation to the North and East.

2355-0030 UT

During this hour, the sunset effect has sharply curtailed the frequency extent of the leading edge of the backscatter to the East, and the slope of the leading edge has become quite large ($\sim$2 msec/MHz). Extensive sporadic E effects are now observed to the North, West, and South. The ionogram to the West still retains the character of a daytime ionosphere, and exhibits a number of enhanced returns due, probably, to sporadic E illumination of ground features. To the North, only sporadic E is clearly observed, and an extension of the 1F vertical incidence return, termed

TABLE II-3

Sunrise and Sunset Times

Latitude - 42° North (1 September)

HT = 200 km				HT = 200 km Longitude 75 Degrees West		
Longitude Degrees West	Sunrise UT	Sunset UT		Latitude °N	Sunrise UT	Sunset UT
0	0415	1945	HT - Sunrise 100 km, add 27 min	0	1007	2353
15	0515	2045	300 km, subtract 19 min	10	1000	0000
30	0615	2145	400 km, subtract 36 min	20	0951	0009
45	0715	2245	1000 km, subtract 1 hr. 51 min	30	0938	0022
60	0815	2345	HT - Sunset	40	0915	0040
75	0915	0045		50	0851	0109
90	1015	0145	100 km, subtract 27 min	60	0758	0202
105	1115	0245	300 km, add 20 min	70	0500	0500
120	1215	0345	400 km, add 36 min			
			1000 km, add 1 hr. 51 min			

slant F begins to be observed. The vertical incidence critical frequency, foF2, is now reduced to about 7 MHz. The comparison between the East and West ionograms illustrates the sunset effect rather dramatically.

0110-0140 UT

The terminator has now crossed the transmitter and receiver sites. All ionograms exhibit slant-F effects, although they are strongest to the West and North. Sporadic E effects are most prominent to the East and the West, with the West also exhibiting ground feature enhancements. The West is still characteristic of daylight propagation, but there is no evidence of effects due to the F1 layer. To the North, at the longer ranges, auroral-type returns begin to appear. The vertical incidence foF2 is now less than 6 MHz; only the fxF2 is observed.

0300-0330 UT

During this hour, sporadic E effects to the East have disappeared but are still evident to the North, South, and West, which are all nighttime ionospheres. Auroral effects as well as strong slant-F are observed to the North. The vertical incidence foF2 is now well below the ionogram lower starting frequency and the interpretation of records become more difficult after this time, particularly the differentiation between slant F and ground backscatter. In experiments where azimuthal scans can be restricted, the rhombic transmitting antenna can be employed, permitting soundings to start as low as 2.5 MHz, which is particularly useful for identification of modes in the auroral ionosphere.

0400-0430 UT

Sporadic E effects have essentially disappeared and all ionograms are nighttime in character. All exhibit what is probably a slant-F return at close ranges. The West ionogram appears to have multiple leading edges for the F backscatter, suggesting a substantial inhomogeneity in the ionosphere.

0500-0530 UT

Meteor echoes are apparent at close ranges in the West and South ionograms, and all but the North exhibit simple F-region backscatter. The West shows evidence of sporadic-E returns not apparent to the North, which is comprised entirely of F-region auroral effects.

0600-0630 UT

The data during this hour are essentially identical to the preceding hour.

0700-0730 UT

The data for the East and South are typical nighttime F layer propagated groundscatter, but the sporadic E to the West dominates the ionogram, with a number of range-discrete enhancements. Auroral returns still dominate to the North.

0800-0830 UT

Except for an increase in the intensity of the backscatter to the East, the data for this hour are essentially similar to the preceding hour.

0900-0930 UT

Sunrise effects begin to be observed to the East as a lesser slope of the ground backscatter range with frequency at the longer ranges. The auroral activity to the North has weakened and there are almost no manifestations except for slant F, but an auroral F return is observed to the West, but no groundscatter.

1000-1030 UT

Sunrise effects become more noticeable to the East, as well as the receiver sensitivity changes due to preselector filter malfunction. No backscatter returns are observed to the West and the South. Some slant F and F-region auroral returns are observed to the North.

1100-1130 UT

The backscatter return to the East has become typical of simple F-region groundscatter under daylight conditions, while the South is beginning to experience sunrise-related changes. Both the North and the West still remain in the nighttime regime.

1200-1230 UT

By this time, propagation conditions have returned to that typical of full daytime conditions, and multi-layer propagation is evident to the East, South, and West, although the F-layer maximum density for the latter two cases is still considerably below that of the East. The lack of returns at low frequencies to the North is probably a result of the receiver malfunction.

1300-1330 UT

The East ionogram is typical of summer daytime conditions with regular E, F1, and F2 groundscatter, as well as weak sporadic E. At the lower frequencies, the E, F1, and F2 returns correspond to the groundscatter leading edges in order of increasing range at any frequency. The West ionogram exhibits only clearly defined E and F2 returns. Equipment difficulties obscure the true nature of the backscatter to the North and the South.

1400-1430 UT

The equipment malfunction became evident to site personnel, particularly for the ionograms at 1420 and 1430 UT, and the experiment was terminated. The ionogram for the West, however, is a good example of regular E layer supported illumination of a ground echo at about 6.8 msec (probably Chicago). This echo was also observed during the nighttime by the sporadic E propagation mode.

2.3 CONCLUSIONS

As a result of this experiment, it was concluded that the sunrise and sunset effects should be studied in greater detail utilizing a more fully instrumented test bed, including a repeater and an oblique ionosonde. This led to the design of the experiment discussed in the next chapter. The removal of the FM/CW receiving equipment to the new field site at Dexter, NY precluded repeating the experiment described in this chapter, and antennas in use at Dexter did not permit a similar experiment to be performed.

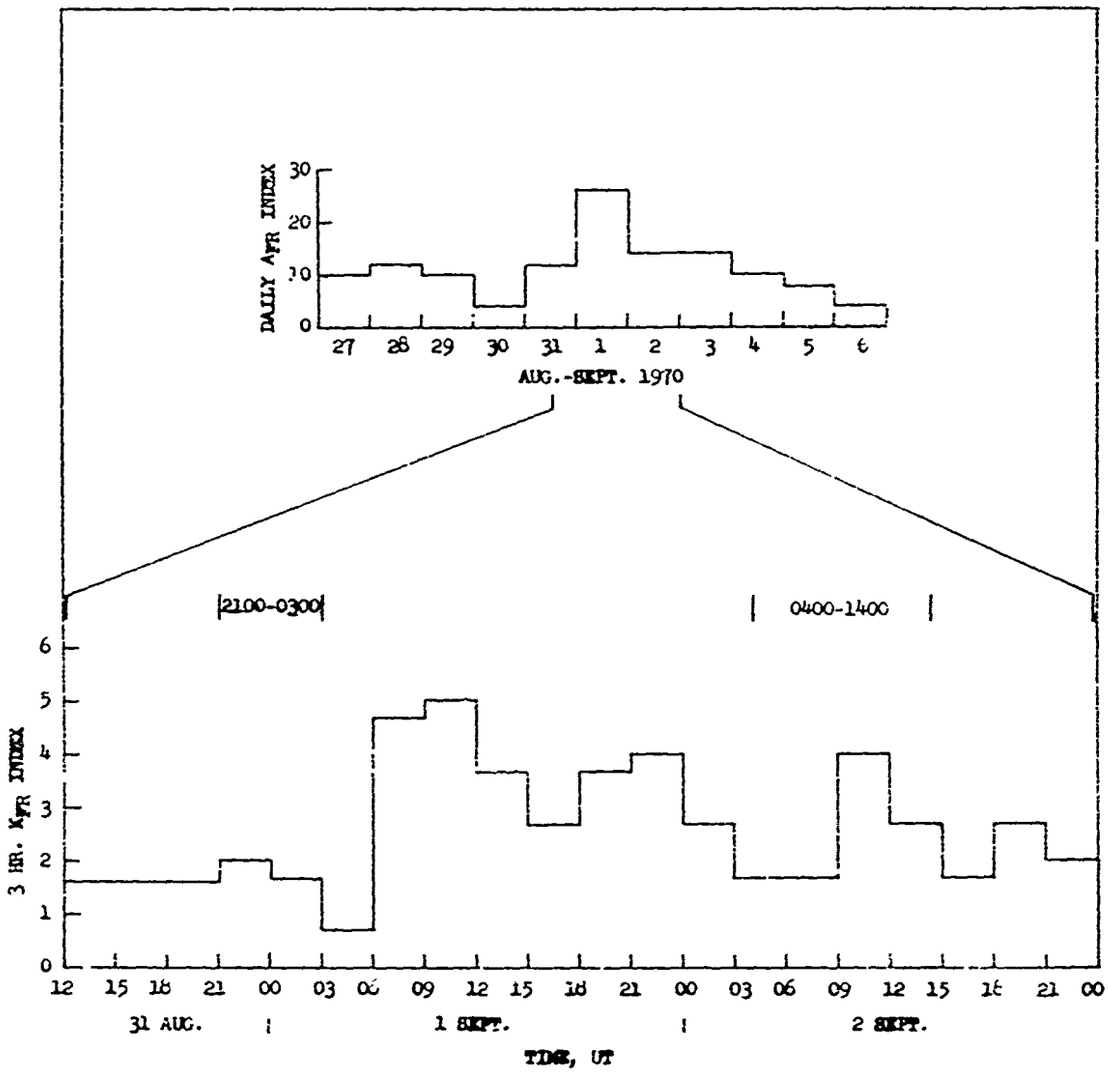

Figure 2-1. Geomagnetic Indices K_{FR} and A_{FR} for the Experimental Period.

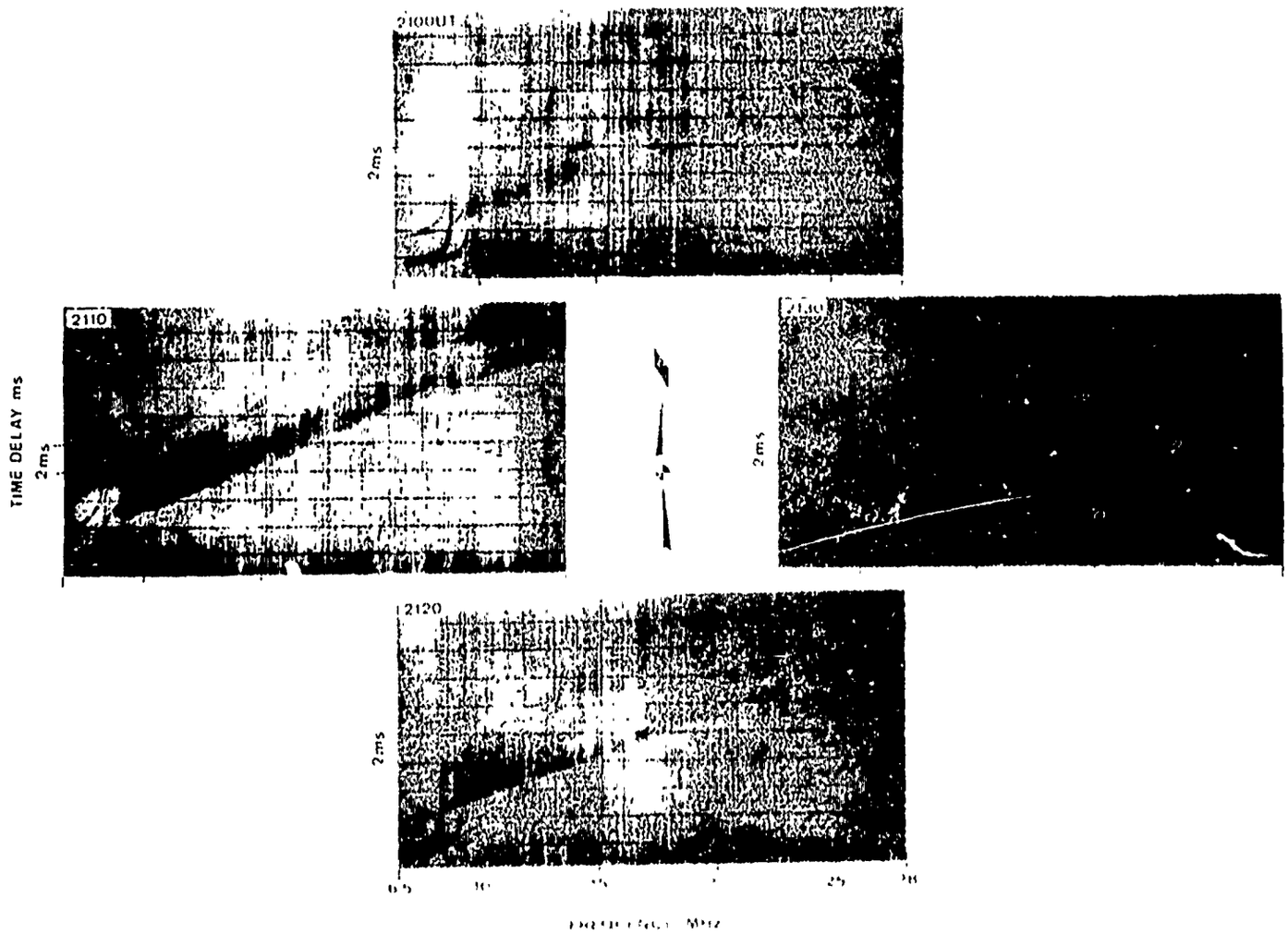

Figure 2-2. Four Quadrant Backscatter Spectrum 2100 [illegible]

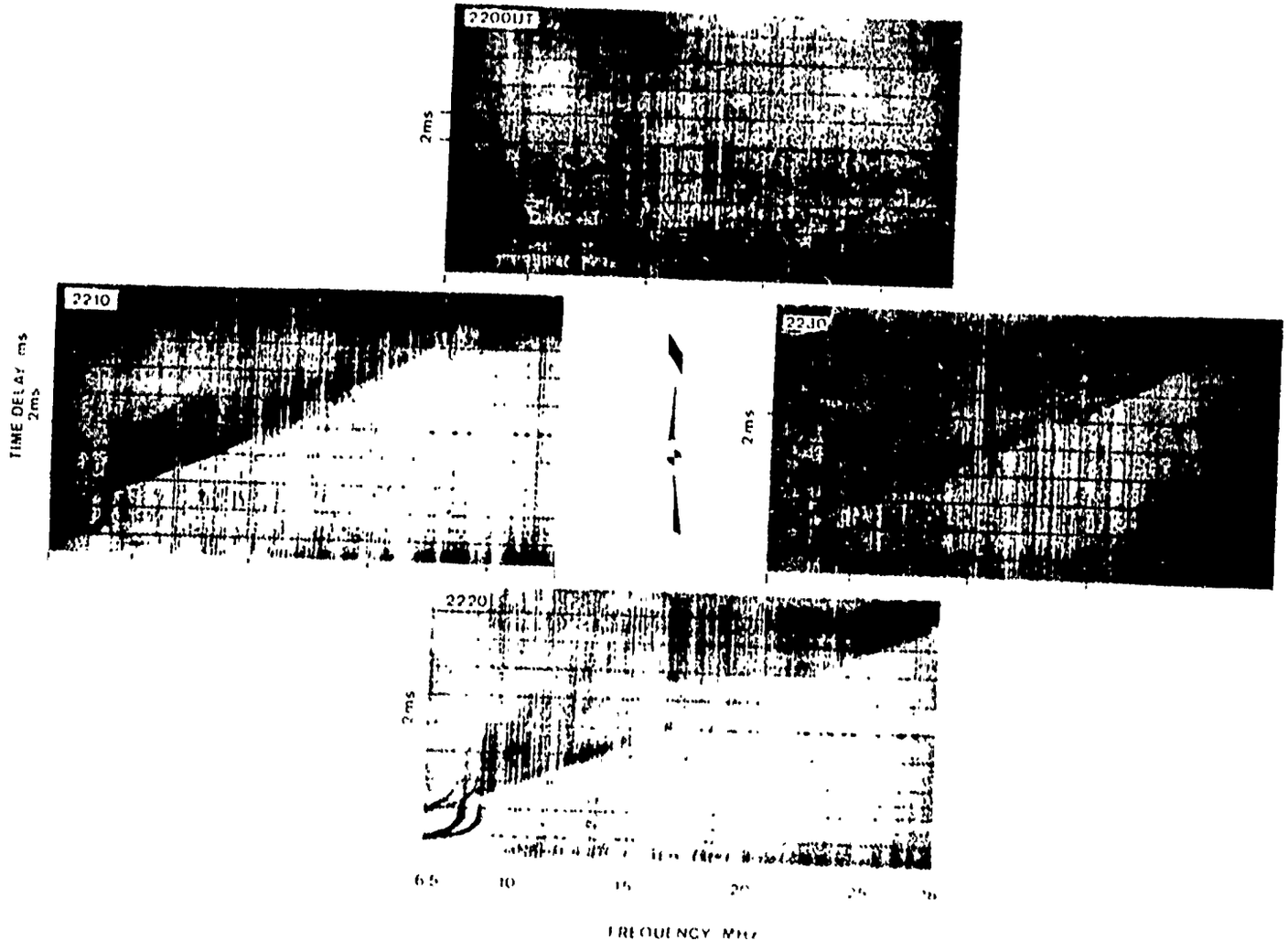

Figure 2-3. Four Quadrant Backscatter Ionograms, 2200-2230 UT.

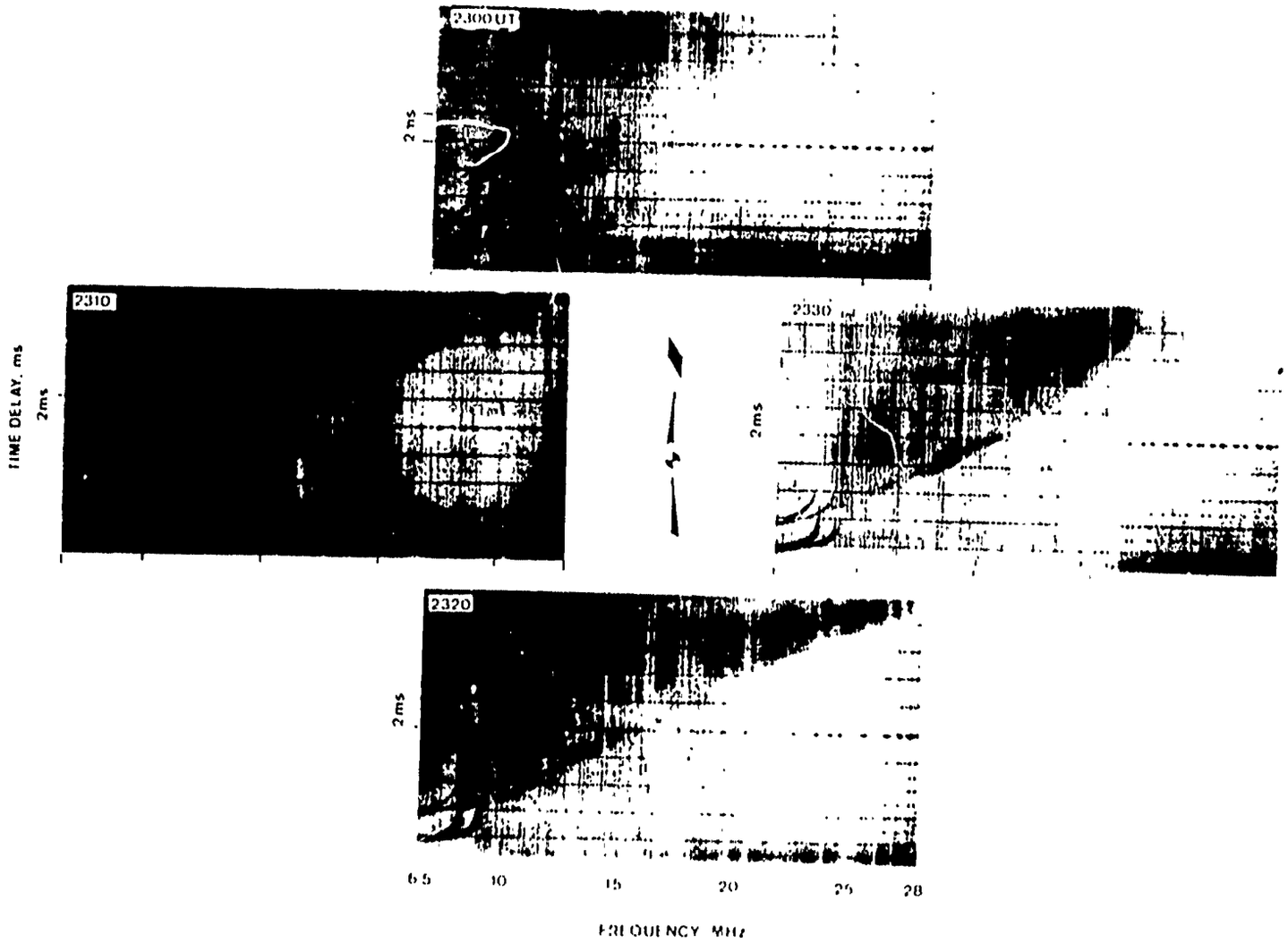

Figure 2-4. Four Quadrant Backscatter Ionograms, 2300-2330 UT

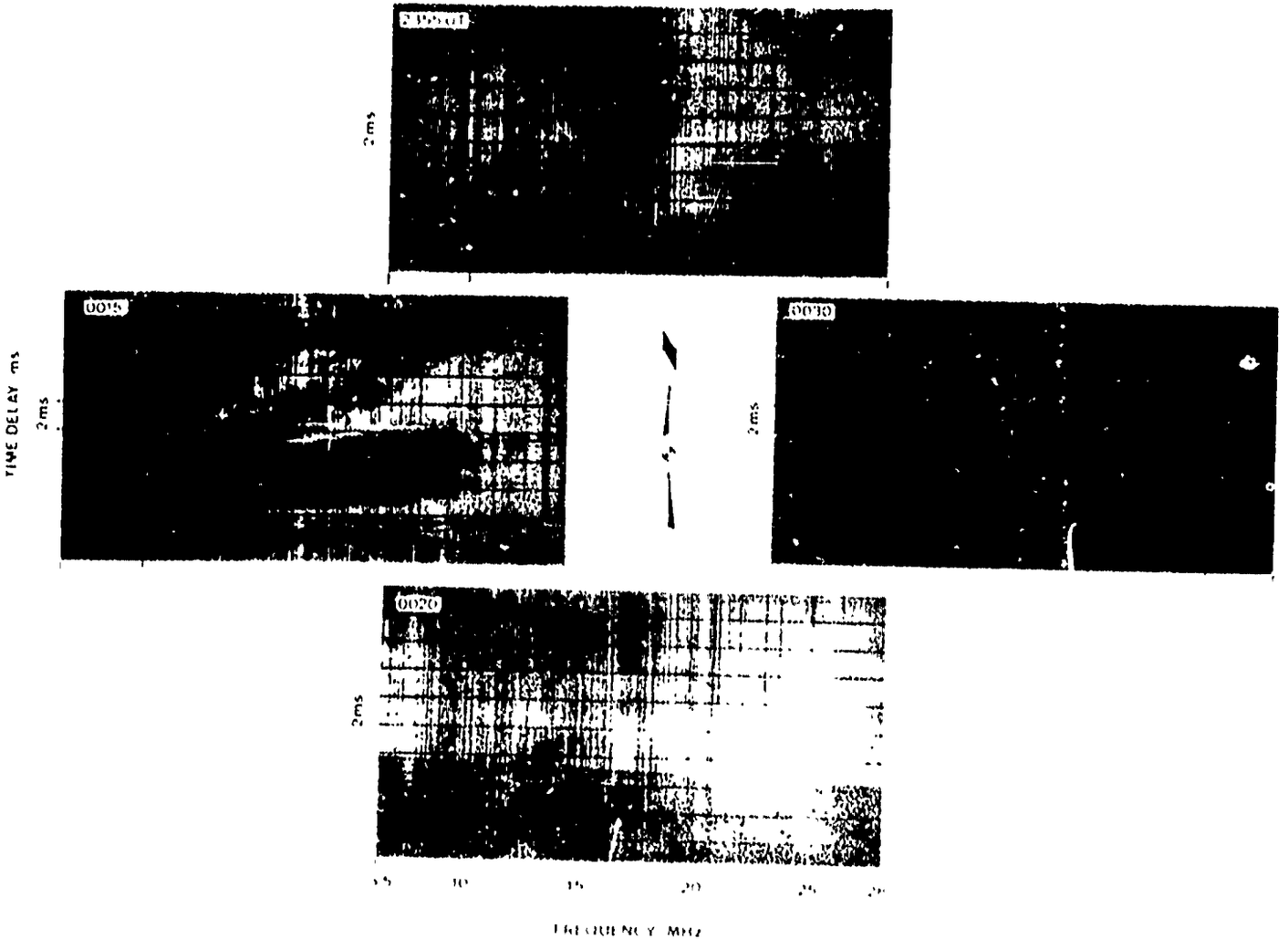

Figure 2-5. Four-Quadrant Backscatter Ionograms, 2555-0030 UT.

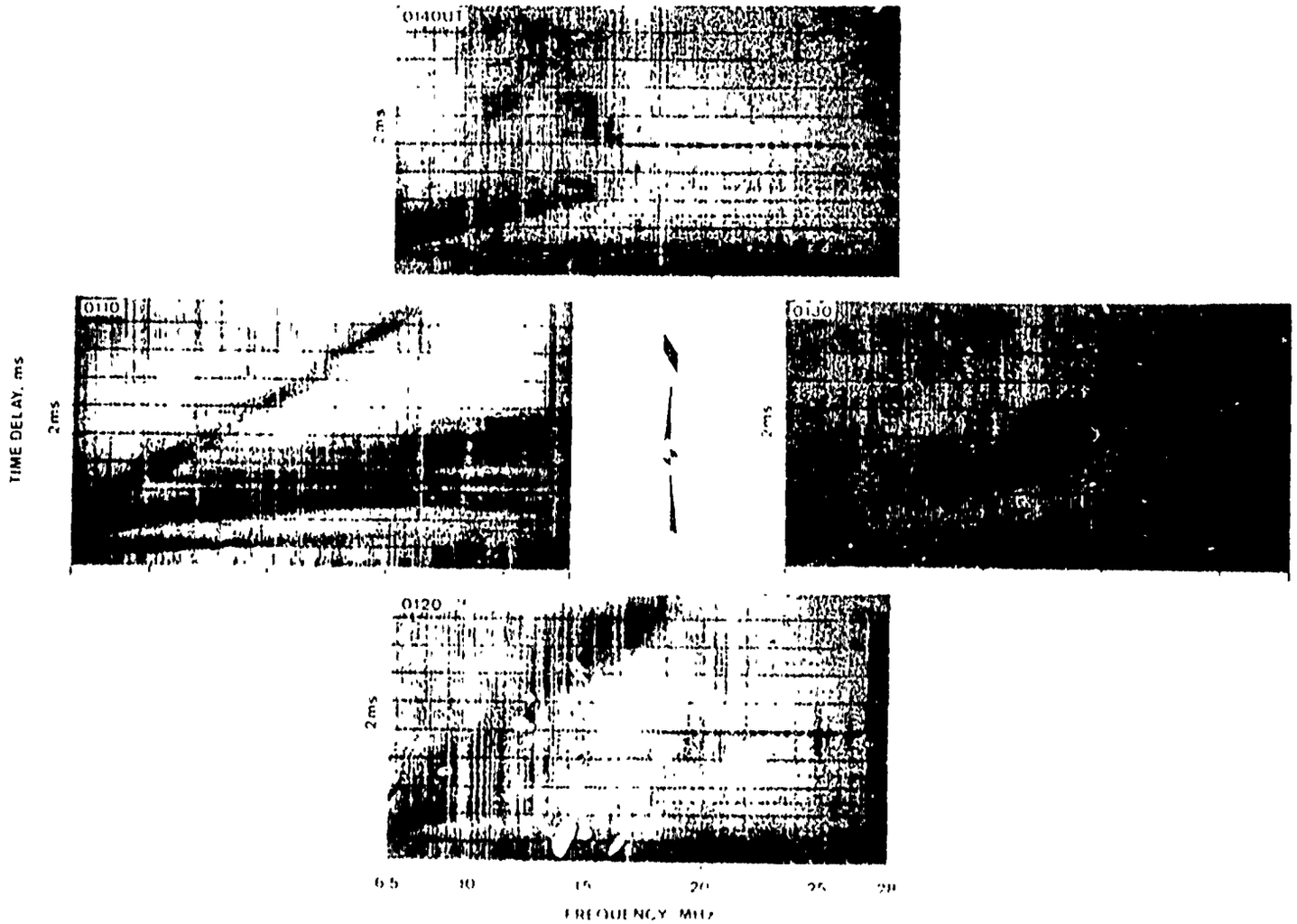

Figure 2-6. Four-Quadrant Backscatter Ionograms, 0110-0140 U.T.

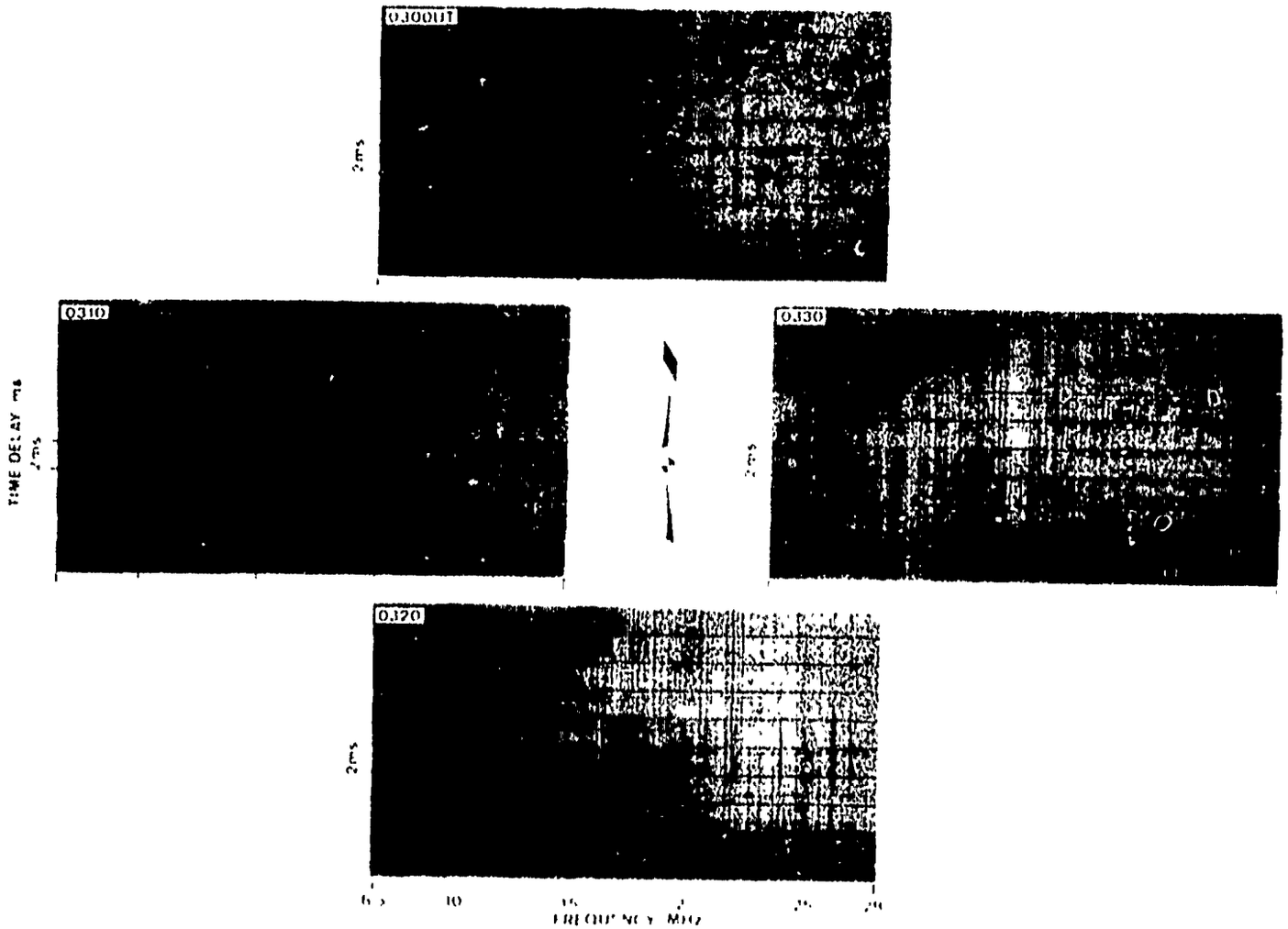

Figure 2-7. Four-Quadrant Backscatter Ionograms, 0300-0330 UT.

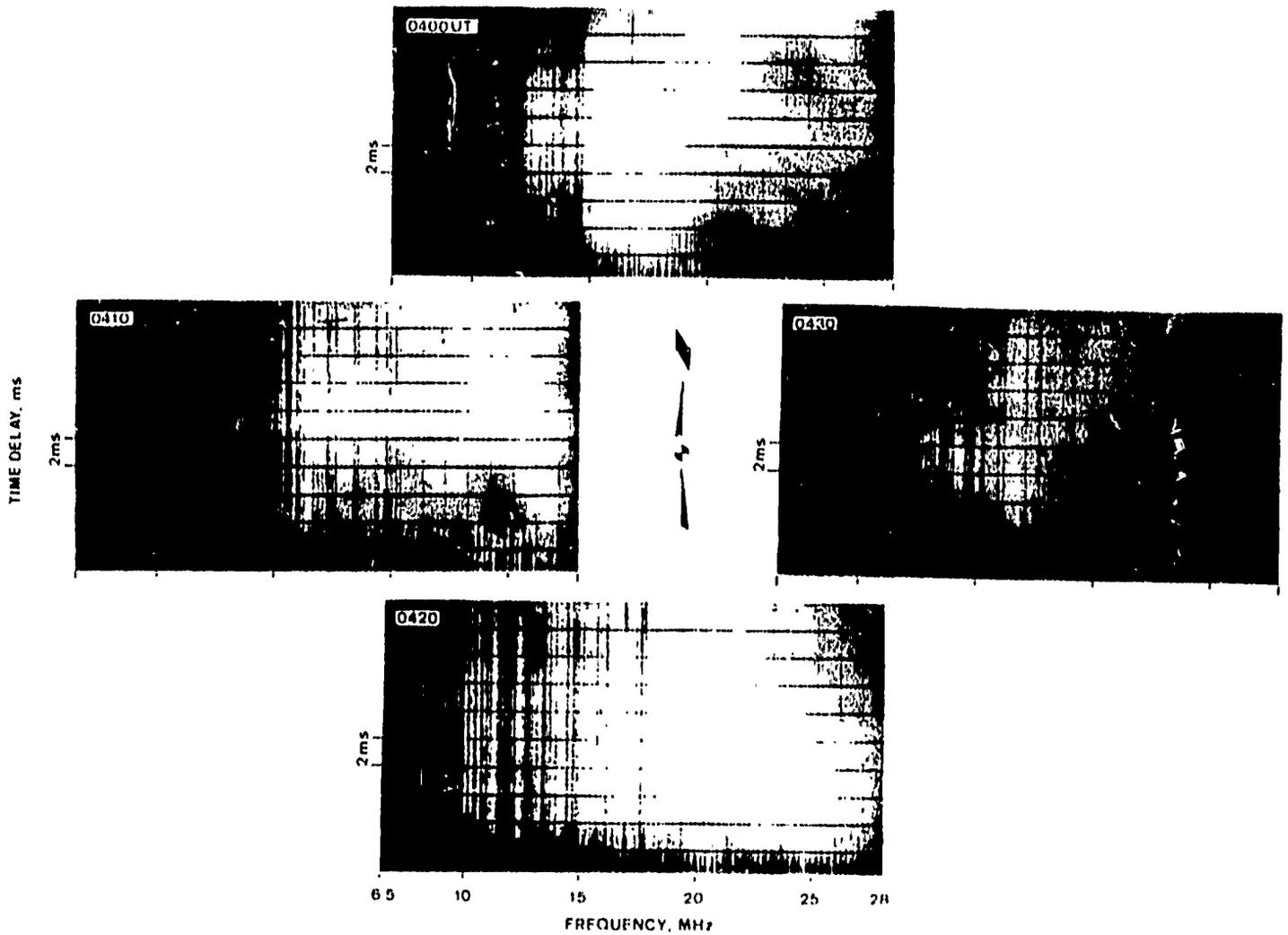

Figure 2-8. Four-Quadrant Backscatter Ionograms, 0400-0430 UT.

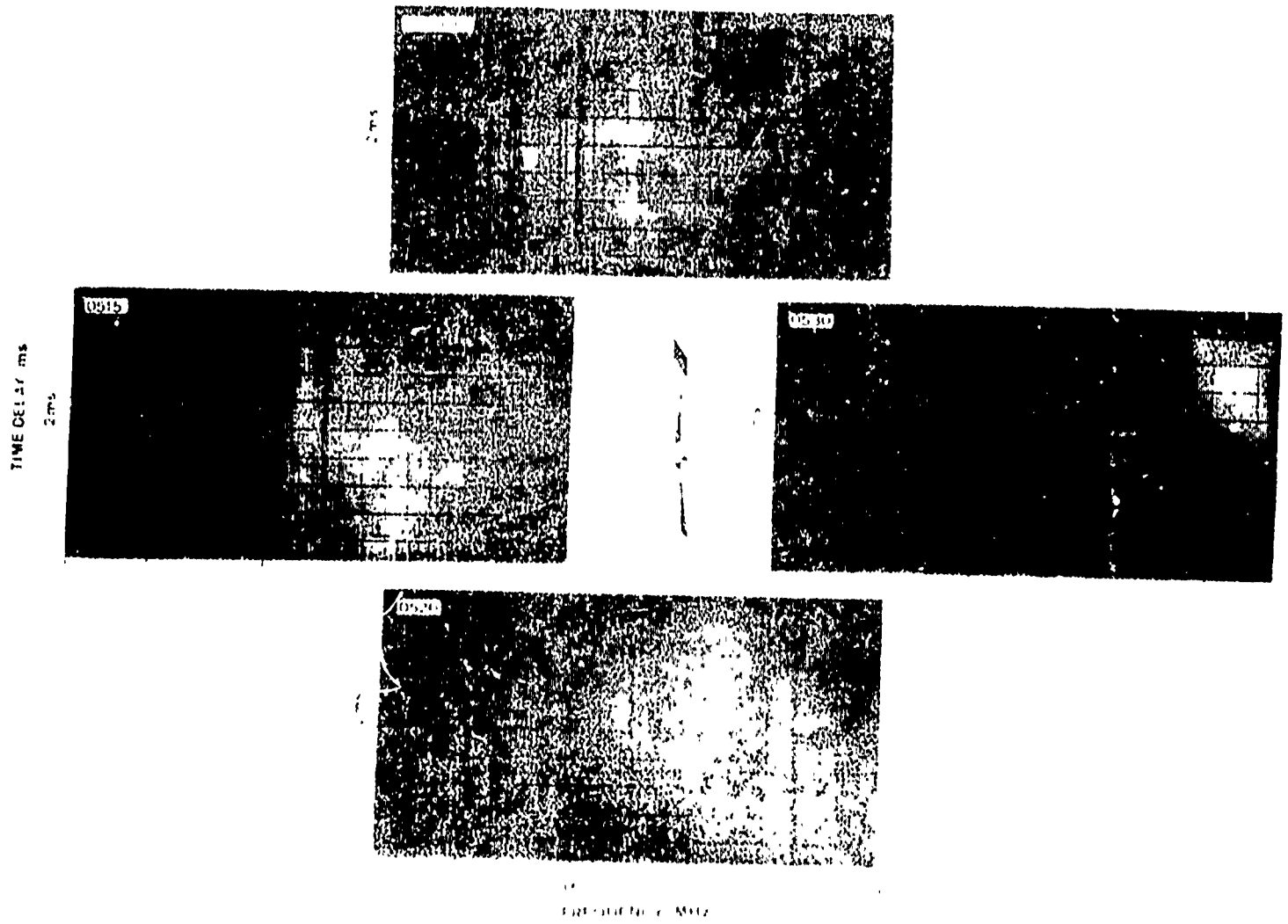

Figure 2-6. Four [illegible]

Reproduced from best available copy.

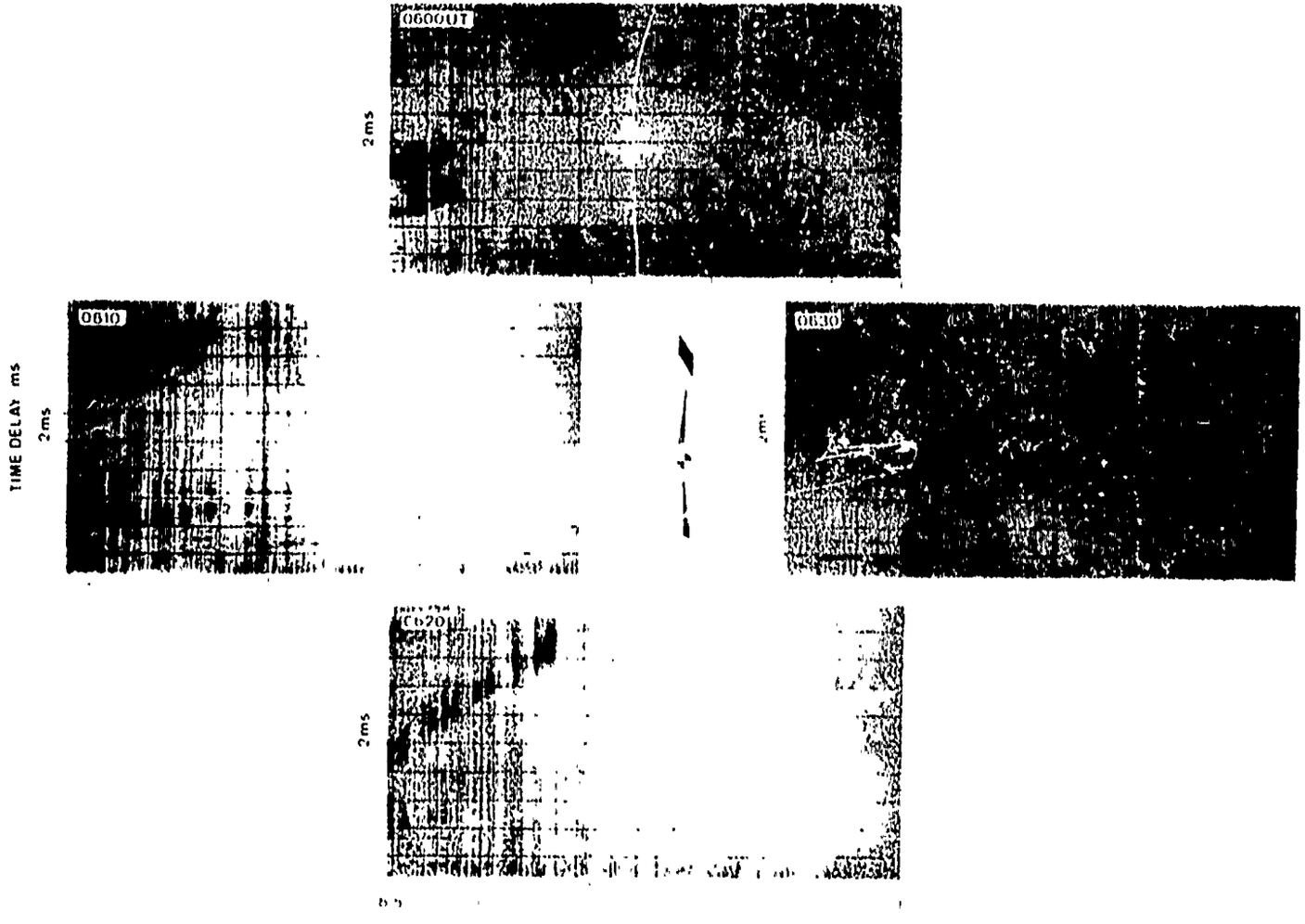

Figure 2-10 Four Quadrant [illegible]

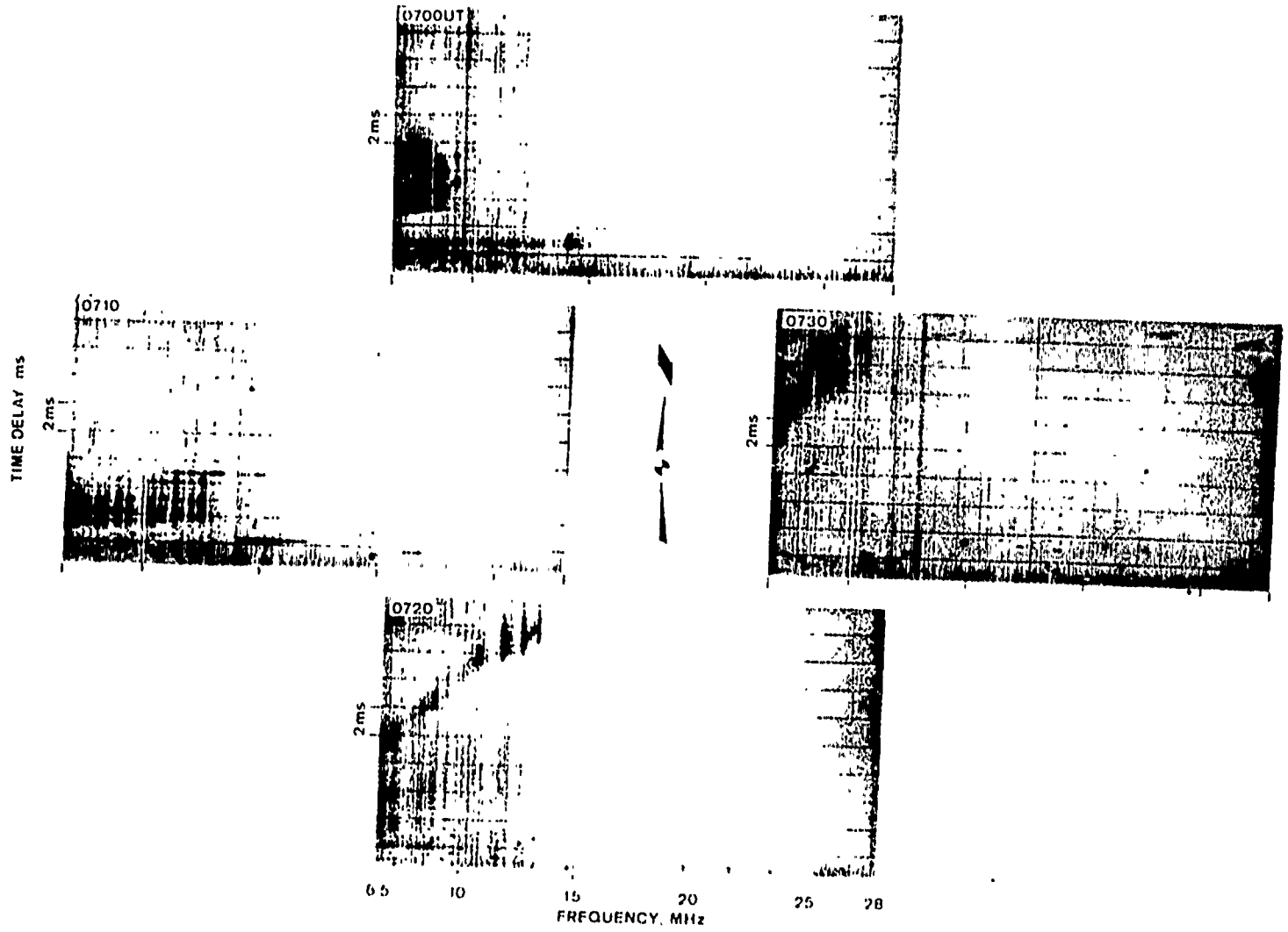

Figure 2-11. Four-Quadrant Backscatter Ionograms, 0700-0730 UT.

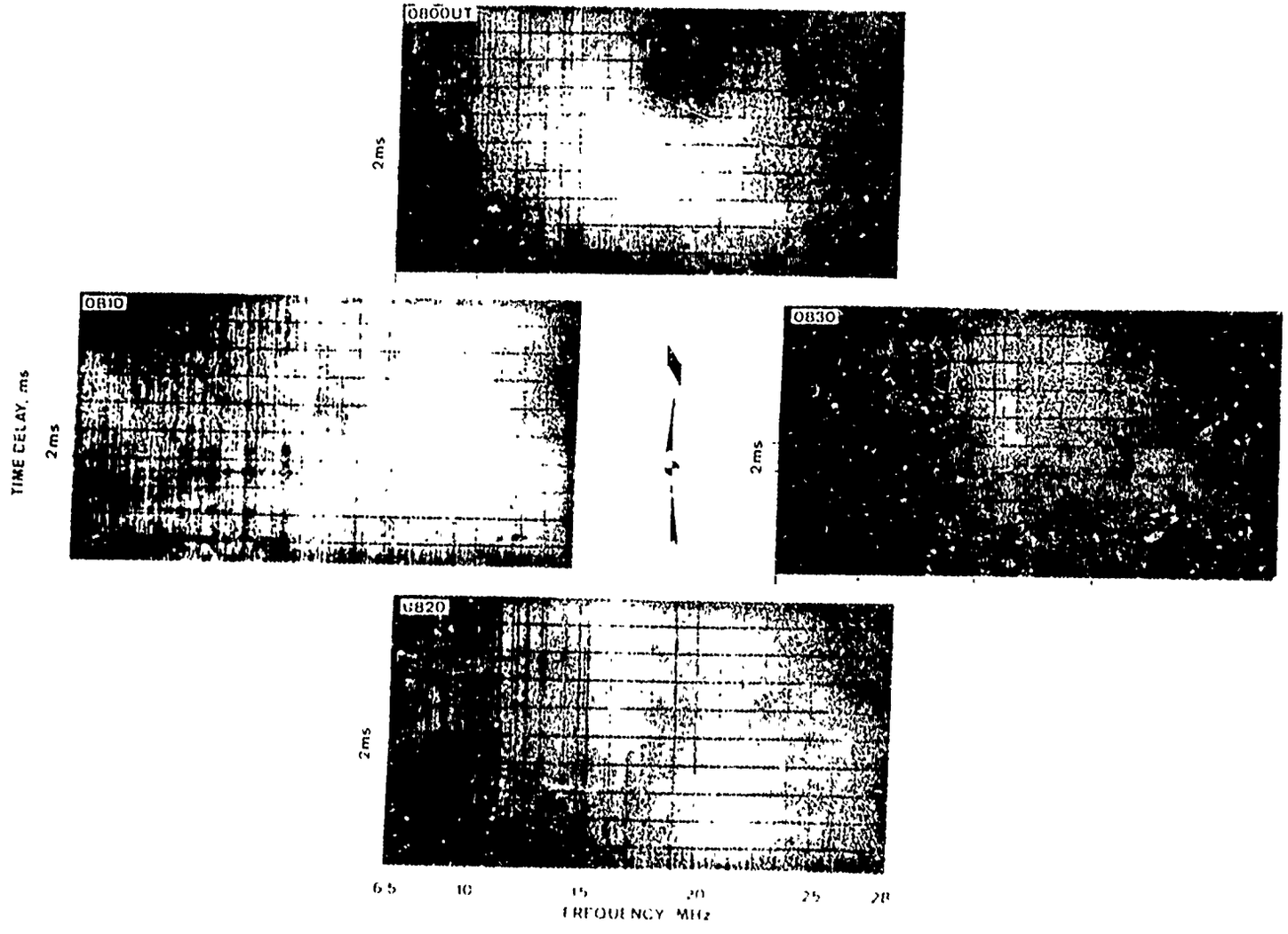

Figure 2-12. Four-Quadrant Backscatter Ionograms, 0800-0830 UT.

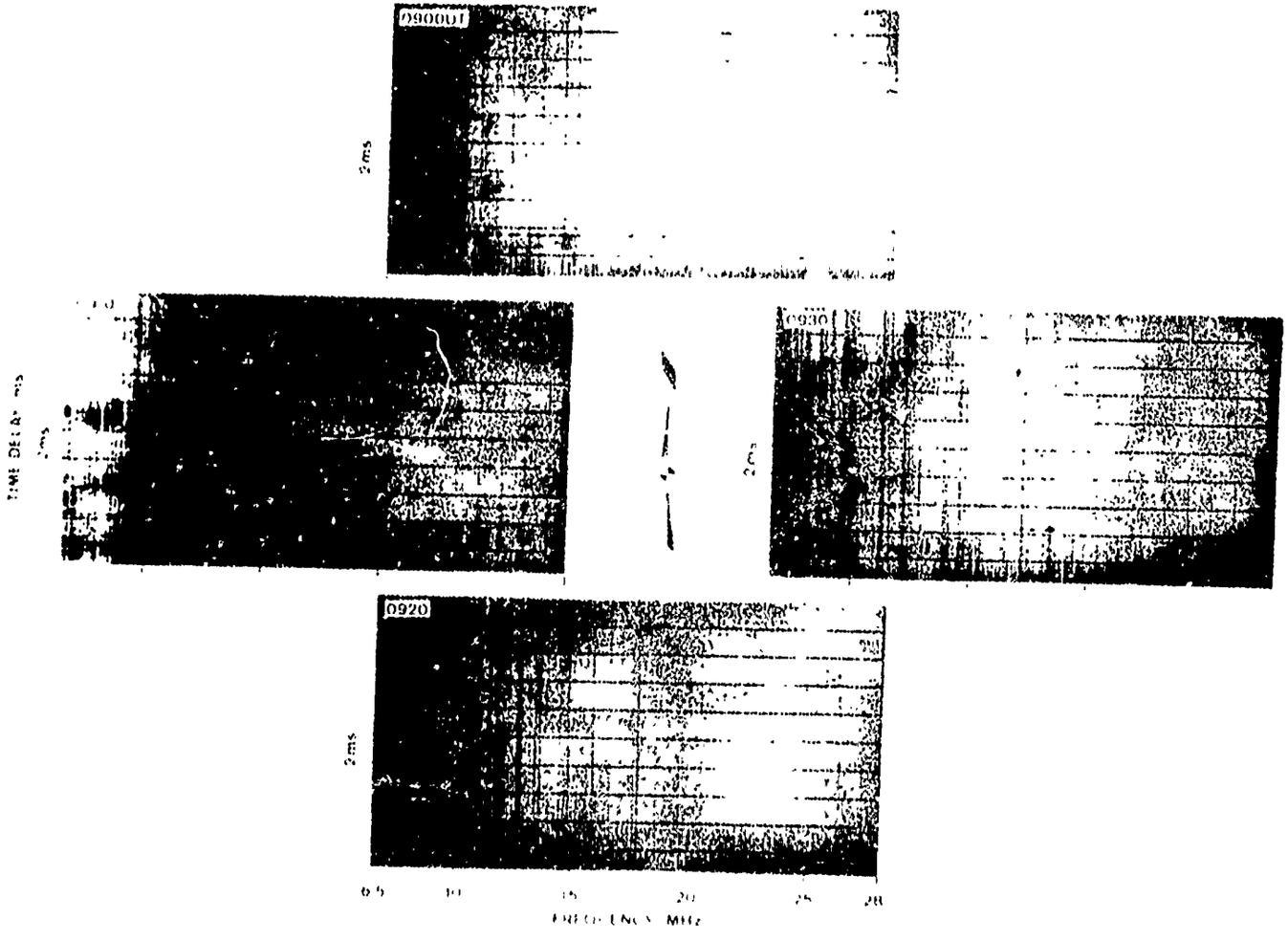

Figure 2-13. Four-Quadrant Backscatter Ionograms, 0900-0930 UT.

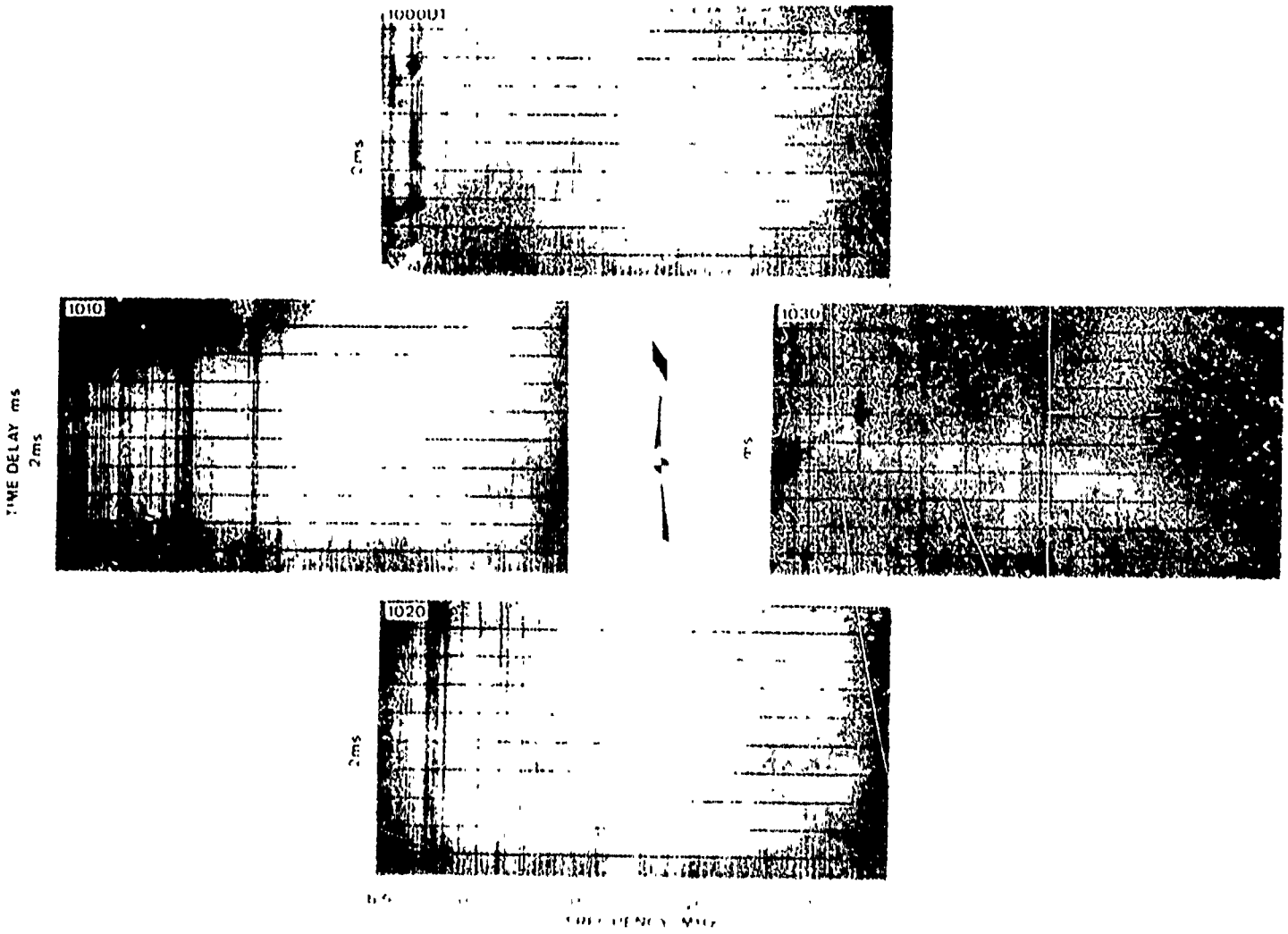

Figure 2-13. Four-Quadrant [illegible]

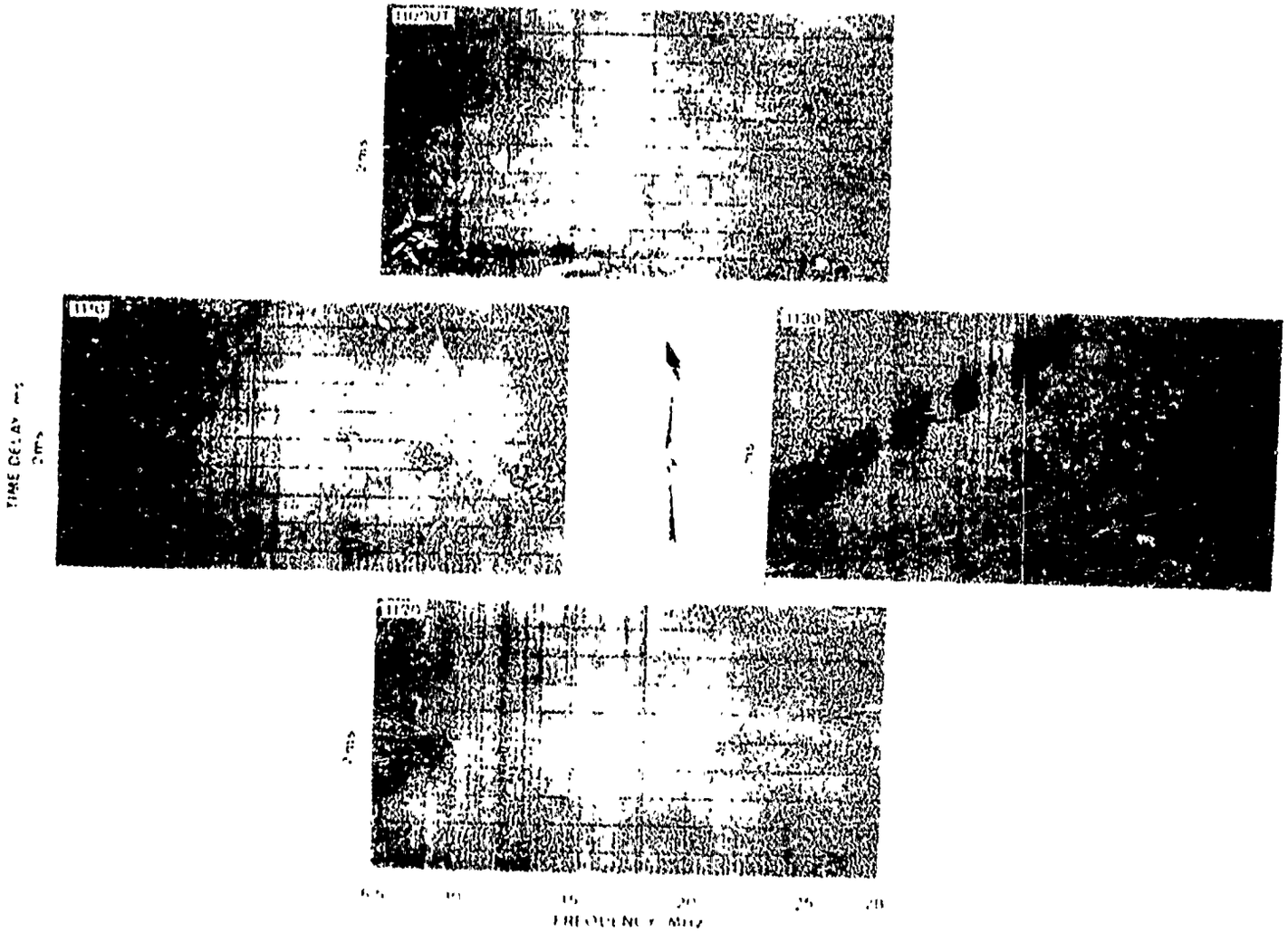

Figure 2-15. Four-Quadrant Backscatter Ionograms, 1100-1130 UT

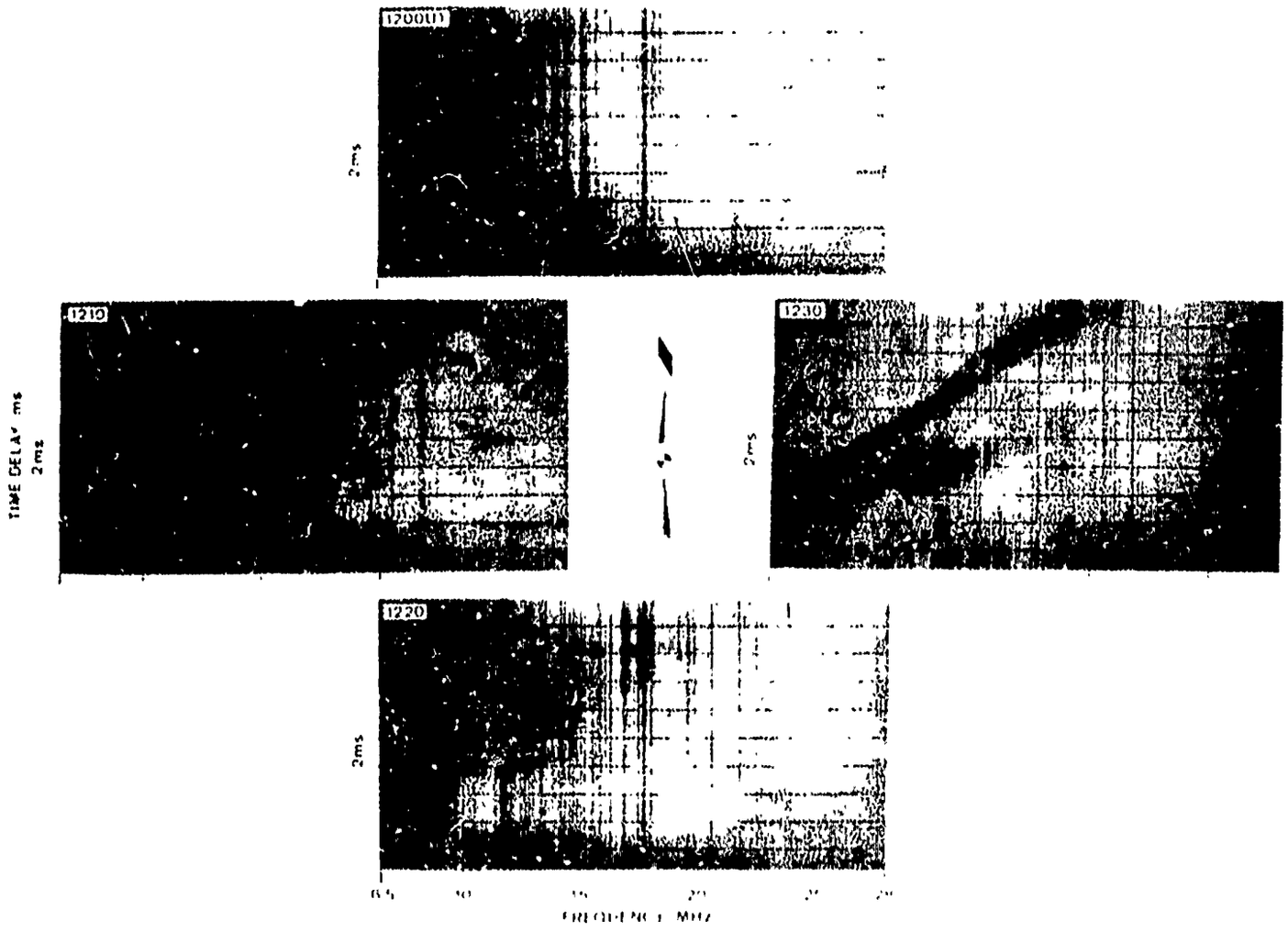

Figure 2-16. Four Quadrant Backscatter Ionograms, 1200-1230 UT.

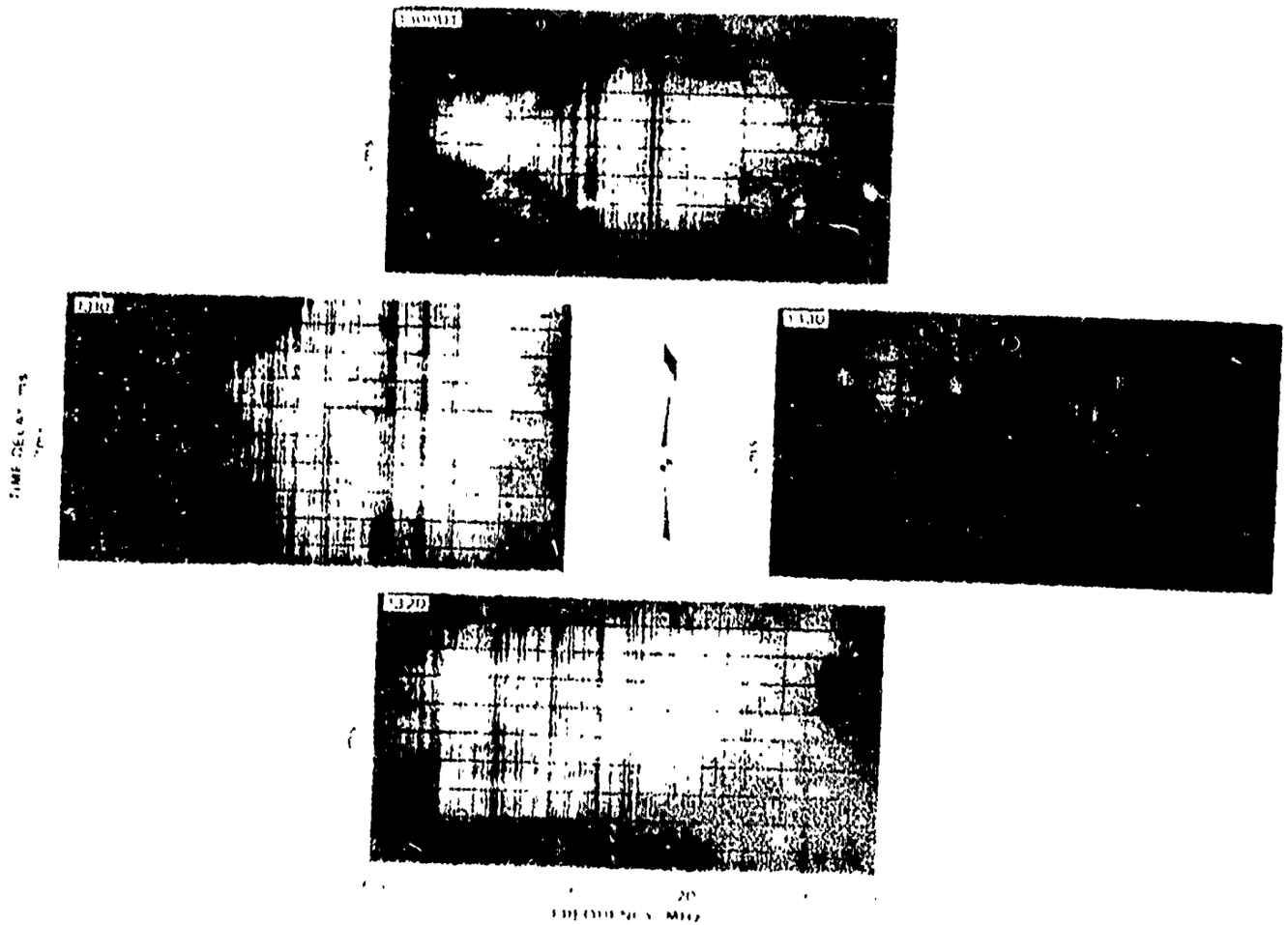

Figure 2-14. Four Quadrant Packet after Longitudinal [illegible]

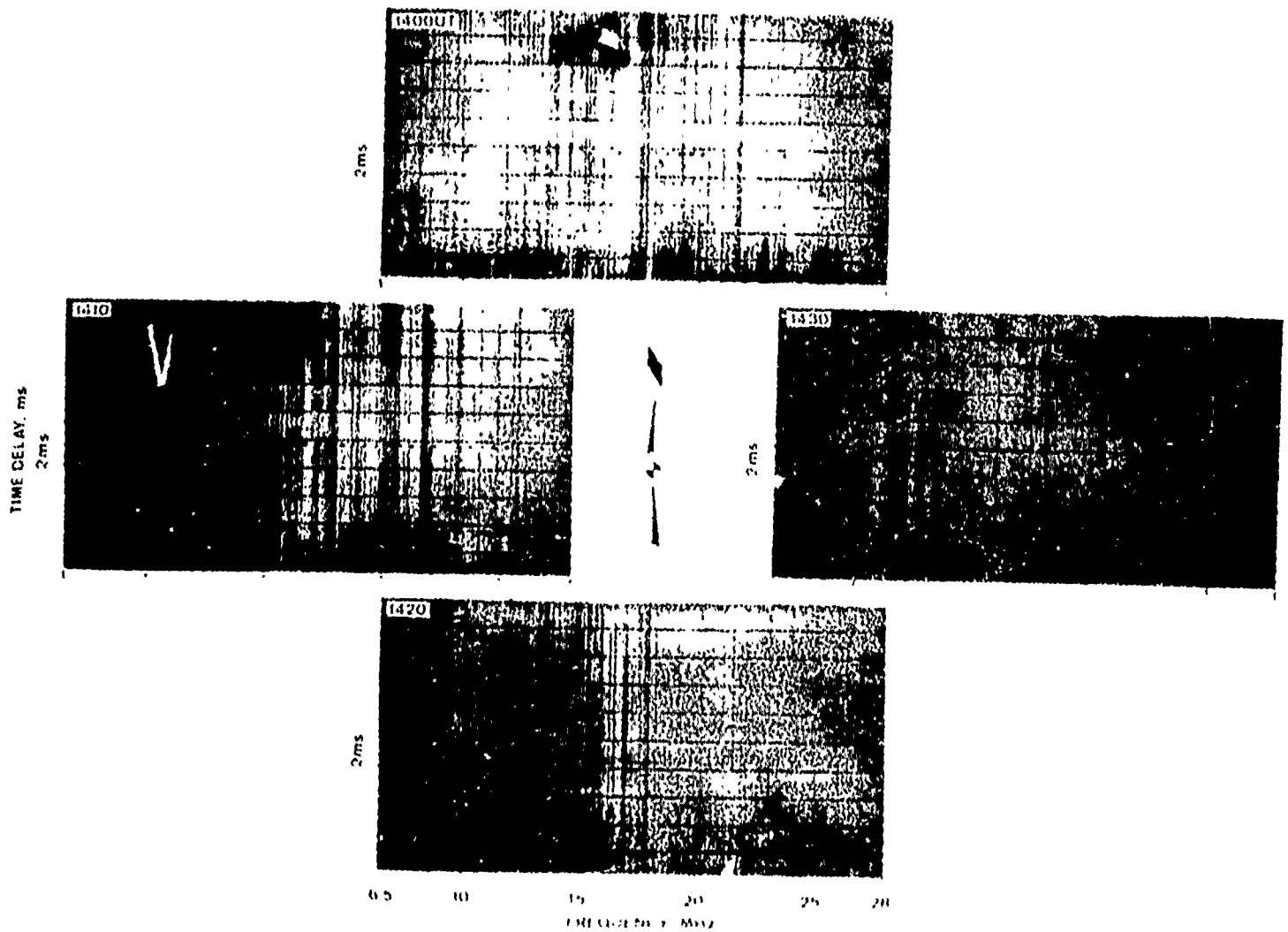

Figure 2-18. Four-Quadrant Back-Scatter [illegible]

3.0 SUNRISE/SUNSET TESTS

3.1 INTRODUCTION

3.1.1 Objective

The sunset and sunrise periods are expected to be times when the operation of an OTH backscatter radar system will experience difficulties. The control of illumination at a specific range demands changes in the operating frequency either to be close to the leading edge of backscatter (focusing effect) or far away from it to increase the signal-to-clutter (S/C) ratio, depending on the objectives of the radar system. Therefore, the position of the leading edge in a frequency-time delay coordinate system has to be predicted or monitored. The ionosphere is far from homogeneous, as we have seen in the previous chapter, layer tilts occur; both effects have to be taken into account.

Because of the expected difficulties of propagation through a day-night transition, tests have often been avoided during such time periods. In order to assess the problem in greater detail, the RADC FM/CW back-scatter system (Ava-Dexter) was operated during one sunset and one sunrise period looking west. The test period was successful; yielding data suitable for detailed study. In this chapter, we analyze the data, interpret the results, and discuss operational procedures.

3.1.2 Summary and Conclusions

Wideband FM/CW backscatter ionograms have been taken for one sunrise and one sunset test period. The ionograms cover the frequency range 6.5-30 MHz with a sweep rate of 250 kHz/sec and an average power of 5 kW. Transmitting facilities at Ava and receiving facilities at Dexter, N.Y. were employed. The antennas looked west (251°T). A transponder was located at the University of Illinois and additional vertical incidence and oblique forward propagation data were taken so that good and reliable ionospheric information for the path are available for analysis. Backscatter ionograms were taken at a rate of three per 10 min.

The ionosphere along the path is approximately homogeneous during daylight and night hours; however, the ionospheric parameters such as foF2 and MUF (1120)F2 undergo variations of about $\pm$ 5 % on a time scale of tens of minutes. During sunset, the maximum frequency range decreases from above 30 MHz to below 10 MHz and the close-in ranges up to 1200 km cannot be illuminated by the equipment because the lowest frequency of the equipment was 6.5 MHz. In order to illuminate close ranges at night, say within 500 km of the transmitter, the lowest operational frequency of the equipment should be 2.5 MHz.

Gradients of the leading edge have been investigated. It is found that average gradients over several msec time delay can be used to infer the ionospheric gross structure along the path. The gradient of the leading edge permits us to estimate the critical frequency at the midpoints to the

nearest integer value. Small irregularities should be disregarded. Two or three linear segments are sufficient to describe the gradient of the leading edge over the whole range of time delays. This method should be tested on a larger sample of backscatter ionograms during daytime and nighttime. Sunset and sunrise make the evaluation of ionospheric parameters along the path more difficult than daytime conditions, because large horizontal gradients of 2 MHz/1000 km or more cause appreciable changes of the gradient.

While ionospheric conditions change slowly during sunset, the conditions change rapidly during sunrise. For a distance of 1100 km, the frequency of the leading edge rose from 6.5 to 16 MHz in about one hour. Hence, frequency selection and frequency switching becomes very important for a time period of one to one and half hours. During sunrise (looking west) the S/N ratio is low, as seen on the transponder signals. This is most probably due to defocusing effects in the skip zone, because ionospheric tilts of several degrees occur. The backscatter ionograms become, at times, quite complicated.

True height electron density profiles from another time period are used to show the ionospheric tilts during sunrise.

Predictions for the leading edge of backscatter records are made using the various ionospheric measurements along the path and comparing the results with the actual backscatter records. For each measurement, a backscatter ionogram is constructed and since the ionospheric parameters

are different, say at Ava and the University of Illinois, two different leading edges result. Four independent measurements along the path gave, in general, four different leading edges. The actual backscatter record agreed best with the synthetic leading edge for the same part of the path. For example, close to the transmitter the actual backscatter agreed best with the predicted leading edge based on vertical incidence data from Ava; for long time delays (ground range 2000 to 3000 km) the actual backscatter record agreed best with the predicted leading edge based on vertical incidence data from University of Illinois. During sunset, the NOAA predictions did not agree with the actual backscatter ionogram. However, late at night the NOAA predictions were useful.

If some ionospheric measurements at the transmitter site or along the path are available, predictions of backscatter ionograms can be made in a simple graphical way without involving special computers. The evaluation of this special test leads to useful results. It shows the change in the backscatter ionogram can be explained and proven by the actual change of ionospheric parameters along the path. It further shows that simple predictions of the leading edge in backscatter ionograms can be made if some vertical incidence ionograms are available.

3.2 BACKGROUND INFORMATION

3.2.1 Leading Edge for Selected Critical Frequencies and Reflection Heights

A simple computation was made to obtain the leading edge for the 1F mode and to distinguish between the influence of $f_{\perp}$ and h'.* Figure 3-1 shows operating frequency from 3 to 30 MHz as abscissa and group path time-delay as ordinate in the form recorded during this test. The ionosphere is assumed uniform and concentric with a maximum electron density corresponding to $f_{\perp}$ = 3, 5, and 10 MHz and height of reflection h' = 200, 250, and 300 km. The gradients of the leading edge of the backscatter trace are quite different for the choices of $f_{\perp}$, the influence of reflection height h' is less important. The corresponding distances of the ground range target are indicated. For $f_{\perp}$ = 10 MHz, the leading edge is a fairly straight line and operating frequencies of over 30 MHz are needed to obtain a leading edge beyond 2000 km. The curvature of the leading edge increases with decreasing frequency. This graphical representation has been used as an overlay of the hard-copy output from the spectrum analyzer.

What is also obvious from this graph is the range limitation for low $f_{\perp}$. If $f_{\perp}$ = 3 MHz and the wideband soundings start at 6.5 MHz, no backscatter from the first 1000 km is received, because it falls below 6.5 MHz.

---

*In this chapter, the frequencies obtained for vertical propagation are indicated by $f_{\perp}$, those for oblique propagation by $f_{\wedge}$, and the virtual ionospheric reflection height by h'.

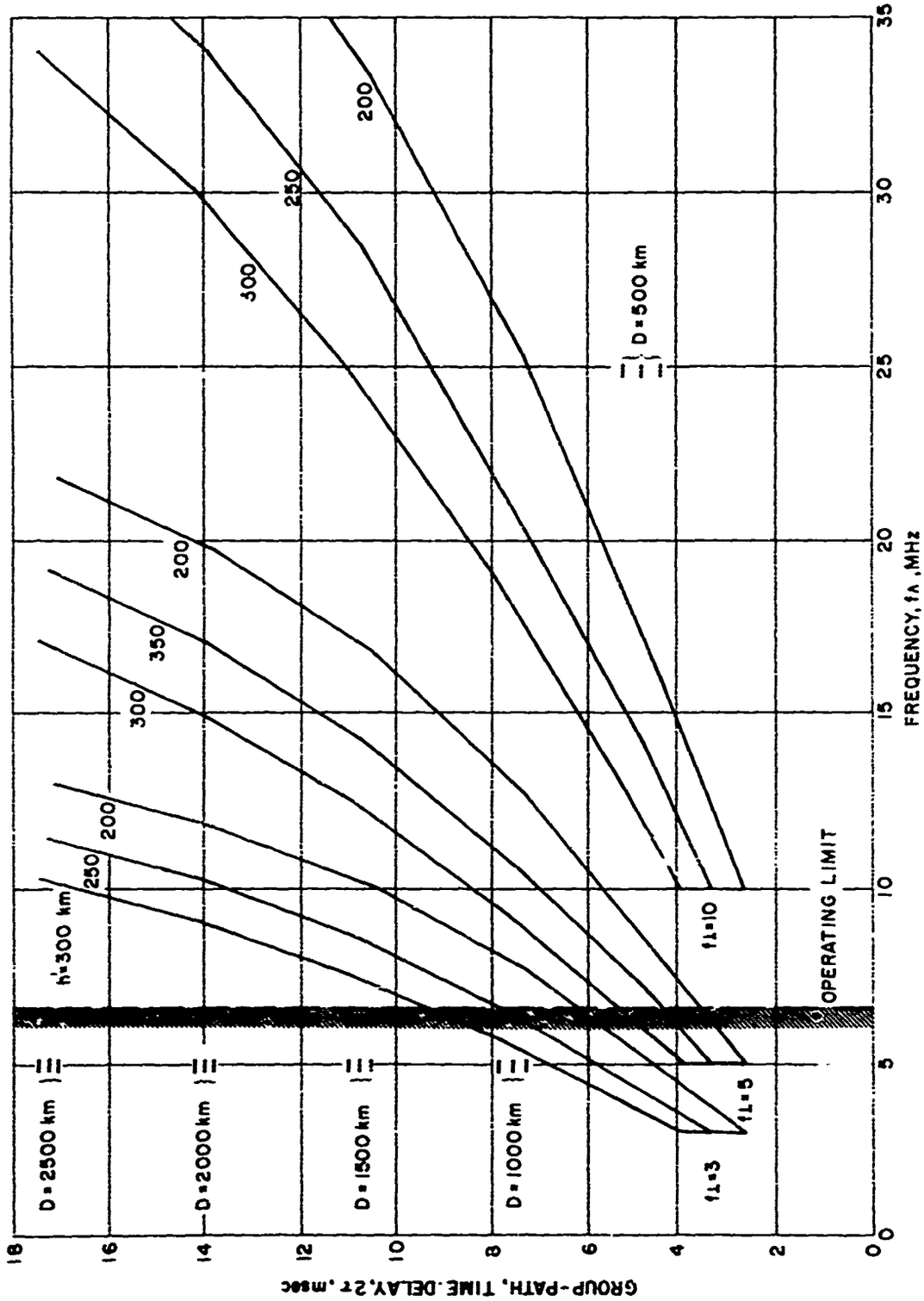

Figure 3-1 Position of Leading Edge in Oblique Backscatter Ionogram for Selected Plasma Frequencies f_L (3, 5, and 10 MHz) and Selected Reflection Heights h' (200, 250, and 300 km).

3.2.2 Mode Identification for the Leading Edge of Backscatter Traces

On wideband backscatter ionograms, several traces can be seen at times and mode identifications of regular and unusual modes have been made (see, for example, Coffey, et al., 1970, Katz, 1970, 1971). If the vertical incidence ionogram appears on the backscatter ionogram, the mode identification is straightforward, because leading edge of each mode can be traced back to the second vertical incidence reflection of the corresponding layer. However, most wideband backscatter soundings start at 5 or 6.5 MHz or even 10 MHz and then no vertical incidence ionogram is recorded or only a small part of it. Without a vertical incidence ionogram, it is sometimes difficult to identify the basic backscatter modes.

During daytime the leading edge of the E, F1 (when present) and F2 modes should appear, as well as mixed or combination modes. Due to skip zone focusing, they may, at times, merge into one wide band. During the night basically only the F2 mode appears, unless a sporadic-E (Es) mode is also present. During daytime, especially in summer and at mid-latitudes, Es occurs very often; thus, an Es mode has to be considered. If sporadic E is strong (blanketing Es) its leading edge can become the predominant backscatter mode.

Based on some actual daytime vertical incidence ionograms from the Boston area (Billerica), we have computed (assuming a uniform ionosphere) the leading edge for each mode (E, F1, F2) using $f_{\perp}$, h' and our tables for group-path time-delay.

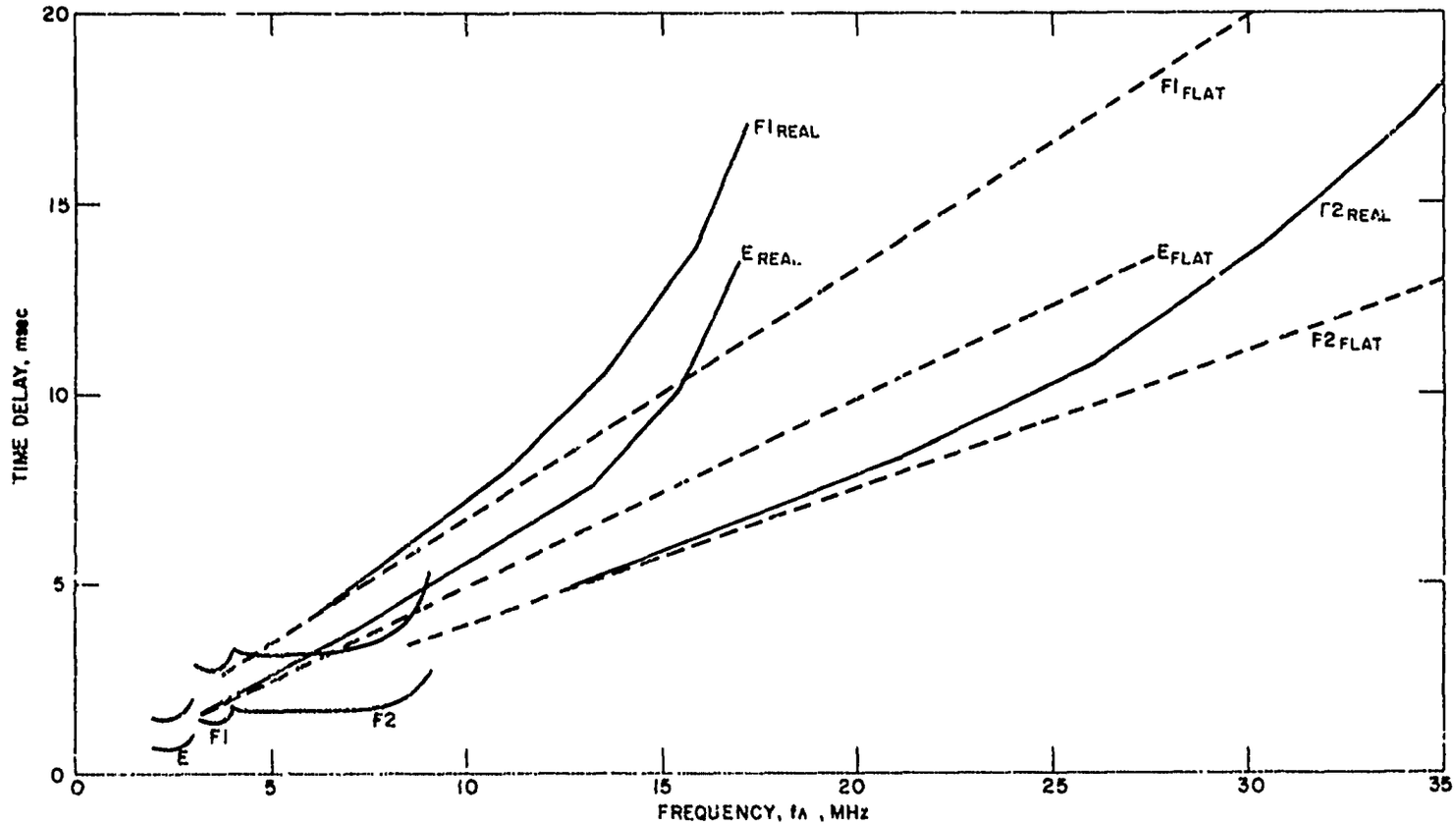

Figure 3--2 Computed Leading Edges in an Oblique Backscatter Ionogram Based on a Real Vertical Incidence Ionogram for a Winter Day (Noon, November, 1970, Boston).

E, F1, and F2 Layers are Present. Leading Edges are for a "flat" and "curved" Earth are Shown.

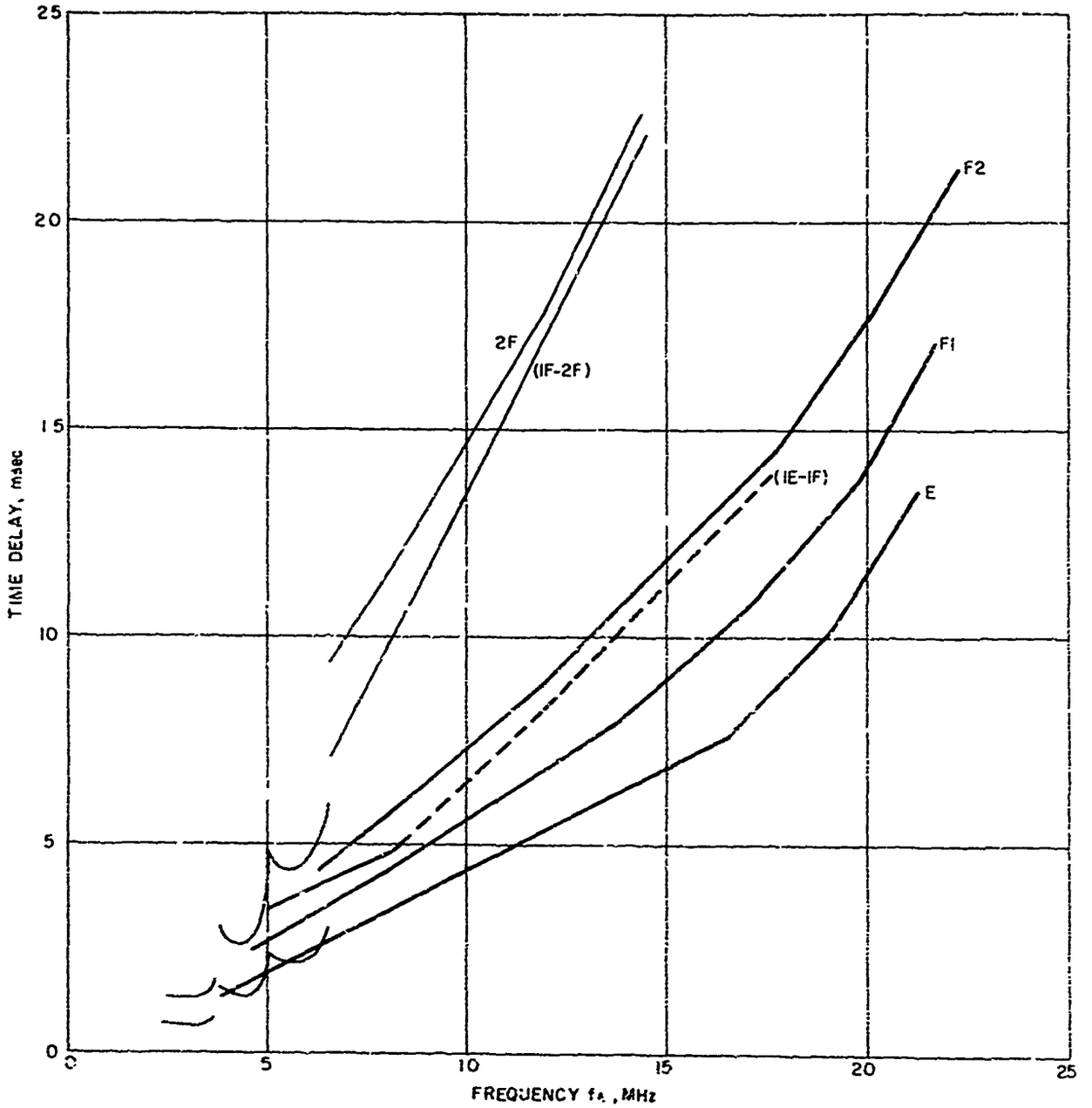

Figure 3-3 Computed Leading Edges in an Oblique Backscatter Ionogram Based on a Real Vertical Incidence Ionogram for a Summer Day (noon, July, 1970, Boston).

E, F1, and F2 Layers are Present. Leading Edges are for Curved Earth. Two Mixed Modes are also Shown.

A winter day (noon, November 1970) is selected with an E layer at 100 km, an F1 and an F2 layer. The critical frequency foF2 is very high compared to foF1, while h'F1 and h'F2 differ by only 40-50 km. In winter, the main leading edge with the shortest time delay is due to the F2 mode; those due to the E and F1 mode are well separated from the F2 mode (Figure 3-2).

A summer day (noon, July, 1970) shows a distinctively different predicted ionogram. The critical frequencies of E, F1, and F2 are close together and the height h' of F1 and F2 are 130 km apart. Consequently, the order of modes for the leading edge changes. The E mode has the shortest time delay, followed by F1, and the F2 is last. All three leading edges are close together. We also include a mixed mode 1E-1F2 which is close in time delay to the F2 mode. The 2F2 mode and the mixed mode 1F2-2F2 are also shown. (Figure 3-3)

For the winter case, Figure 3-2, we have added the leading edges assuming a flat earth-flat ionosphere, solely for illustrative purposes. The curves are straight lines and indicate the error in time delay for large distances if such a simplified assumption is made.

3.2.3 Test Configuration

The data for this study were obtained during November/December 1970. Sunset conditions were observed by operation between 30 November 17 UT (12 EST) and 1 December 3 UT (22 EST), while sunrise conditions were observed by operation on 2 December from 10 UT (5 EST) to 15 UT (10 EST).

Backscatter ionograms were obtained over the frequency range 6.5-30 MHz with transmissions at a sweep rate (positive sense) of 250 kHz/sec and an average power of 5 kW; a rhombic antenna was utilized for transmission. The receiving site at Dexter, NY, employed a phased array receiving antenna comprised of Beverage antenna elements and steered to 251°T, which is within the half power beamwidth of the transmitting antenna at the range of operation and the bearing of the University of Illinois. An FM/CW generator at the receiving site was utilized to de-ramp the backscatter return, with signal processing which has been described in detail in previous reports.

At the University of Illinois were located a wideband transponder and a receiver for oblique incidence FM/CW ionograms. The transponder imposed a double-sideband suppressed carrier modulation of 500 Hz on the re-transmitted signal, equivalent to a range shift of $\pm$ 2 msec at the sweep rate employed. The purpose of the offset is to permit separation of the transponder echo from the ground clutter, permitting more accurate scaling of data from the transponder echo.

Ionograms were obtained commencing at 1, 4, and 7 minutes of each ten minute interval, but the transponder was activated for only one of the three soundings. The received data was recorded on analog magnetic tape and processed to yield ionogram displays at the DRC of RADC. The processed data was inspected and scaled at least every ten minutes; the ionogram containing the transponder information was always scaled.

Vertical incidence ionograms were obtained by a Granger ionosonde at the University of Illinois; the vertical incidence data from the Granger sounder at RADC was lost due to improper operation.

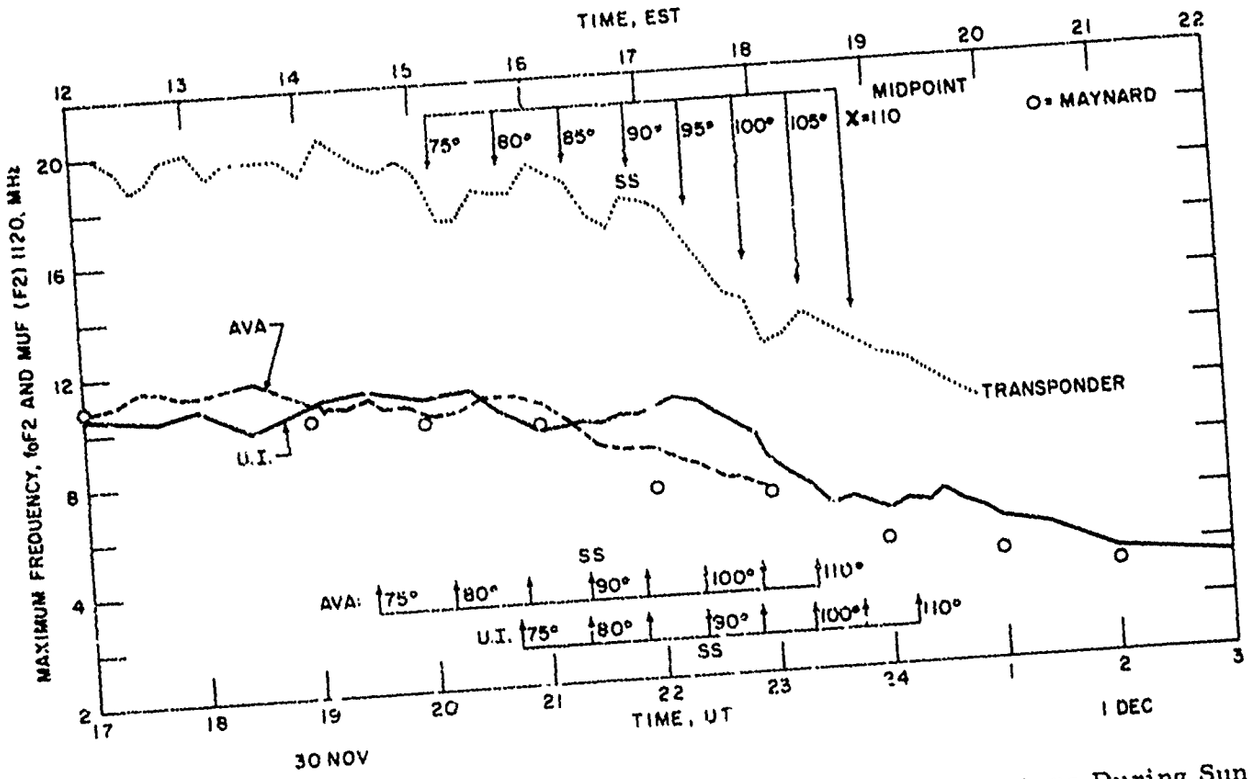

Figure 3-4 Observed Temporal Variations of Ionospheric Parameters During Sunset Test Period.

Shown are foF2 at Ava and University of Illinois (U. I.) at 10 min intervals. Open circles are hourly values of foF2 at Maynard, Mass. MUF from transponder at U. I. Solar zenith distance χ every 5° for Ava, U. I., and path midpoint. SS = ground sunset.

3.3 SUNSET TEST

3.3.1 Ionospheric Variations During Test Period

The ionosphere changes its structure (electron density and layer height) drastically during sunrise and sunset periods (Penndorf and Katz, 1969). But, it also undergoes continuously some small scale irregular changes during day and night. One can say that foF2, during a quiet daytime, varies at least $\pm$ 5% around its average hourly value if it is monitored continuously.

In Figure 3-4 we show the scaled foF2 data for Ava and University of Illinois (U. I.) as a function of time (one data point every 10 min), which indicate such small scale irregular variations. For clarity reasons, we omit the fxF2 traces, although they have been scaled too. Some slight variations in the difference (fxF2-foF2) appear in the data, indicating small ionospheric irregularities. During daytime, foF2 differs between Ava and U. I., implying horizontal gradients up to 1.5 MHz exist over this distance scale. Such differences become, of course, most pronounced during sunset and here they reach up to 2 MHz. The normal sunset decrease starts at Ava at $\cos\chi = +0.1$ (solar zenith distance $=\chi$), which is normal. At U. I. it starts later, at $\cos\chi \approx 0$. The critical frequency decreases below 6.5 MHz* at Ava when $\chi \approx 110^{\circ}$; at U. I. it reaches a minimum of 3.5 MHz at the end of the test at 3 UT (21 LST). The hourly foF2 values for

*The equipment was limited to 6.5 MHz, thus no smaller frequencies can be measured.

Maynard, Mass., are also indicated. The conditions at the path midpoint are obtained from the transponder data and from the oblique forward propagation, both of which agree most of the time, as expected. While the forward propagation is from Ava to U. I., the transponder path is from Ava to U. I. and back from U. I. to Dexter. Thus, the ionosphere over the two paths Ava-U. I. and Dexter-U. I. may not always be identical, although the paths are very close together. The observed differences in the MUF are a few tenths of a MHz, with the single path MUF being larger, except at a few times after 0000 UT. The diagram gives the transponder data because they are more complete. The MUF for this path also varies by about $\pm$ 5% during daytime around an hourly average value. The decrease in MUF starts at $\cos\chi \approx +0.1$ reaching about 10 MHz at 0040 UT; then the signal strength of the transponder becomes weak and disappears at about 8 MHz at 0130 UT. Figure 3-4 also shows the zenith angle χ for midpoint and the two stations as function of UT time. ESSA foF2 predictions at 20, 22, and 24 UT are computed for ionospheric conditions observed at U. I. They agree roughly with the measured values. but deviations from about -0.8 to +0.4 MHz occur during this time period. Further discussion of the consequences of such differences are discussed in Sections 3.5.1 and 3.5.2.

Using foF2 data from Ava and U. I. and comparing them with the MUF leads to a MUF factor (k sec ϕ) of 1.75 for the average during daytime and a distance of 1120 km.

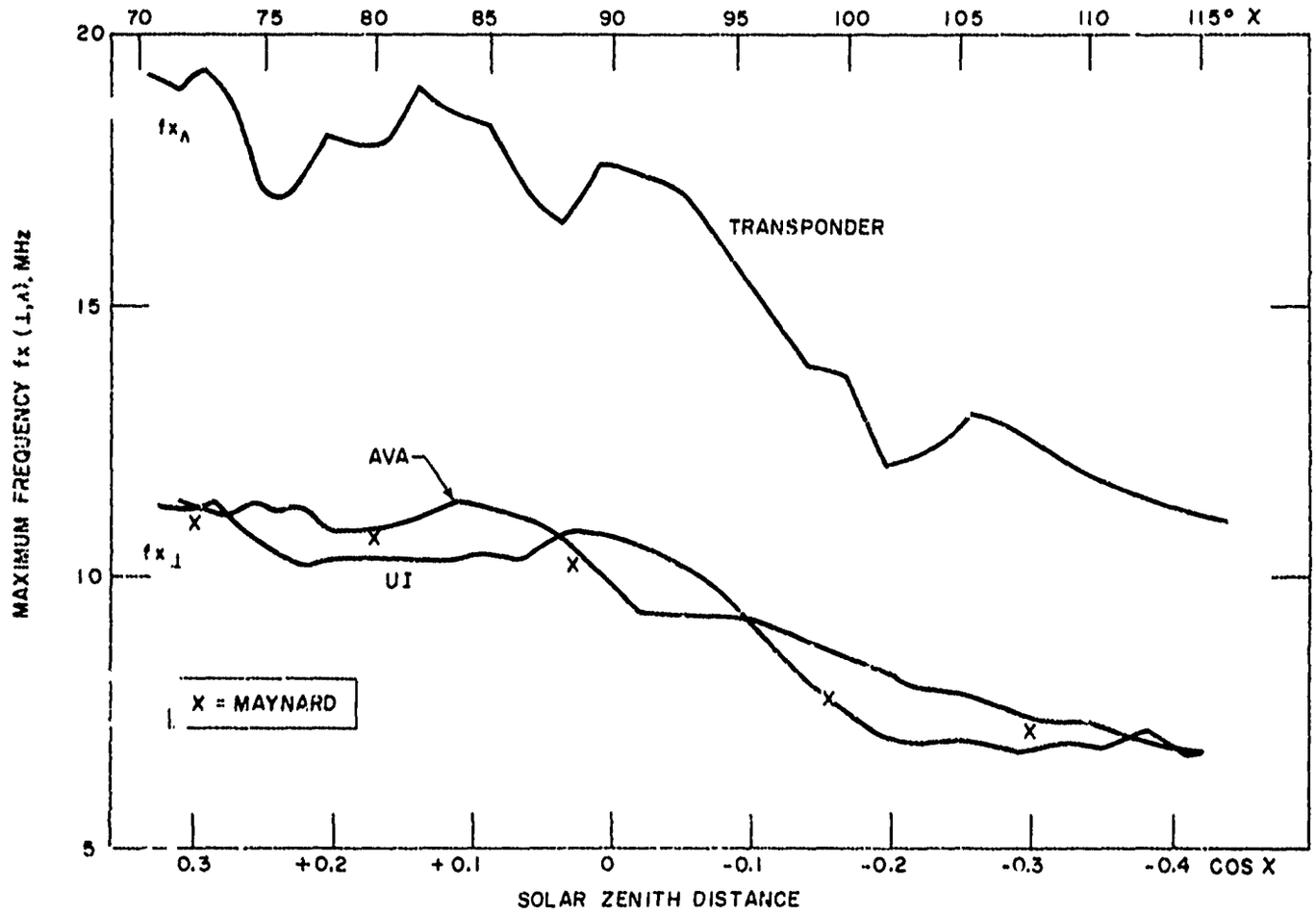

Figure 3-5 Observed Temporal Variations of fxF2 and fxF2 during Sunset Test Period.

Same data as in Figure 3.4 (except fx instead of fo) normalized for same solar zenith distance. Similar trend in all three curves, but local variations are obvious.

Since the test was performed looking west, there should be a horizontal gradient in the ionosphere during sunset and it is necessary to investigate the ionosphere for the same zenith distance χ. In Figure 3-5 the maximum frequencies $fxF2_{\perp}$ at Ava and U. I., and $fxF2_{\wedge}$ between Ava and U. I. are plotted as functions of cos χ instead of UT, which clearly indicate that the general trend of all three curves is similar, but local variations do not agree with those observed for $fxF2_{\wedge}$ (Ava-U. I.). The general decrease in electron density starts at all three locations at about cos χ = + 0.1, which is expected. The hourly data for Maynard, Mass. fit into the general trend.

Using the carefully scaled data and the overlay, we constructed oblique ionograms in the f-h' coordinate system using the forward oblique data from Ava to U. I., the transponder data (Ava-U. I. -Dexter), and the vertical ionograms from U. I. The ionograms from Ava could not be used, because the trace was not too well resolved (too thick) in time delay for lower frequencies. Data for about 31 zenith distances have been compared. The value of such an investigation is related to predictions. How useful are ionospheric data for one station or one path to predict the MUF (or leading edge) to other points along the path? We compare the data for the same zenith distance and express the results in MUF for an 1100 km path (Ava-U. I.). Let us mention just two cases. For cos χ = + 0.25 the observed MUF is 18.5 MHz for the transponder, 19.5 MHz for the oblique forward path; 18.5 MHz is computed using U. I. ionosonde data, but

about 19.9 MHz using Ava ionosonde data (the Ava ionosonde data uses an average MUF factor of 1.75). At $\cos\chi = +0.12$ the observed MUF is 18.5 MHz for the transponder, 19.5 MHz for the forward oblique path; and we derive 18.0 MHz using the U. L. ionosonde and about 20.0 MHz for the Ava ionosonde data.

The agreement between such data is, therefore, within about 1 MHz for an 1100 km path using simple graphical methods. Computer methods may improve the data, but, at present, we feel that there is no need for higher accuracies.

From the ionospheric data and the constructed oblique ionograms, we conclude:

a) Under quiet conditions the ionosphere undergoes regular quasi-periodic variations (maximum-to-maximum in foF2 or MUF) on a time scale of tens of minutes to 1 to 2 hours, with amplitudes (MHz) on the order of at least $\pm$ 5% around the hourly average value. That means variations of such amplitudes have to be considered in applying a measured foF2 value or a MUF from a transponder, if frequency predictions are made. Such variations go undetected in any regular ionospheric probing system (vertical or oblique) which scales more or less only one value per hour.

b) There exist horizontal gradients in electron density as a consequence of the variations just stated. One can also call them "clouds" with a scale size of about 100 to 500 km. Such clouds also go undetected in any ground based vertical incidence ionosonde network because stations are very far apart. This means that for MUF predictions (see section 3.5.4)one has to build in a certain "error", whether one uses the ESSA predictions or those based on ionograms at the transmitting site.

c) The pathloss during sunset should be measured more accurately. The signal strength from the transponder decreases around 1 UT, although the frequency is well above the threshold value. There are several reasons for this decrease, certainly absorption is not the cause. The ionosphere has tilts and the raypath must deviate from the "normal" path. Thus, the signal may be received at angles where the antenna gain is very low. This point needs further testing using calibration signals and digital processing.

3.3.2 Frequency Limits of Backscatter and Limit of Illuminated Ranges

From the backscatter records, we read the maximum frequency at which the leading edge of backscatter returns is seen and also the maximum and minimum time delay.

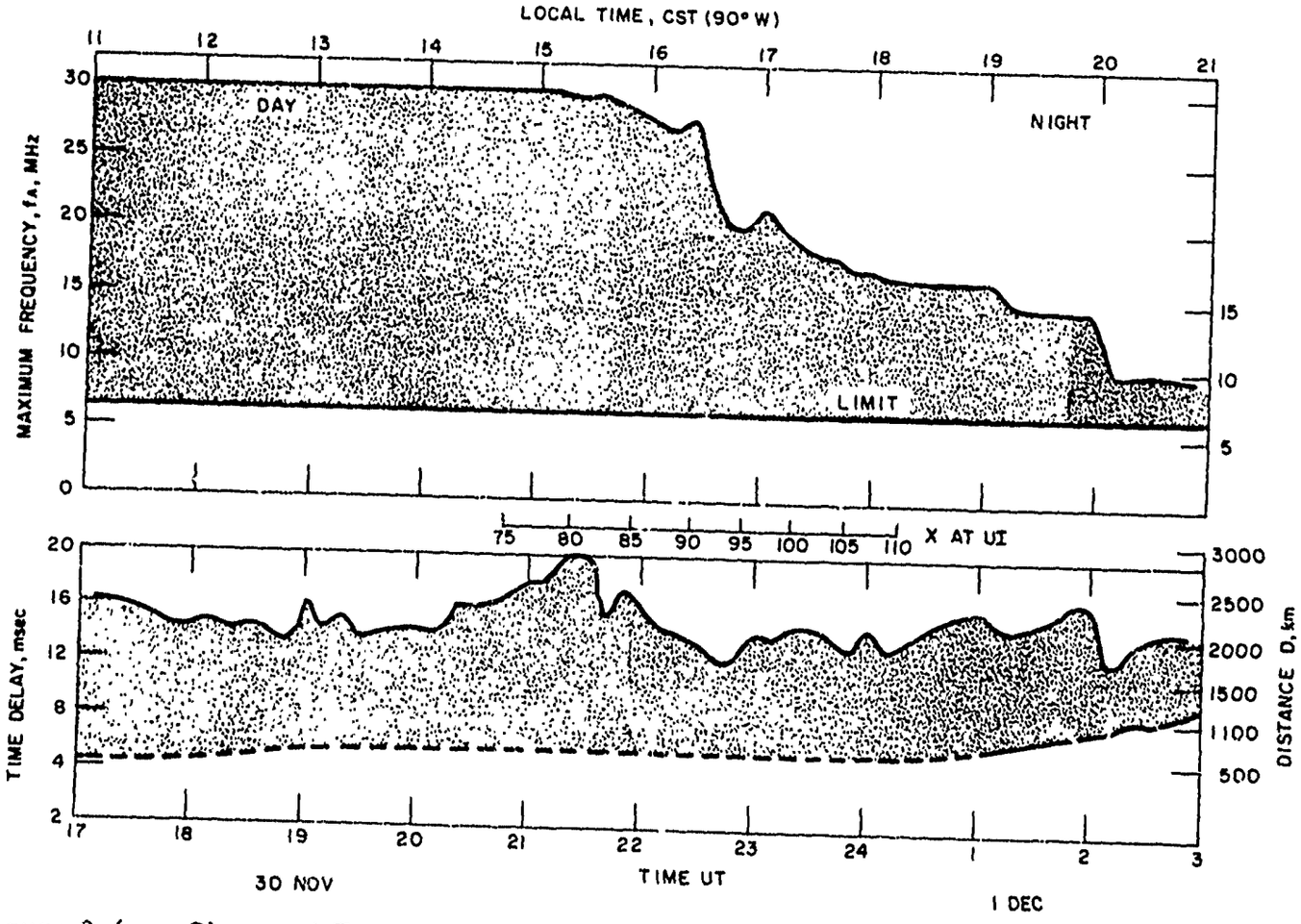

Figure 3-6 Observed Frequency and Time Delay Limits During Sunset Test Period.

The results are shown in Figure 3-6. The upper part shows the maximum observed frequency for the visible backscatter traces (leading edge). The lower figure shows the shortest and largest time delay (without regard to frequency) for a visible leading edge. The distance D in km on the right hand side indicates distances for corresponding time delays, assuming a layer height of h' = 300 km.

During daytime the upper frequency limit of the leading edge of backscatter is always $>$ 30 MHz and the corresponding time delay is about 14-16 msec. Thus, during daytime the whole frequency range from 6.5 to 30 MHz is useful. When the zenith distance of the sun reaches about 80° the maximum frequency of the leading edge begins to drop below 30 MHz and at such times the full time-delay range up to 20 msec is seen. As the sun sets over the path, the maximum time delay drops at first rapidly to about 16-17 MHz, but also the time delay range drops back to 12-15 msec, i.e., strong backscatter returns beyond D = 2000 km are not received. During the night, the maximum frequency drops to about 10 MHz, leaving a very small frequency range of only 6.5 MHz to 10 MHz for backscatter operation. At the same time, the time-delay window shrinks.

During daytime, the lower limit is about 4 msec and the upper limit 14-16 msec (at a frequency $f_\wedge$ of 30 MHz). During sunset, the maximum time delay reaches the 20 msec limit and drops later on to around 14-16 msec. The minimum time increases during the night from 6-9 msec, because the shorter distances are reached only by frequencies

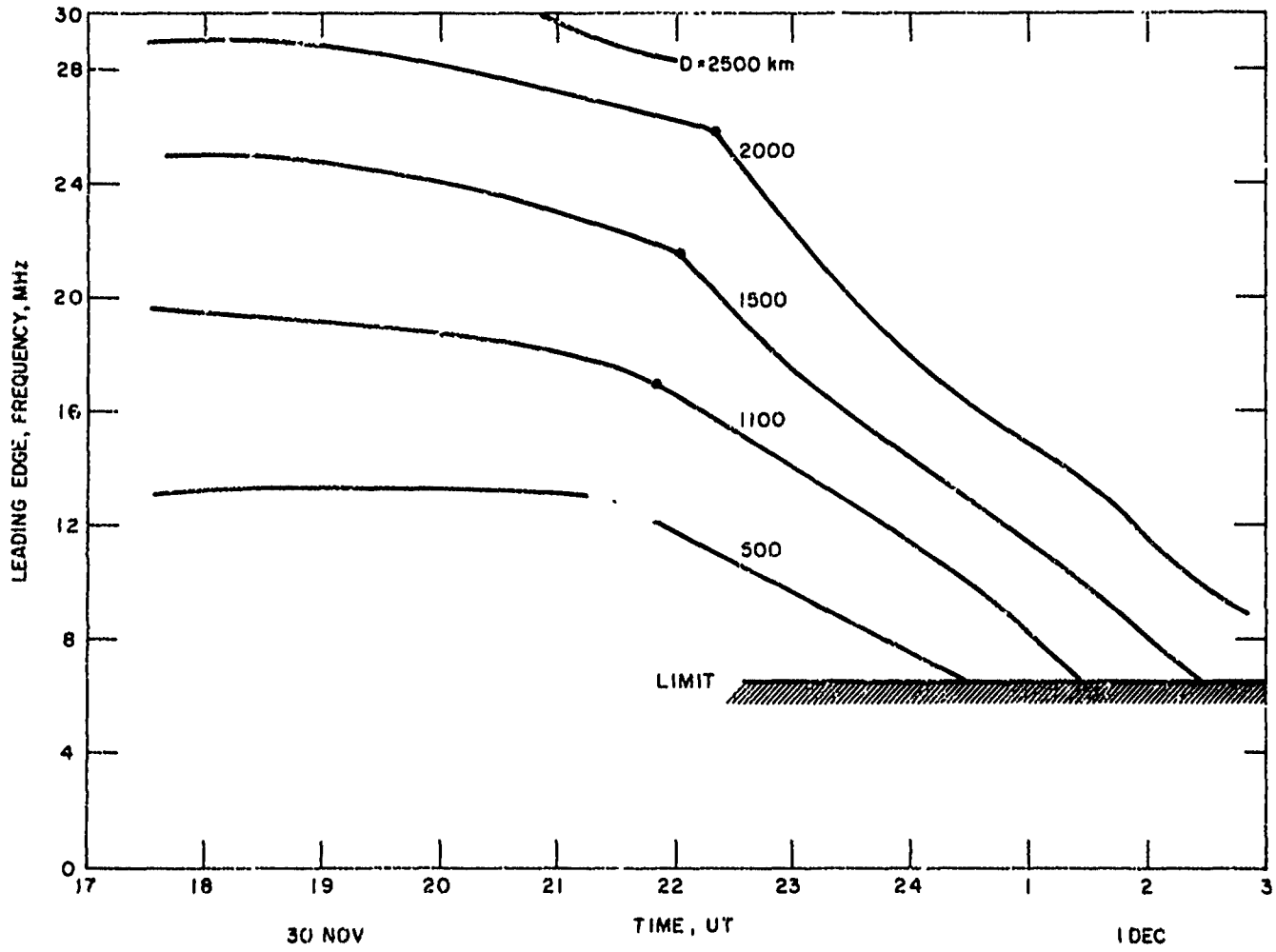

Figure 3-7 Frequency of Leading Edge for Selected Ground Ranges up to D = 2500 km During Sunset Test Period.

Data are smoothed. Due to lower frequency limit of 6.5 MHz, targets closer than specified ground range cannot be seen after 1 UT.

below 6.5 MHz. Thus, the time delay window shrinks at night to 9-12 msec for the leading edge, or a range window of about 1200 to 2000 km. Thus, at night, we have a small frequency band and a small range band for surveying. It seems necessary to have transmitters and receivers available to operate below 6.5 MHz; 3 MHz seems to us a necessary lower limit if we want to see closer in than 1200 km. If $f_{\perp}$ drops below 3 MHz, as in polar troughs, and also during nights in low sunspot years, the low frequencies are needed for OTH operations.

In Figure 3-7, we show in a schematic way the frequency of the leading edge for fixed ranges D = 500, 1100, 1500, and 2000 km. The range is based on an assumed reflection height h' = 300 km throughout this period. Since this assumption does not hold true for all ranges and all the time, we have averaged the measured points and show the results in more or less straight lines. There is a slight decrease in frequency $f_{\wedge}$ for the leading edge of the backscatter from daytime to the evening. At about sunset ($\chi = 90^{o}$) at the path midpoint, which is indicated for each distance by a dot, the frequency falls off rapidly with time. The 6.5 MHz limit for surveying, using the leading edge only, is reached for D = 500 km at about 1 UT, for D = 1100 km at 1.30 UT, and for D = 1500 km at 3 UT. Targets at smaller ranges cannot be detected after those times. This information clearly shows the range limitations that an OTH radar will experience at night if the operational lower frequency is set at 6.5 MHz. The present (1971) equipment at Dexter eliminates this constraint.

3.3.3 Gradients of Leading Edge of Backscatter

The backscatter records during sunrise or sunset show the gradient of the leading edge, $\Gamma = dp'/df_\wedge$, changes with time, i.e., with the frequency $f_\perp$ at the midpoint. At any given time, the gradient changes also with range, D, for constant $f_\perp$ and constant h'. The path length is p' and the frequency operating over this path is $f_\wedge$. The gradient is easy to measure and indicates if propagation behaves normally or not. This seems helpful in assessing predicted operating frequencies for narrowband surveillance.

A very simplified derivation for flat earth approximation indicates the expected relationship of $dp'/df_\wedge$ with range, D, and frequency, $f_\perp$, at midpoint.

It follows

$$f_\wedge = f_\perp \sec \phi$$

$$\sec \phi = p'/s$$

with s = distance for flat earth.

Thus, $$f_\wedge = f_\perp \frac{p'}{s}$$

For backscatter, the path length for the skip distance has to be doubled, leading to

$$f_\wedge = (f_\perp \, 2p')/s.$$

Differentiation yields

$$\frac{dp'}{df} = \frac{s}{2f_\perp}.$$

In a first approximation, $s = D$; but, for large distances, $s \neq D$, although this error is small. Other assumptions in the derivation are causing larger errors, for example, changes in the reflection height h'. Using better geometries, such as curved earth, leads to very awkward expressions, without gaining a better insight. In short, the gradient increases with D and inversely with $f_{\perp}$.

For the ideal case of a homogeneous and concentric ionosphere, we calculated the leading edge of backscatter (Figure 3-1) and determined the instantaneous gradient $\Gamma = dp'/df$ in units of km/MHz at the leading edge for a time delay corresponding to D = 500, 1000, 1500, and 2000 km and h' = 200, 250, 300, and 400 km. The values Γ are thus based on the true geometry and the results are given in Table III. 1. The relation $\Gamma = \text{const}/f_{\perp}$ for a fixed distance D and a constant height of reflection h' is quite strong, and it increases slightly with distance D for fixed $f_{\perp}$. The gradient is not really linear with distance D and approximations can be obtained, although we find them not too useful, such as

$$\Gamma = (1/f_{\perp})(ap'_5 + bD^{2.8})$$

where a and b are constants and p'_5 is p' for a distance of 500 km.

Turning now to the actual backscatter records, we determined Γ in two ways. First, we measured the instantaneous gradient at selected points of the leading edge. We choose fixed ranges D = 500 (500) 2500. It did not lead to useful data because small scale irregularities at the leading edge become magnified (too much noise), as shown in Figure 3-8.

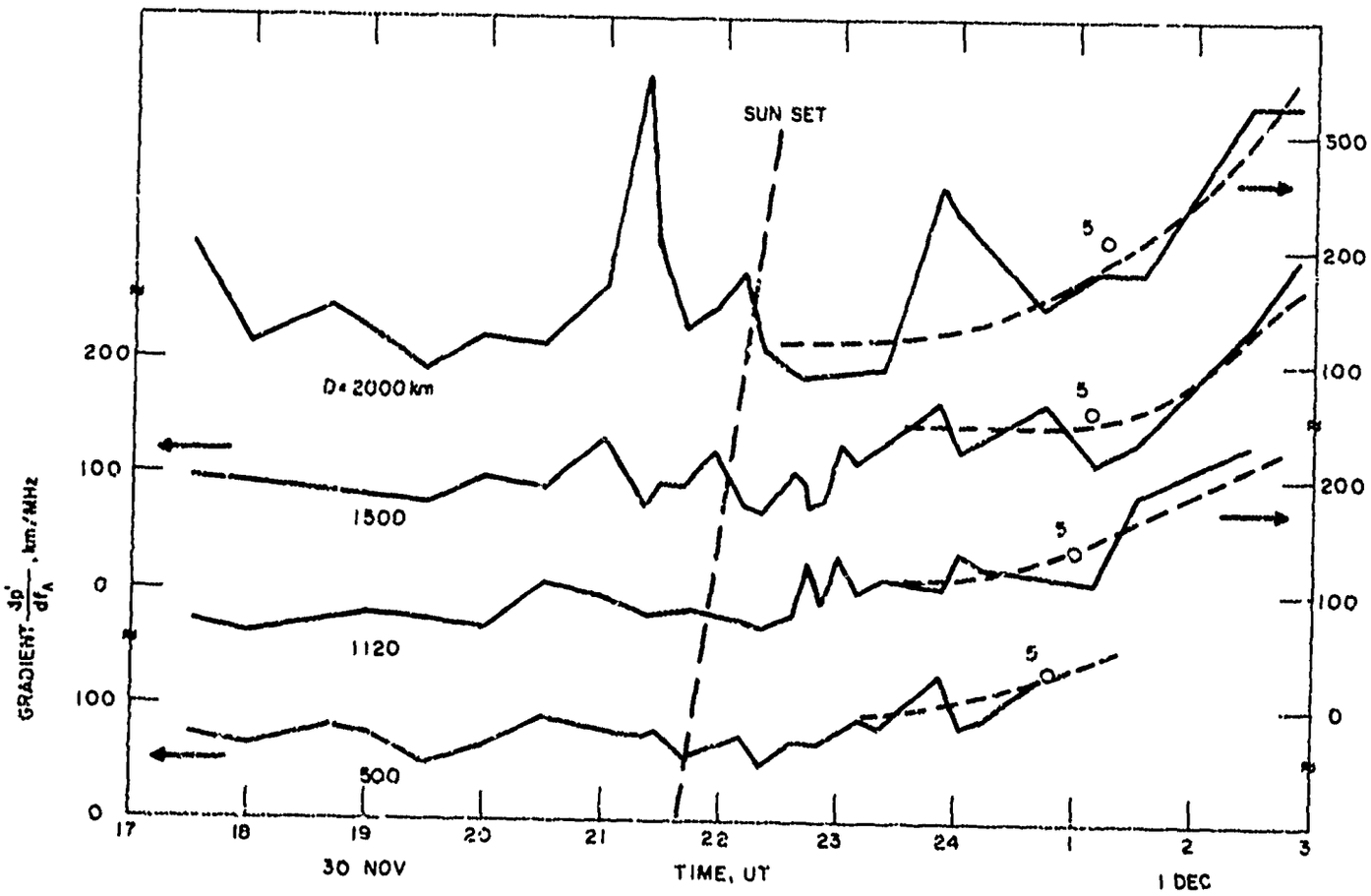

Figure 3-8 Observed Gradient $\Gamma = dp'/df_A$ for Selected Ground Ranges.

Ordinate Scale for each ground range alternate between right-hand and left-hand side. Dashed line indicates average and "circle 5" indicates theoretical value for $f_\perp$ = 5 MHz.

TABLE III. 1

Gradient Γ of Leading Edge of Backscatter for Selected $f_\perp$, h', and D. Theoretical Values Based on Uniform Ionosphere

	h' in km	D in km 500	1000	1500	2000
A) $f_\perp$ = 10 MHz					
	200	42	45	61	---
	250	55	60	72	100
	300	64	70	80	108
	400	82	90	101	120
B) $f_\perp$ = 5 MHz					
	200	87	107	136	193
	250	109	124	150	201
	300	130	135	169	211
	400	169	175	207	227
C) $f_\perp$ = 3 MHz					
	200	150	175	236	306
	250	175	198	248	325
	300	206	225	274	345
	400	289	306	323	393

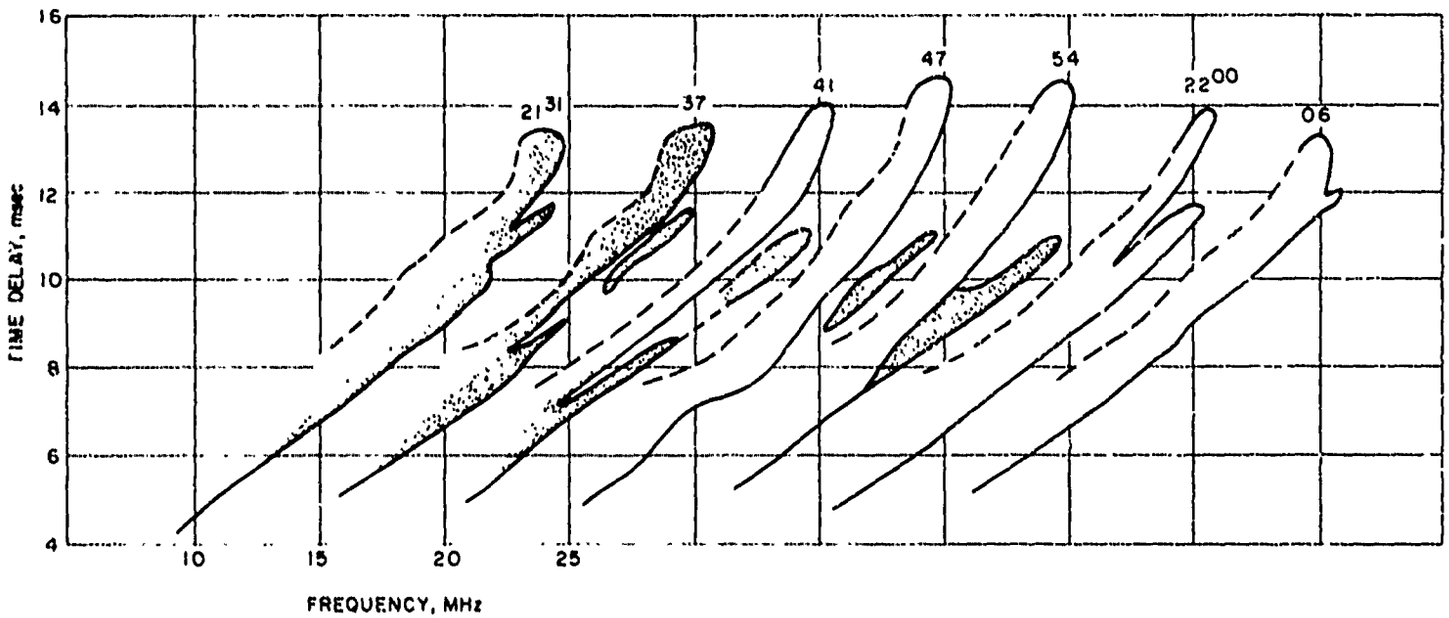

Figure 3-9 Backscatter Ionograms Between 2131 and 2206 UT.

Leading Edges and darkest areas have been copied from original. Each ionogram has been displaced by 5 MHz. Note appearance of two distinct traces.

The order of magnitude of Γ, however, is correct and compares with Table III-1

The second approach uses an average Γ for a time delay range of several msec. This leads to representative values for such a range because small scale modulations are disregarded. The reason for this approach is seen in Table III-1, where for $f_{\perp} > 5$ MHz, Γ increases only by 25 to 35%, while D increases from 500 to 1500 km.

We checked this approach with data for the time period from 2131 to 2206 UT. At this time, $f_{\perp}$ is about 10 MHz and irregularities in the leading edge appear (Figure 3-9). One leading edge prevails, but a second one with larger time delay appears during this period. The explanation is a change in the horizontal gradient of electron density in the direction of propagation (see section 3.5.2). Table III-2 lists the results of our evaluation.

TABLE III-2

Observed Gradients $\Gamma = dp'/df_{\wedge}$ in km/MHz for the Time Period 2130-2206 UT. Backscatter Received at Dexter, N. Y.

Time Delay Range $\Delta\tau$ in msec

Time UT	First Trace				Second Trace			
	$\Delta\tau$	Γ	$\Delta\tau$	Γ'	$\Delta\tau$	Γ	$\Delta\tau$	Γ
2130	4-10		10.5-11.75	71			11-13	105
2137	6.5-12	71			8.5-11	71	11-13	105
2141	5-7	71	7-11	63	7-11	71	12-14	230
2147	5-7	71	7.5-11	69	8-12	105	12-14	230
2159	5-7	71	7-11	61	10-13	105	12-14	230
2200	6-11	71			10.5-13	105		
2200	5-12	71						

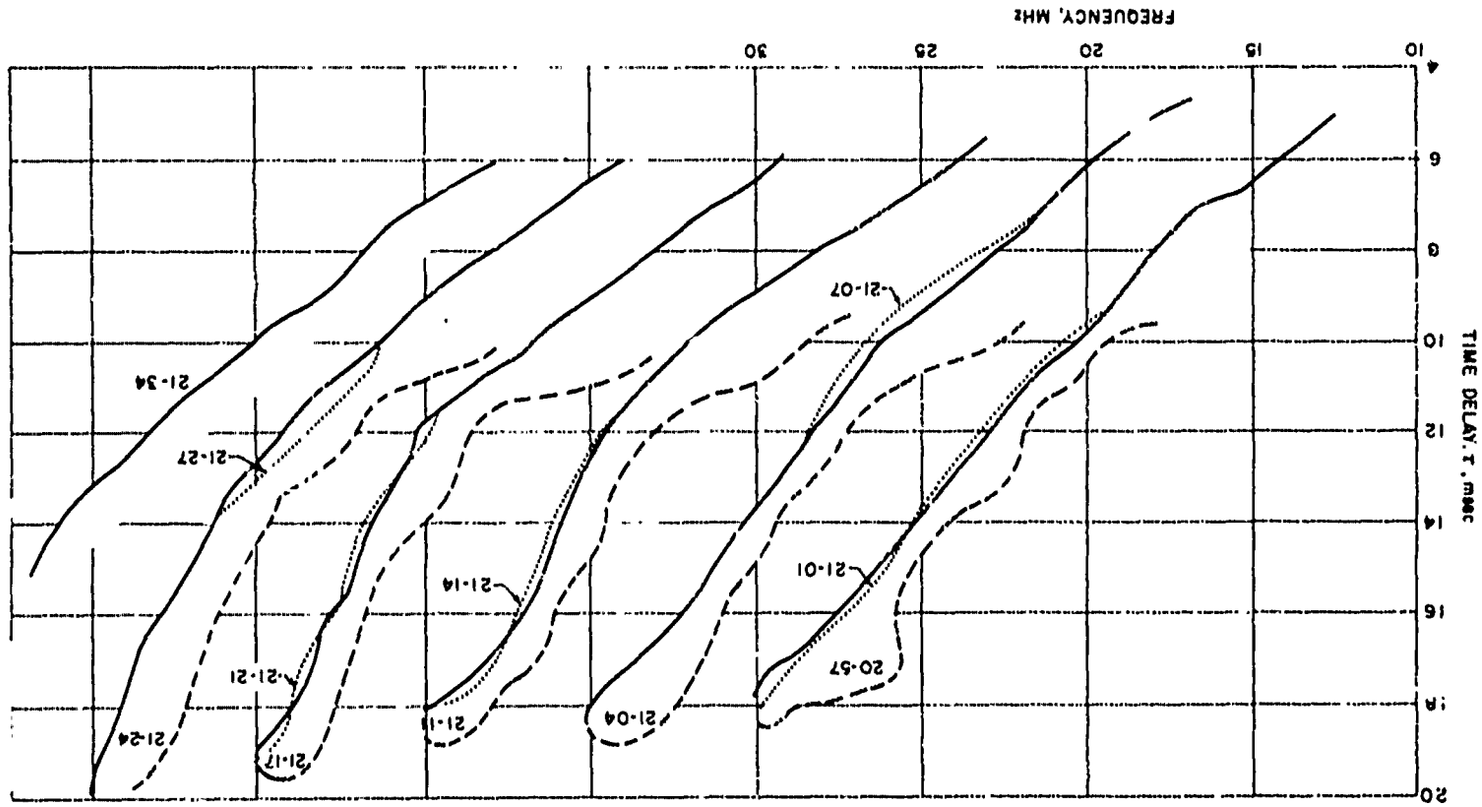

Figure 3-10 Backscatter Ionograms Between 2057 and 2134 UT.

Same basic system as in Figure 3.9. Note irregularities in gradient of leading edge after 2111 UT.

The first leading edge has a gradient of Γ = 71 km/MHz, extending to at least 7, but sometimes out to 12 msec. The second leading edge has a similar Γ at the beginning of the time period, and could be a mixed mode, but from 2147 UT on the gradient is larger, 105 km/MHz. The top beyond 11 or 12 msec has a fairly larger gradient of about 230 km/MHz.

Another case is that for the period 2057 to 2134 UT just before sunset over the path. Figure 3-10 shows the backscatter received at Dexter. The leading edge is indicated by a heavy line, the upper end of the "dark" trace by a dashed line. It seems best to ignore the small undulations in the leading edge and approximate the leading edge by as few straight lines as possible, 2 or 3 segments are sufficient. Table 3.3 shows the interpretation of the data. The leading edge with a gradient of about 80 km/MHz extends first out to 6-7 msec, later to 10-11.7 msec. Such a gradient corresponds to a $f_\perp$ of just under 10 MHz assuming a height h' = 300 km, similar to the case above. For the longer time delays of 10-20 msec (D > 1500 km), the gradient starts with 120 km/MHz and increases to 220 km/MHz at the end of the period, corresponding to $f_\perp$ of 8-9 MHz. The time delay at which the break between these gradients occurs increases from 6 to 11 msec during this period. A very strong irregularity occurs at 2111 and 2114 UT, but it lasts perhaps only 10 min. During such a time, no reliable $f_\perp$ can be determined.

TABLE III-3

Average Gradients at the Leading Edge
Backscatter Received at Dexter, New York
Γ in km/MHz; Time Delay Range $\Delta\tau$ in msec

Time, UT	$\Delta\tau$	Γ	$\Delta\tau$	Γ	$\Delta\tau$	Γ	$\Delta\tau$	Γ
20.57	4-6	78			7-18	121		
21.01	4-6.7	78	7-14	120	15-18	121		
.04	4-10.0	90			10-18	145		
.07	4-10.3	78	10.3-13	243	13-18	145		
.11	4-10.4	78	10.4-12	127	12-15.5	265	16-18	110
.14	4-10.4	78	10.4-12	110	12-16.5	265	16.5-18	< 100
.17	4-11.7	78			11.7-19	220		
.21	4-11.5	78	11.5-14	150	14-19	280		
.24	4-10.4	78	10-13.2	110	13.2-20	220		
.27	4-10.0	78	10.14	110	14.20	220		
.34	4-11	90	11-13	110	13-15	220		

The conclusion we can draw here is that the gradients $\Gamma = dp'/df_{\wedge}$ can be used to infer the ionospheric gross structure along the path. If the gradient of the leading edge is more or less smooth, it corresponds to $f_{\perp}$ at the midpoint. Thus, the gradient Γ permits an estimate of $f_{\perp}$ to the nearest integer values assuming reasonable values for h' by using Table III-1. Small irregularities in the leading edge should be disregarded. There are often "breaks" in the gradient, but two or three linear segments are sufficient to determine Γ over the whole range of time delays. The method should be tested on a larger sample during daytime or nighttime. Sunset is not the most appropriate time because large horizontal gradients occur in the ionosphere. Irregularities are found during sunset, but their duration is of the order of 10 min. Explanations of such irregularities will be discussed in Section 3.5.2.

3.3.4 Samples of Backscatter Records

Backscatter records obtained with the FM/CW waveform and the RADC equipment have been published including mode identification. Therefore, no extensive reproduction of samples are given here. Just for illustrative purposes, samples are selected and reproduced in Figures 3-11 and 3-13. In this type of recording, the frequency increases from right to left, starting at 6.5 MHz and ending at 30 MHz. The vertical lines are frequency markers, 1 MHz apart. The horizontal lines are time-delay markers, 2 msec apart. They give relative time delay; the determination of converting them into absolute time delay is discussed in Appendix A. The ordinate in Figures 3-11 to 3-13 shows absolute time.

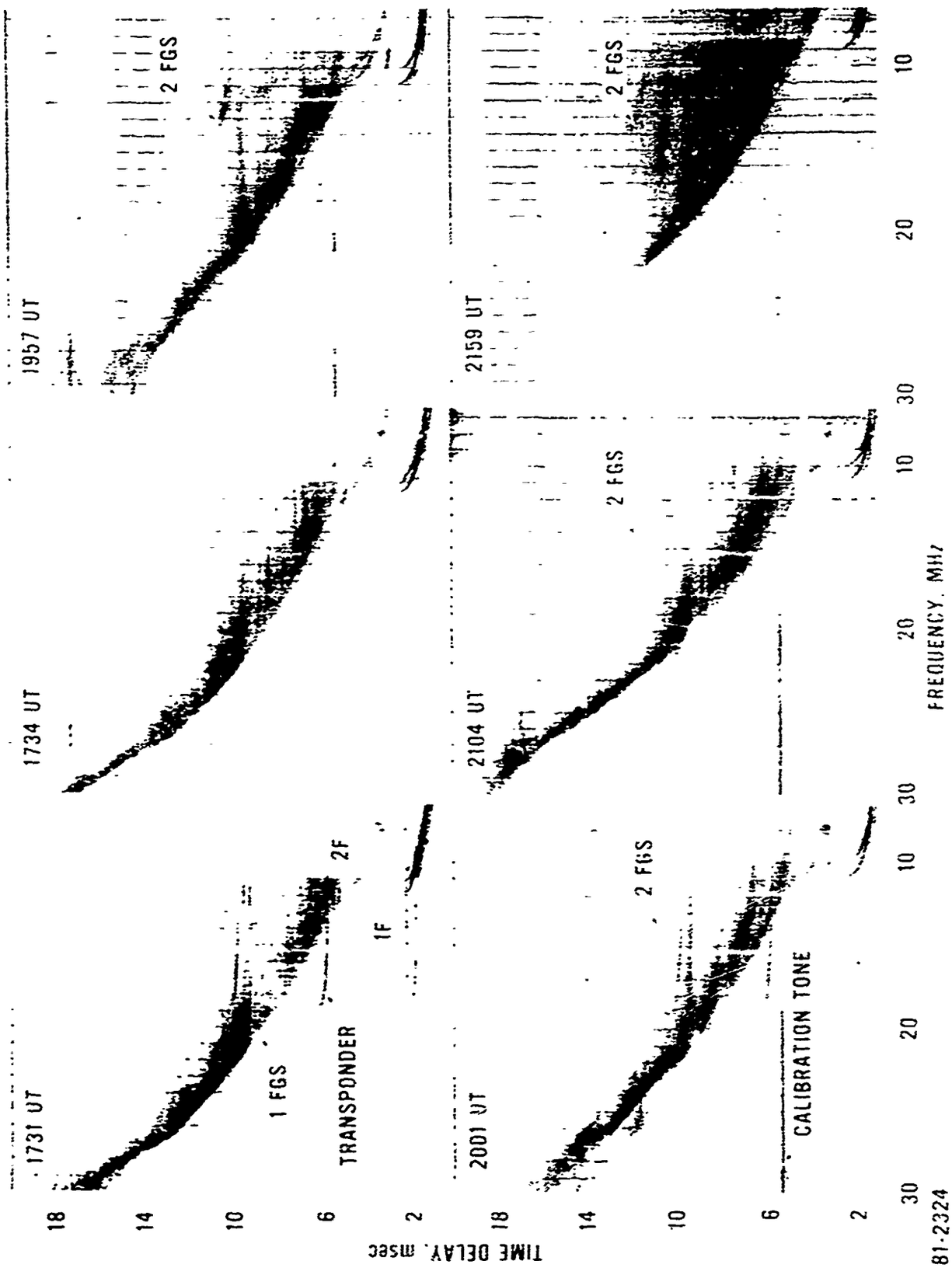

Figure 3-11 Samples of Original Backscatter Ionograms for 30 November 1970.

The selection of samples is somewhat arbitrary. Figure 3-11 contains the conditions before sunset over the path, while Figure 3-12 represents those at and after sunset. On two samples (1731 and 2001 UT) the transponder traces appear. The transponder is offset by 2 msec. so that the signal falls outside the leading edge for better visibility and scaling. The repetitive traces are caused by harmonics in the transponder modulation waveform. For a large number of backscatter records, sketches have been prepared which helped in the analysis but which are not reproduced here. No study of unusual modes or ground targets is made.

For daytime one can see the general character of backscatter. The width (in time delay) of the strong backscatter signal changes a bit from one frame to the next; at some time delays (for example, τ = 14 msec), the backscatter extends over a large frequency range, indicating backscatter from special ground targets. The leading edge has, at times, a "weak" precursor, with a time delay difference of 0.6 to 0.7 msec between the weak and solid leading edge. Since this time delay difference extends over a large frequency range up to 30 MHz, it cannot be caused by different basic modes; both returns must be 1F modes, but the path length is about 100 km different over a wide range of frequencies and time delays are probably caused by minor tilts or blobs of ionization acting as a type of "beamsplitter".

Later at night the samples in Figure 3-12 show the strong backscatter is limited to a small frequency range and the gradient of the leading edge becomes steeper as a consequence of the reduction of $f_{\perp}$.

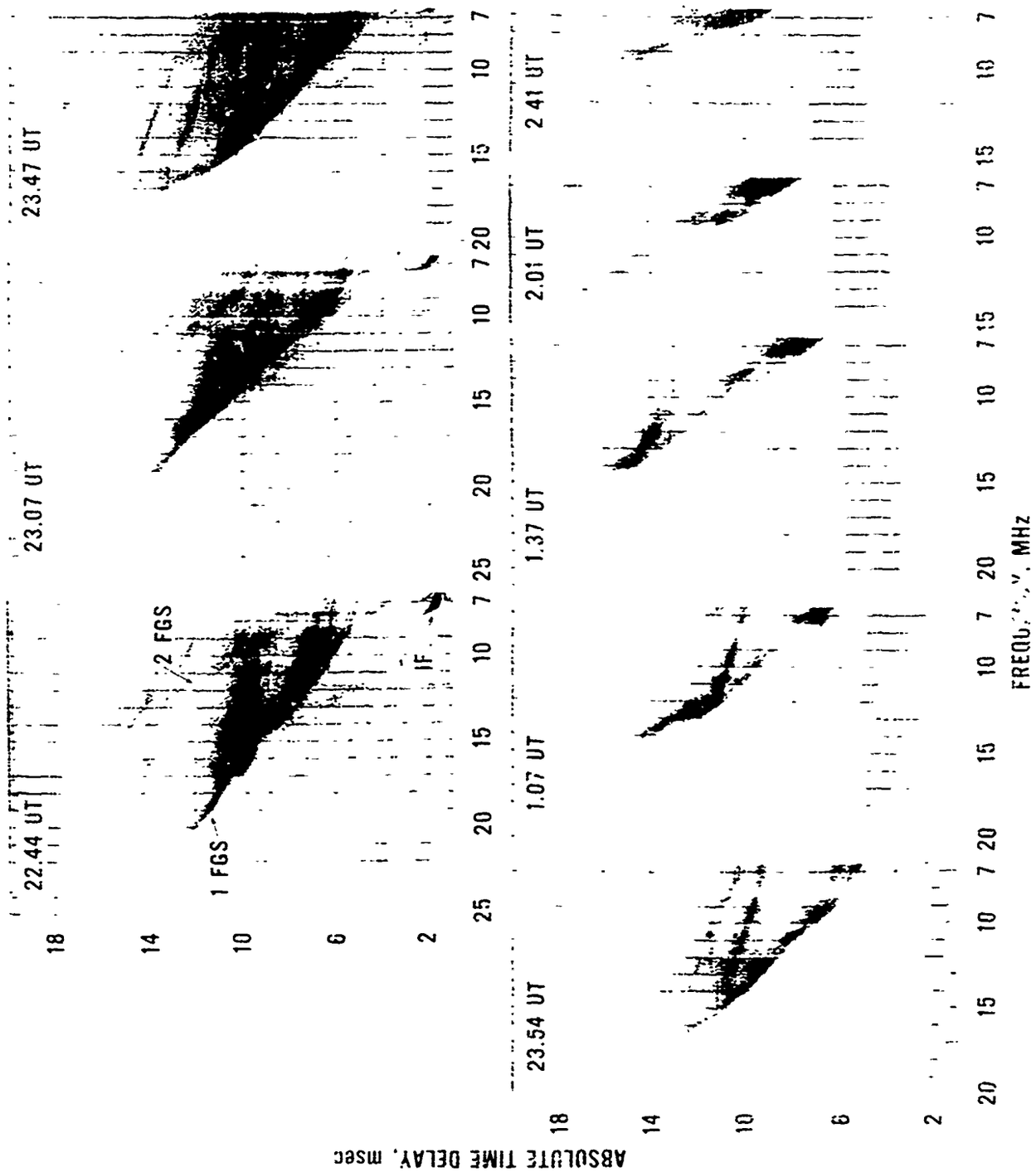

Figure 3-12 Samples of Original Backscatter Ionograms for 30 November/ 1 December 1970.

Conditions after sunset over path.

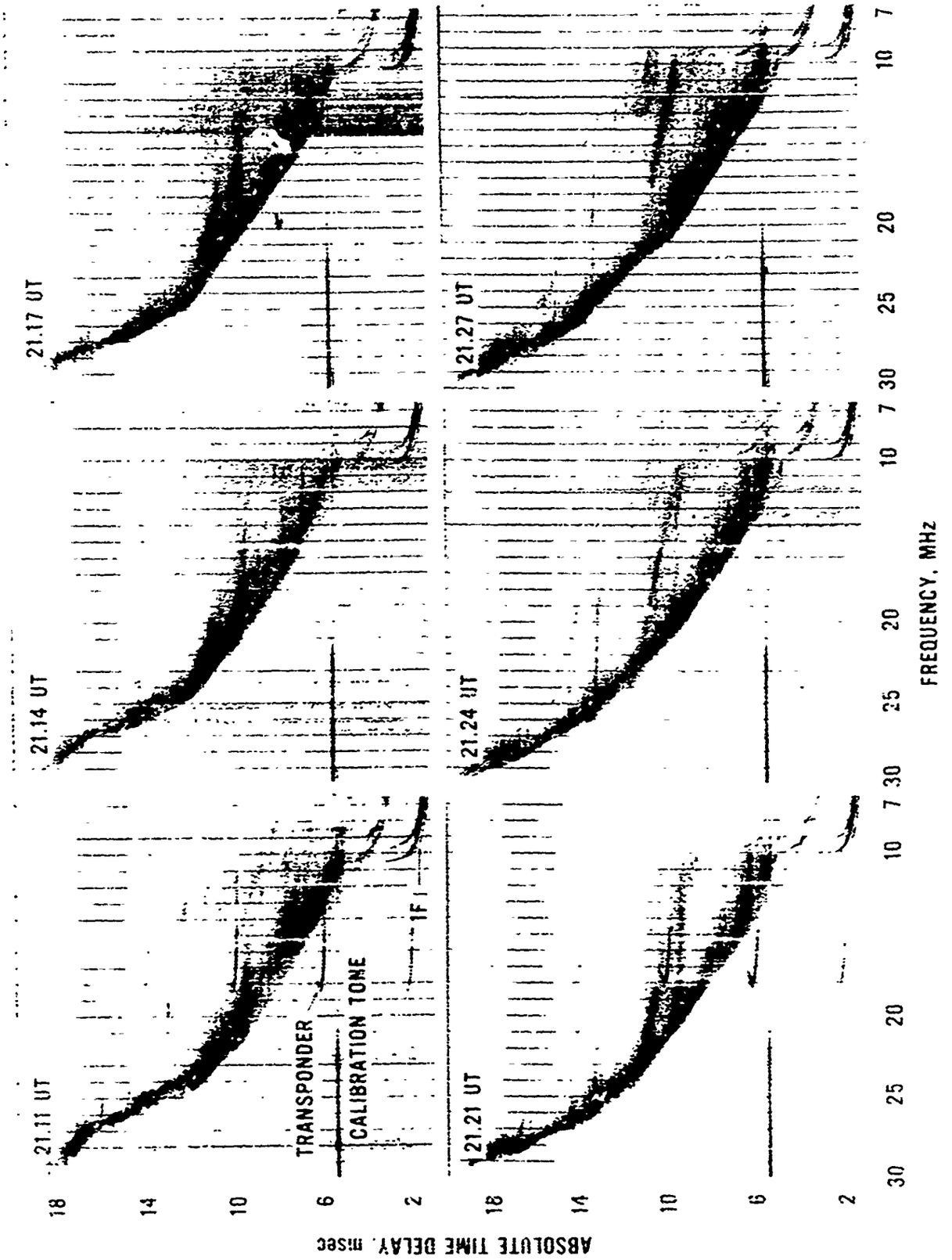

Figure 3-13 Samples of Original Backscatter Ionograms 30 November 1970.

Compare with tracings shown in Figure 3-10.

Figure 3-13 covers part of the period shown in Figure 3-10; the unusual gradient beyond 12 msec. The tracings can be compared with the series of original backscatter records.

3.3.5 Transponder Visibility

All transponder traces have been copied for the evaluation reported in Section 3.1. During daytime from 1711 to 2031 UT (1531 EST) one always sees an E mode, and a mixed mode (E + F) up to 2011 UT in addition to the usual F mode (see original for 1731 UT in Figure 3-11).

The nose and the splitting of the trace in fo and fx is often clearly observed. The high-angle ray is rarely seen at daytime, except at 1831 and 2001 UT. It becomes, however, a regular feature after sunset over the path and the high-angle ray has enough signal strength to be recorded from 2101 to 0001 UT (see samples in Figure 3-13). From 0031 UT, the signal from the transponder becomes very weak and is at times not recorded, although the maximum frequency of the transponder signal is well above the limit of 6.5 MHz. This weakening of the signal may be caused by the arrival angles at this time, and an investigation of the antenna pattern and some ray tracing could shed some light on this problem.

3.4 SUNRISE TEST

3.4.1 Ionospheric Variations During Test Period

During the sunrise test period on 2 December 1970 from 10 to 15 UT (5 to 10 EST) the ionosonde at U. I. did not operate. Therefore, we have no data for the ionospheric structure below 6.5 MHz over the illuminated path. However, the hourly values for Maynard, Mass., about 200 mi (320 km) west of Ava, N. Y. are available (Geophysics and Space Data Bulletin) and are very useful, because they list foF2, foE, MUF (3000)F2, and other ionospheric parameters. The ionosonde data of the preceding day, 1 December, for U. I. are also available, but are useful only as a general guide. Figure 3-14 shows fxF2 data from Ava received at Dexter; the lower limit is 6.5 MHz and, therefore, no data before 1221 UT are available. The hourly foF2 data for Maynard at 13 and 15 UT agree, more or less, with the Ava data. Half-hourly data from U. I. for the previous day also agree with the Ava data except after 1330 UT, where they remain below the Ava data. The increase in foF2 starts at $\chi \approx 100^{\circ}$ which is normal.

There are undulations in the foF2 data for Ava with a period of about one hour and amplitudes of $\pm$ 6%; similar results have been mentioned in Section 3.1 for the sunset test period.

The electron density in the E layer is large enough to be recorded at Maynard after 13 UT (8 EST) with foE = 2.4 MHz at 13 UT and 2.9 MHz at 15 UT. Thus we can estimate E modes to exist during some hours.

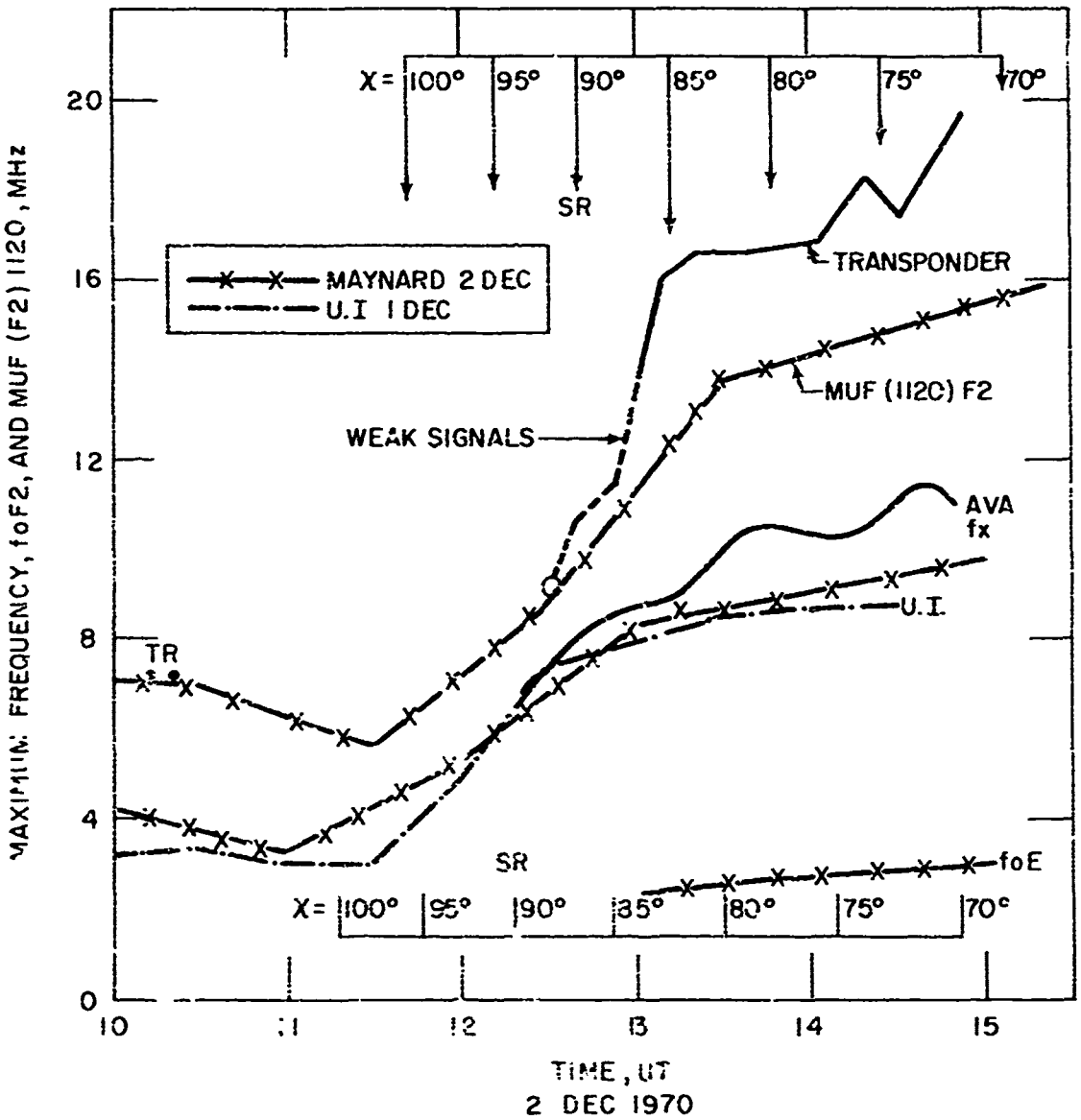

Figure 3-14 Observed Temporal Variations of Ionospheric Parameters During Sunrise Test Period.

Solid lines are fxF2 for Ava and transponder at University of Illinois (U. I.) received at Dexter. Maynard based on hourly fxF2; fxF2 from U. I. from previous day. MUF (1120) F2 computed from Maynard data and shifted by 30 min. Solar zenith angle χ for Ava at bottom, for midpoint at top. SR = ground sunrise.

The transponder returns have been scaled and are very clear after 13 UT, but very weak before. There are some questionable transponder traces of 7.2 MHz at 1011 and 1021 UT. As we will discuss below, they can be real. No transponder returns are recorded between 1021 and 1231 UT. At 1231 UT, a trace between 8-9 MHz appears at the correct time delay which seems to be the reappearance of the transponder, but it is a weak signal. At 1241 and 1251 UT, the weak transponder signal is noted with maximum frequencies of 10.5 and 11.5 MHz, respectively. The nose frequency of the transponder, shown in Figure 3-14, rises rapidly until 1311 UT and the weak signals fit into this rise very well.

Using the Maynard foF2 and MUF (3000)F2 data, MUF (zero)F2 can be determined and using the old ESSA prediction method (Davies, 1965, p. 289) MUF (1120)F2 is determined. Since sunrise over the midpoint Ava-U.I. is about 35 min later than over Maynard, we have plotted the MUF (1120)F2 values based on Maynard's ionosonde data shifted by 30 min. It is seen that between 1000 and 1045 UT this MUF is above 6.5 MHz; therefore, the weak transponder signals at 1011 and 1021 UT are possibly real and at the right frequency. There should be no transponder signal between about 1045 and 1145 UT because it would have a maximum frequency below 6.5 MHz. At 1230 UT, the first observed weak transponder signal at 9 MHz agrees with the MUF computed from Maynard's ionosonde data. The fast rise of the observed MUF is steeper than the one computed from Maynard. However, the identification of the weak transponder signals is

now verified using the Maynard data. The steep rise corresponds to χ = 95 to 85°. The Maynard scalings give a MUF (1120)F2 factor of 1.50 (1.45 to 1.52), while the Ava ionosonde and U. I. transponder data give a MUF factor of 1.65, about 10% higher than Maynard after sunrise. Thus, the actual transponder data lead to a better estimate of the actual ionospheric conditions over the path than the vertical incidence ionograms. If improvements of MUF transmission curves should be made, those suggested by Kobayashi (1962) could be tested.

There are several important conclusions to be drawn:

a) The vertical ionogram of the transmitter site or even east of the transmitter site is useful in estimating the leading edge for west-looking backscatter radars during sunrise.

b) Such measurements may be needed because frequencies for transponders can be below lowest operating frequency for the late night or before dawn periods.

c) The transponder was not seen before sunrise, because the ionospheric conditions did not permit propagation at frequencies above 6.5 MHz for that distance.

d) The transponder signals are very weak around sunrise, at least until about 87°.

e) The frequency change during the sunrise period is very rapid. For a distance of 1100 km, the frequency of the leading edge rose from 6.5 to 16 MHz in about one hour. Hence, frequency selection and frequency switching becomes very important.

3.4.2 Frequency Limits of Backscatter and Limits of Illuminated Ranges

From the backscatter records, we read the maximum frequency at which the leading edge of backscatter return is seen and also the maximum and minimum time delay, similarly to that discussed in Section 3.2 for the sunset test period. The backscatter records are more complicated during sunrise than during sunset and some explanations will be proposed in Section 3.5.3.

The frequency and time delay limits are shown in Figure 3-15 and the most obvious fact is that very weak backscatter records are obtained between 1124 UT and 1157 UT. Using the Maynard data for 11 UT, the maximum frequencies are 5.2 MHz at 1000 km, 6.6 MHz at 1500 km, 8.0 MHz at 2000 km, 9.0 MHz at 2500 km, and 11.0 MHz at 3000 km. Thus, up to a range of 1500 km, no backscatter signal could have been received with the equipment, because of its lower frequency limit (6.5 MHz). That only weak returns have been recorded from 1700-2100 km indicates that either the ground-backscatter signal was weak due to defocusing effects or that the antenna pattern for rays at those frequencies arriving from ranges beyond 1600 km was possibly unfavorable, i.e., the rays arrived at the nulls in the pattern.

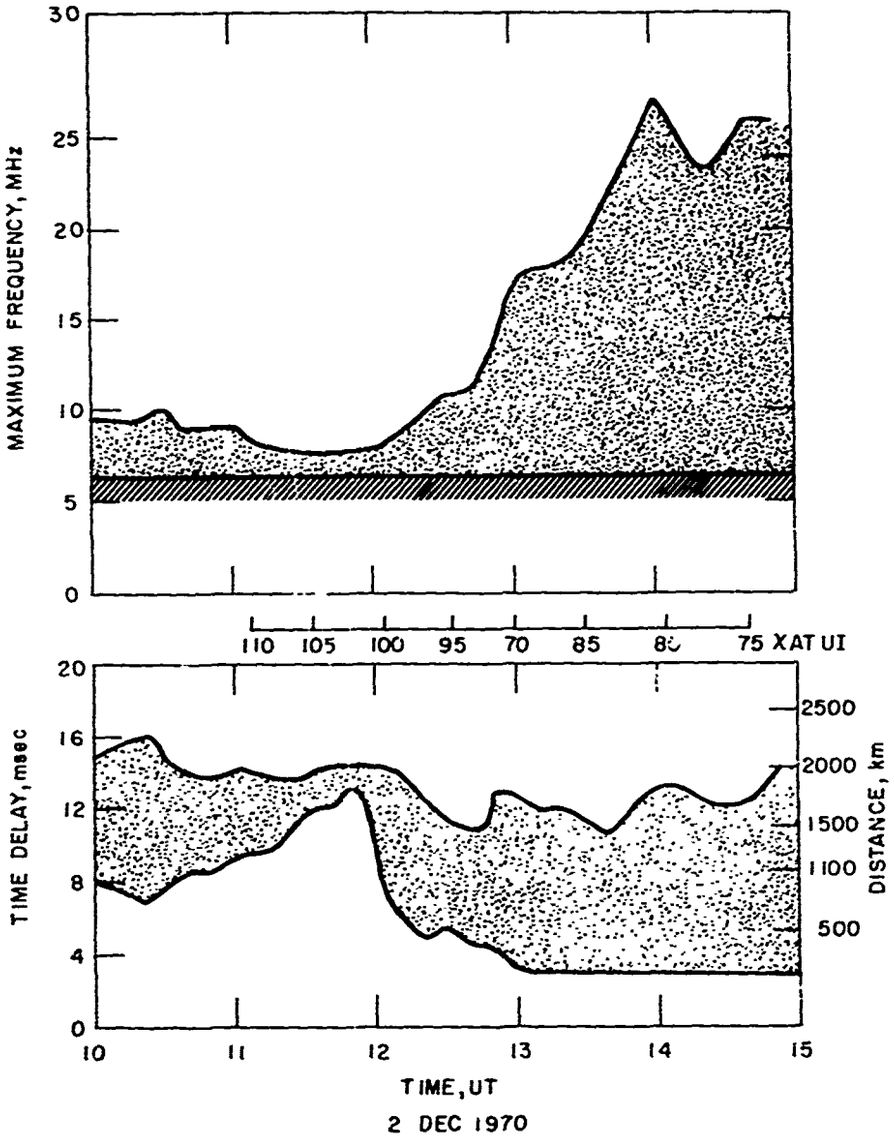

Figure 3-15 Observed Frequency and Time Delay Limits During Sunrise Test Period.

Solar zenith distance χ at U. I. Usable frequencies increase rapidly when $\chi < 100^{\circ}$.

The maximum frequency of the leading edge at night is 9-10 MHz, dropping to about 7.5 MHz before sunrise. Due to the low signal strength the top frequency can be given only to the nearest 0.5 MHz. From 12-14 UT, the leading edge rises rapidly from 7.5 to $>$ 25 MHz at a rate of 9 MHz/h. Thus, for a two-hour period, large frequency changes seem to be required for surveillance.

The time delay range of strong backscatter returns is, in general, good. At night we have a lower limit of about 8 msec increasing to nearly 10 msec which means that no ground backscatter from ranges less than 1000 km is received. The upper limit is 14-16 msec, or about 2000 km. During the weak signal period from 11 to 12 UT, the lower limit rises to 12-13 msec ($D \approx 1750$ km) while the upper limit stays around 14-15 msec. When the signals begin to come in strong again, at 12 UT, the lower limit decreases from 7 to 3 msec and the upper limit is at about 12-14 msec, varying due to the unusual structure of the backscatter. But, in general, no ground backscatter from 2000 km with strong signals is received for this type of processing. Digital processing has not been done, but can be accomplished if warranted from the original tapes.

Of great interest are the questions: What frequencies illuminate a given range? Are the frequencies fairly constant over a time period of an hour? How fast should you change frequencies to illuminate a given range?

Scaling the frequency of the leading edge at fixed distances D is shown in Figure 3-16. The scaling is done every 10 minutes, which is probably sufficient to obtain the general trend. To convert time delay τ into range D, a fixed reflection height of h' = 300 km is assumed. (We also read data for h' = 250 km, but since the results differ very little for both assumptions, only those for h' = 300 km are shown and discussed.) During the late night hours, backscatter from a range D = 1500 km is always present in the frequency range 7-8 MHz, slightly decreasing in frequency with time and disappearing after 1111 UT. The range D = 1100 km is seen only at the beginning of the test period and at 1051 UT; at other times no backscatter from this range is received. The 2000 km range appears with strong backscatter early in the test period and at 1107 UT. Using the Maynard data(section 3.4.1)we find the frequency of the leading edge at about 1030 UT for D = 1500 km is 8.6 MHz, for D = 2000 km it is 11 MHz. The actually observed frequencies are lower. The Maynard data are indicated by circles on Figure 3-16 where M2 means computed leading edge for D = 2000 km.

Only weak backscatter is seen from 1111 to 1211 UT, as stated above, which corresponds to ground ranges of greater than 1650 km to about 2100 km. Using Maynard data for 1100 UT and moving the data by 30 min, the frequencies are 6.6 MHz and 8.0 MHz for D = 1500 and 2000 km, respectively. The agreement with the observations is good, because the backscatter from 1500 km is so close to the equipment limit, that a

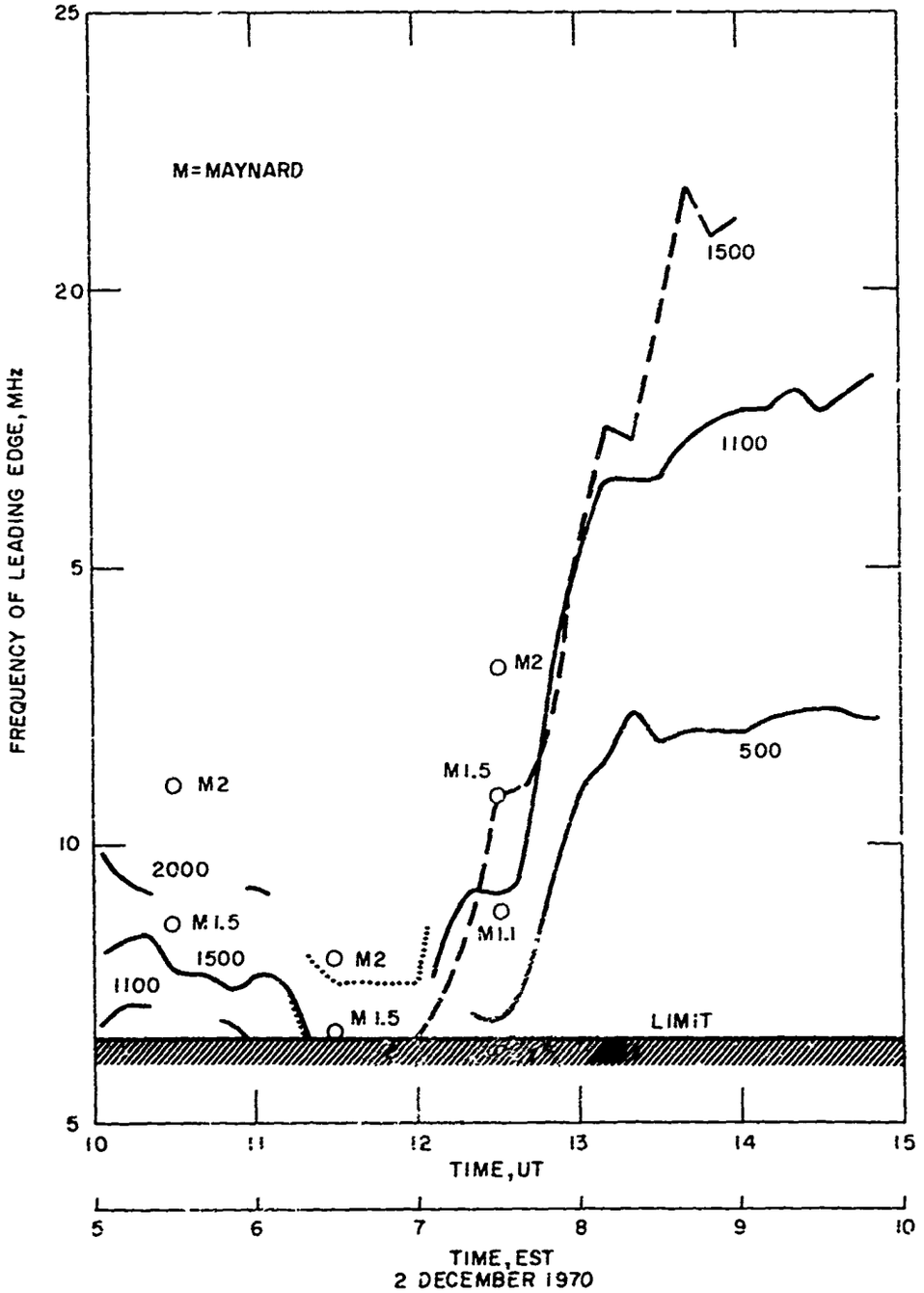

Figure 3-16 Frequency of Leading Edge for Selected Ground Ranges During Sunrise Test Period.

Circles mean leading edge computed from Maynard data, M2 means leading edge for D = 2000 km.

slight change is only needed to make it impossible to record the leading edge of ground backscatter. The backscatter from a range D = 2000 km (dotted line) agrees with the Maynard data. For this range, it has been very weak for the hour before and some defocusing must have taken place. A more sophisticated computation may also lead to a slightly lower MUF value.

At 1211 UT ground backscatter is coming back at the 1100 km range, and shortly thereafter also at 500 and 1500 km ranges. The frequency of the leading edge for these three selected ranges increases very rapidly at a rate of 5 MHz/h for D = 500 km, 8 MHz/h for D = 1100 and 1500 km. This rapid increase ("sunrise effects") lasts for about one hour. At 1230 UT, the Maynard data leads to 8.8 MHz, 10.9 MHz, and 13.2 MHz for D = 1100, 1500, and 2000 km. respectively. The agreement between actual observation of the leading edge and computations using Maynard data is very good.

3.4.3 Gradient of Leading Edge of Backscatter

For the sunrise test period, we measured the average gradient of the leading edge of backscatter every 10 minutes. In Section 3.3, it was shown that an average gradient Γ is most expedient. Again, a division of the full trace into two segments is sufficient; however, at some times, the backscatter is very complicated as our tracings in Figure 3-17 and 3-18 demonstrate and that will be discussed later. Table III-4 shows the results, namely, average gradients Γ for selected time delay ranges and the corresponding ground D for which this Γ value applies.

TABLE III-4

Observed Average Gradient Γ of Leading Edge for Sunrise Period

Time UT	Γ km/MHz	Time Delay Range msec	Largest Distance km	Γ km/MHz	Time Delay Range msec	Largest Distance km
1004	280	7.8-13	1800			
1011	280	8.2-11	1500	470	11-15	2100
1021	280	7-11.5	1550	470	12.5-15	2100
1041	280	8.5-9	1200		12.5-14	1950
1051	280	8.2-10	1350	180	11-13	1800
1101	280	8-14	1950			
1111	280	10-11.5	1550			
1211	210	5.8-9	1200			
1221	160	5-8	1000			
1231	215	5.5-8	1000	200	8.5-11	1500
1241	?			200 (2F)	7.5-9.5	1250
1251	135	5-8.5	1100	200 (2F)	8.5-12	1650
1301	115	3-10	1350	130 (2F)	10-12	1650
1311	90	4-8	1000	?		
1321	65	6-8	1000	?		
1341	80	3-11	1500	280	11-12.5	1700
1351	70	3-11	1500	98	11-13	1700
1401	80	3-11	1500	60	11-13	1700

At night, Γ is high, about 280 km/MHz which corresponds to $f_{\perp} \approx 3$ MHz according to Table III-1. For large time delays, Γ is about 470 km/MHz, values which would correspond to $f_{\perp} < 3$ MHz. During sunrise over the path (1211 to 1311 UT), Γ drops from 210 to 90 meaning the increase of $f_{\perp}$ from 3 to 10 MHz in agreement with proper interpretation of figure 3-14.

After sunrise over the path (after 1311 UT for D < 1500 km) the gradient stabilizes around 80 km/MHz, but so does $f_{\perp}$ (Figure 3-14). Due to tilts in the ionosphere, the gradients at larger time delays behave at times quite erratically because of large irregularities and tilts in the F region, but they also drop from about 200 to 60-80 km/MHz.

We conclude that the gradient Γ when averaged over a segment of time-delay range corresponds to $f_{\perp}$ at midpoints. Thus, it can be used as a guide to infer ionospheric conditions over the path. If Γ corresponds to a more or less uniform $f_{\perp}$ over the whole frequency domain (although it increases with D, as shown in Table III-1), the ionospheric conditions are stable. If, however, Γ assumes very large or very small values over a restricted time-delay range, an ionospheric irregularity occurs at the corresponding midpoint for this ground range. Thus. we believe, monitoring of Γ can be useful for OTH range determination, although further investigations using a larger data base are needed.

3.4.4 Samples of Backscatter Records

Backscatter records are displayed in Figure 3-17, but are not always easy to interpret due to the reduction in size and the loss of contrast in photography and printing. Samples are given for several important time periods and especially the most disturbed one, from 1231 to 1251 UT is shown completely. The leading edge is mostly quite diffuse indicating that focusing effects are not as well pronounced as during daytime; the energy is spread over a larger range. Again, the frequency increases from right to left, while tracings show the conventional coordinate system.

Backscatter records have also been traced every 10 minutes and assembled in Figure 3-18. Solid lines indicate a strong leading edge, dashed lines a weak or fuzzy leading edge, which is certainly subjective, but sufficient for this investigation. Evaluatin the data recorded on magnetic tape can put such distinction on a solid foundation. After sunrise strong groundscatter from hard targets is often seen and indicated by solid lines; again this is a subjective choice and no effort has been made to identify such targets. If the transponder signals are included. a "TR" is added to identify this particular trace. The transponder signal was easy to identify because it appears only at the 01, 11... min frames, but not at the 03, 07 min frames. From 1301 UT on, the transponder signal has been left out.

From 1000 to 1111 UT, the limited frequency range as well as its steady decrease with time are quite obvious. The time delay range shrinks

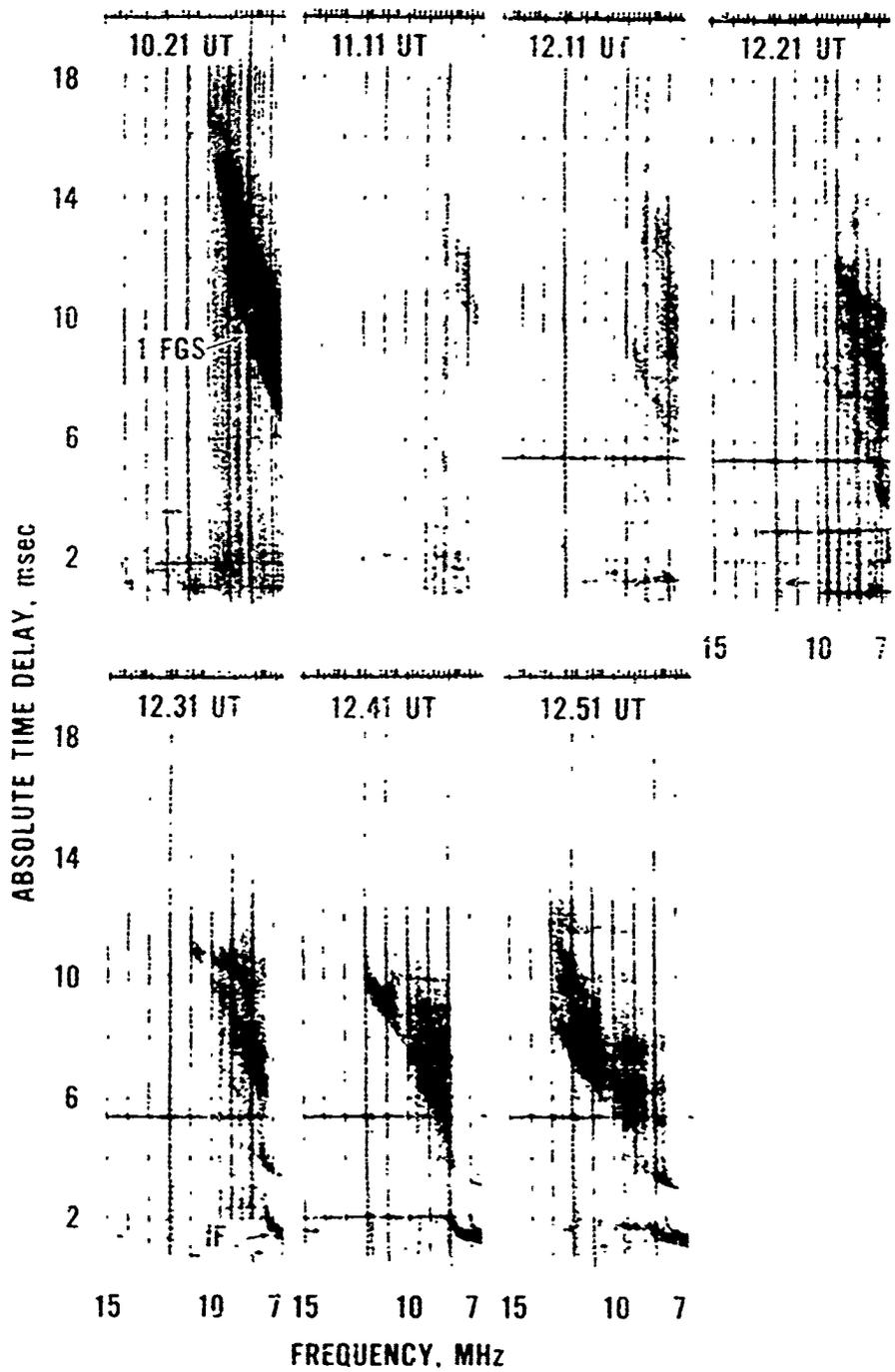

Figure 3-17 Samples of Backscatter Ionograms During Sunrise Test Period.

Frequency increases from right to left. Strong signal near 6 msec time delay is calibration tone. Recorded with automatic gain control. Vertical incidence ionograms are recorded in lower three ionograms only.

too because $f_{\perp}$ decreases steadily. The gradient of the leading edge is more or less constant. There are, however, irregularities. Some are seen clearly beyond 12 msec at 1004 and 1021 UT, others between 10 and 12 msec and 1041 and 1051 UT. They do not last very long and are, therefore, not important for continuous surveys, but indicate that for short time-intervals surveillance will experience difficulties. Such irregularities are related to short term ionospheric irregularities, a fact we have mentioned previously at several occasions. No tracings are shown between 1111 and 1211 UT because the leading edges are extremely fuzzy and any lines would be entirely subjective.

The most unusual backscatter records are seen immediately after sunrise along the path, i. e., after the reappearance of strong ground backscatter at 1211 UT. This period lasts for about one hour. During that period, there are essentially returns from two well separated ranges, one shorter than 8 msec, the other beyond 10 msec. Between these two strong ground backscatter areas, there is a region of weak backscatter signals.

The short range backscatter has a strong leading edge which ends at about 8.3 msec from 1211 to 1251 UT. While its gradient decreases during this time period (see Table 3.4), its maximum frequency increases from 8.5 to 13 MHz. The longer range backscatter appears from 12 to 13.5 msec at 1211 UT, 10 minutes later, at a shorter time delay, 10 to 12 msec, but stronger. Again another 10 minutes later,

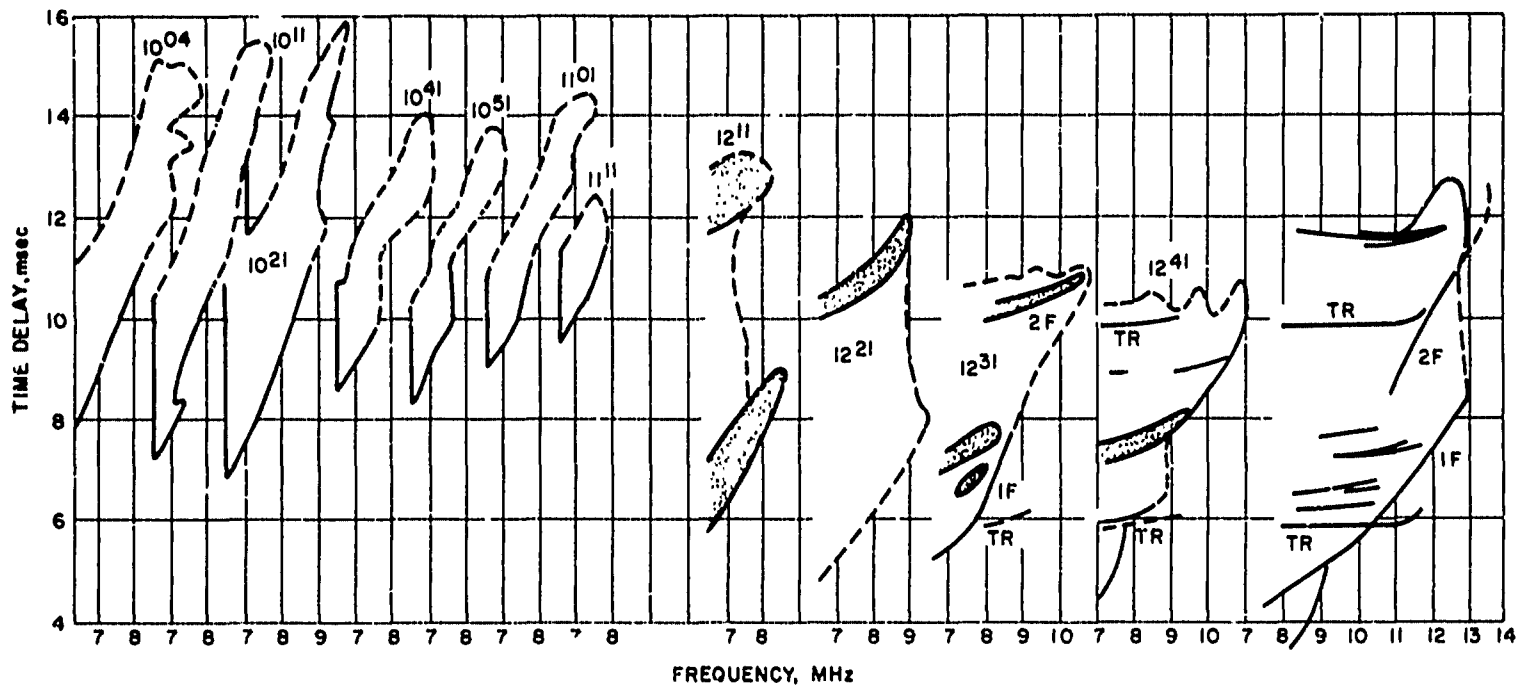

Figure 3-18a. Tracings of Backscatter Ionograms During Sunrise Test Period.

Ionograms are displayed every 10 min. TR = transponder trace. Fuzzy leading edge indicated by dashed line. 1F, 2F mean 1FGS and 2FGS mode. Solid traces at more or less constant time delay are possibly returns from hard targets.

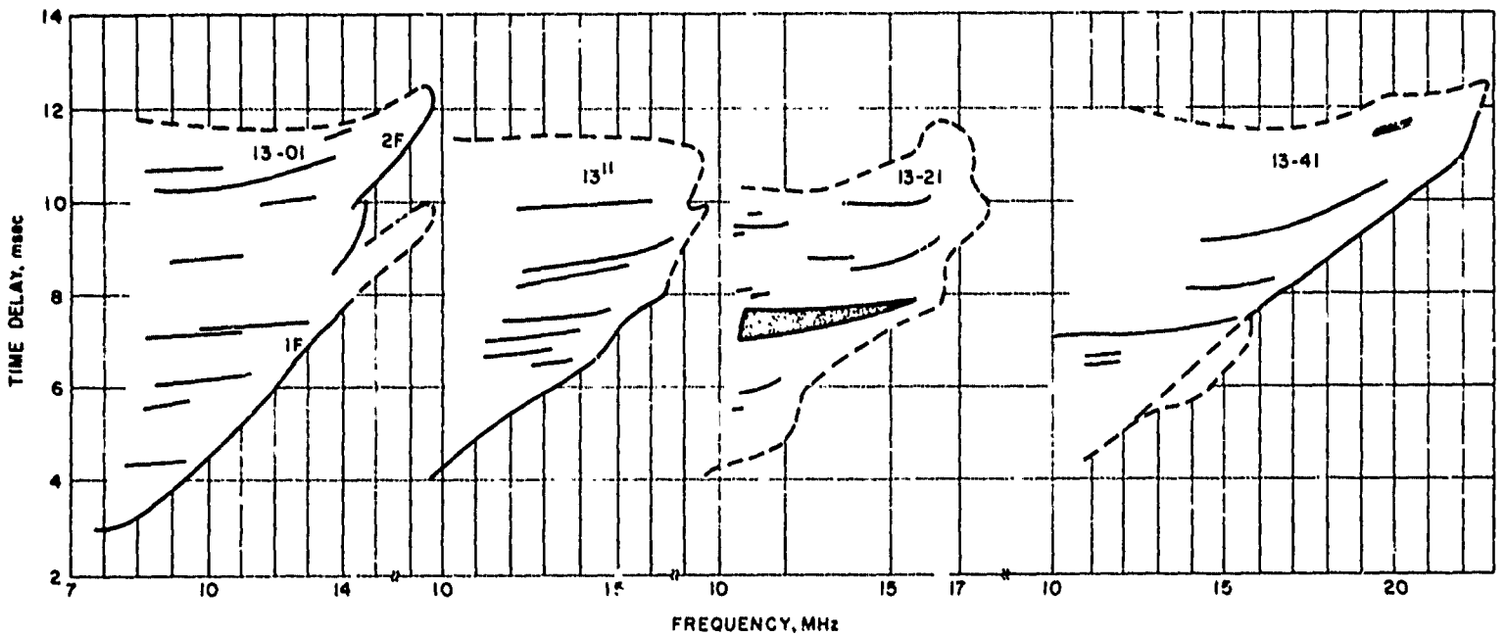

Figure 3-18b. Continued.

the time delay range shortens to 10 to 11 msec and it looks more like another mode than 1F. Its frequency range increases rapidly, as seen on Figure 3-18b, sometimes very clear as at 1301, but very vague at 1311 and 1321 UT. Finally, at 1341, the ground backscatter has the "normal" daytime appearance of one good leading edge. The most irregular form of the leading edge is noticed at 1241 UT. Careful investigation convinces us that the upper trace is the 2F mode, definitely from 1227 to 1237 UT and from 1247 to 1301 UT. Some of the heavy traces are probably hard targets.

3.5 EXPLANATION OF TEST RESULTS AND PREDICTION OF BACKSCATTER

3.5.1 Non-Uniform Ionosphere

The leading edge from wideband backscatter ionograms permits one to select proper narrowband frequency for target illumination.

For a daytime (or nighttime) ionosphere, uniform conditions over large distances are a reasonable assumption, and the frequency time delay diagram will show a "regular" leading edge of the ground backscatter. The actual position of the leading edge depends essentially on one ionospheric parameter, namely the maximum electron density of each layer (E, F1, and F2), which can be measured by an ionosonde. The height of the peak has some influence, but is of secondary importance, as seen in Figure 3-1. The form of the vertical electron density profile has, of course, some influence, but again it is of secondary importance. One normally chooses a simple mathematical form (parabolic layer, Chapman like or similar form) or takes the actual electron distribution from a true-height analysis of an ionogram.

During the day, the leading edge from the E and F1 layer can be of some importance but only out to perhaps 2000 km (Figures 3-2 and 3-3). The mixture of backscatter from E and F layer is clearly seen on computer produced synthetic backscatter ionograms, published by Stephenson and George (1969) and an example is shown in Figure 3-19, redrawn in linear scale. Here we see clearly a leading edge of the E mode separated from the F2 mode. Other cases are published by Croft (1965).

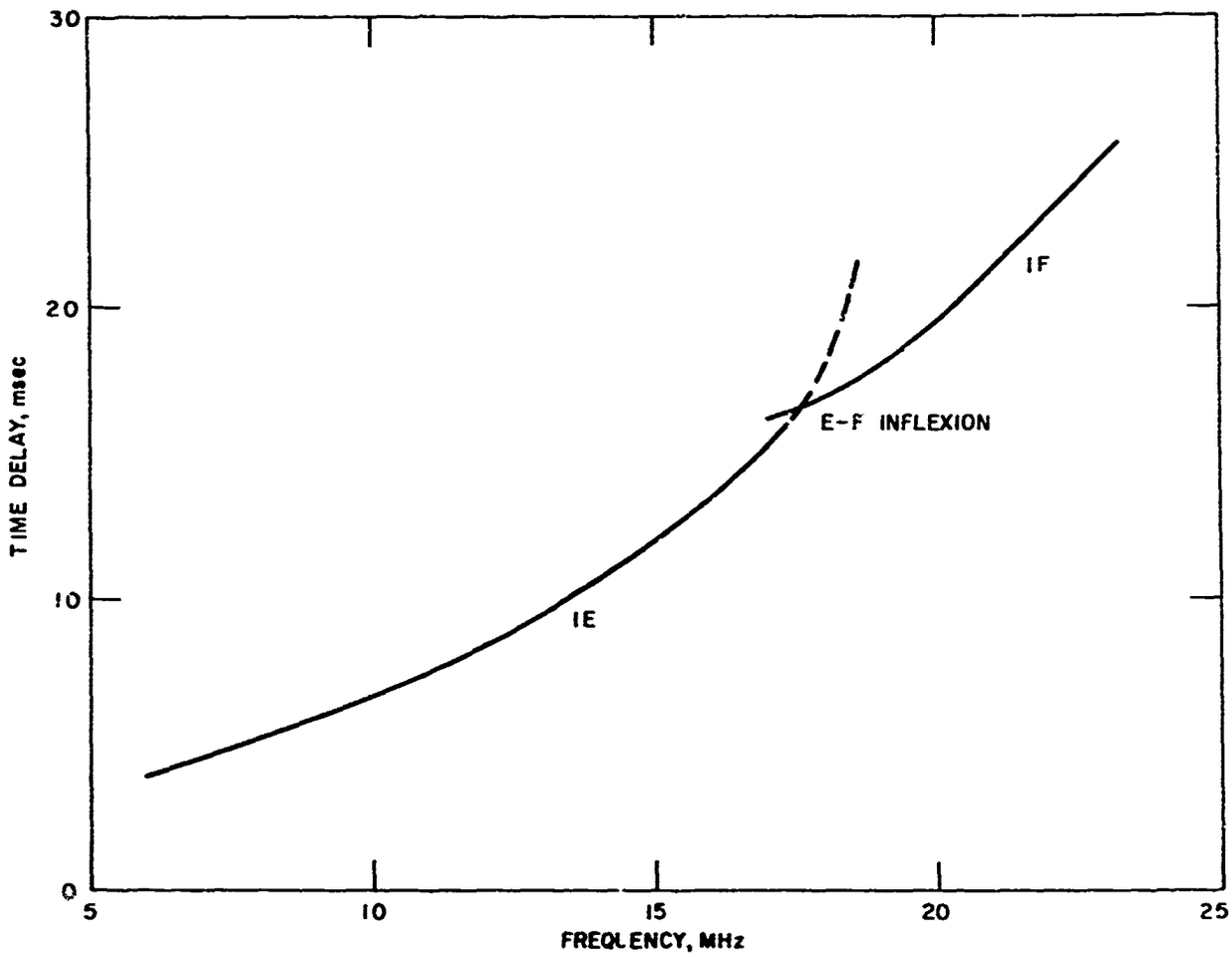

Figure 3-19 **Overlapping Leading Edges of 1EGS and 1FGS Modes.**

Redrawn from computer produced synthetic backscatter ionograms.

During dawn or dusk, general assumptions are not valid, because the ionosphere is not homogeneous, but the maximum critical frequency foF2 either increases or decreases westward during such times. The gradient d(foF2)/dD, when D is the distance along the surface of the earth is of the order of 1 to 2 MHz/1000 km.

From an earlier investigation (Penndorf, Katz, 1969) we select two maps (Figure 3-20), one showing the height for the maximum of the F2 layer during the sunrise period on 15 December 1960. These are the true heights (h) and are above 320 km in the night side and less than 280 km after sunrise in the day side. A gradient parallel to the isolines of solar zenith distance χ exists. The height of a fixed electron density (in this case 1×10^{11} el/m^3 = 2.8 MHz) shows the same tendency, namely low height on the day side, great heights in the night side, and a strong gradient, parallel to χ, around sunrise ($\cos\chi = 0$). Thus, we have to expect tilts in the ionosphere during dawn and dusk.

Inhomogeneities occur, of course, also during the day, but at such times the gradient d(foF2)/dD may be positive or negative for distances of a few hundred km only. That they occur is clearly seen from the variations of foF2 and they are about of the order of 10 percent of foF2, as discussed in Section 3.1 and seen in Figure 3-4.

For selected gradients and an foF2 = 3.5 MHz at the transmitter site, backscatter curves have been computed and published by Bartholomew et al (1968). For a particular ionospheric profile (layer semithickness 75km)

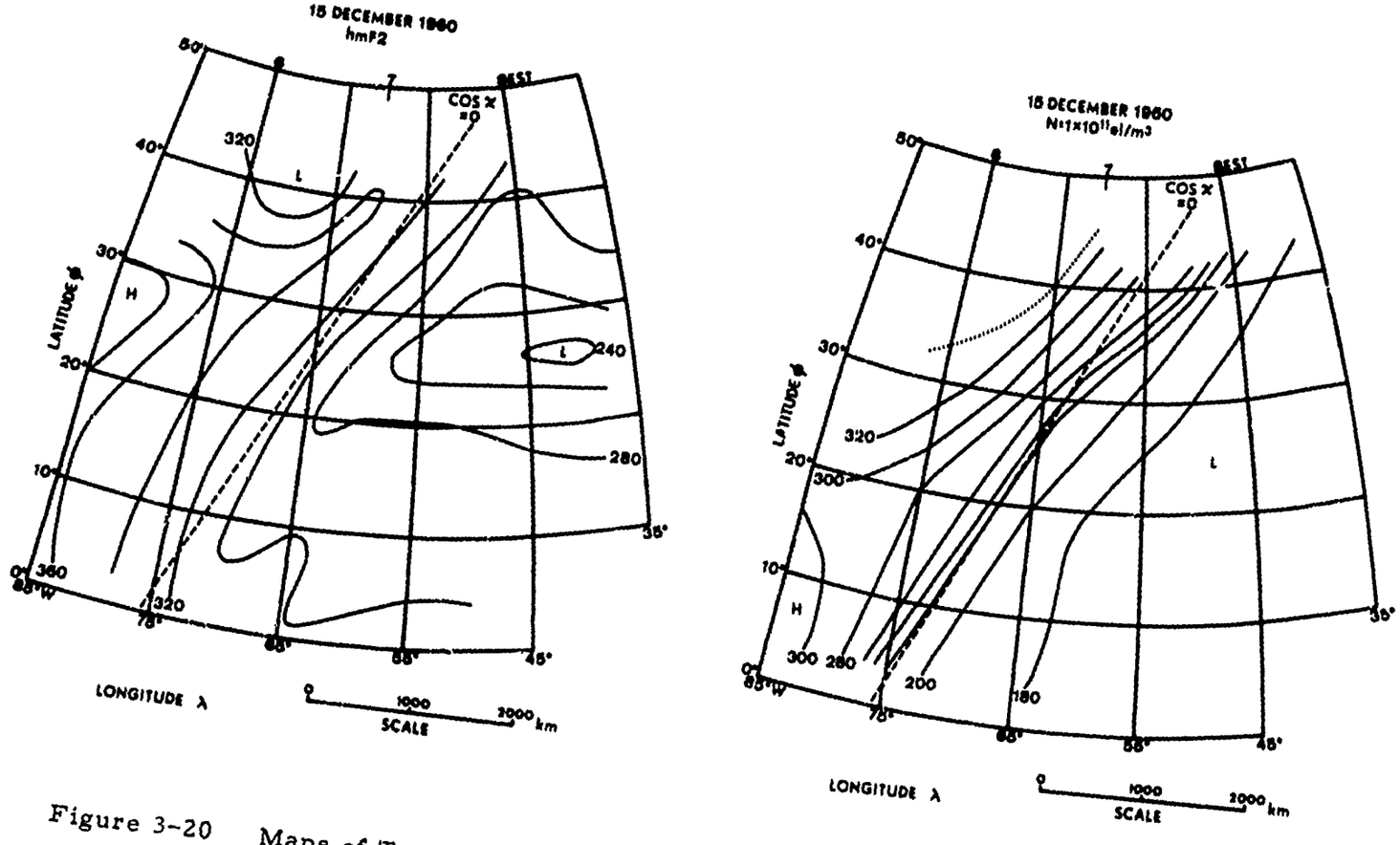

Figure 3-20 Maps of True Height of Maximum of F2 Layer and of Constant Electron Density for 15 December 1960.

a) True height hmF2.

b) Electron density $N = 10^{11}$ el/m^3. Dashed line is $\cos\chi = 0$ (ground sunrise).

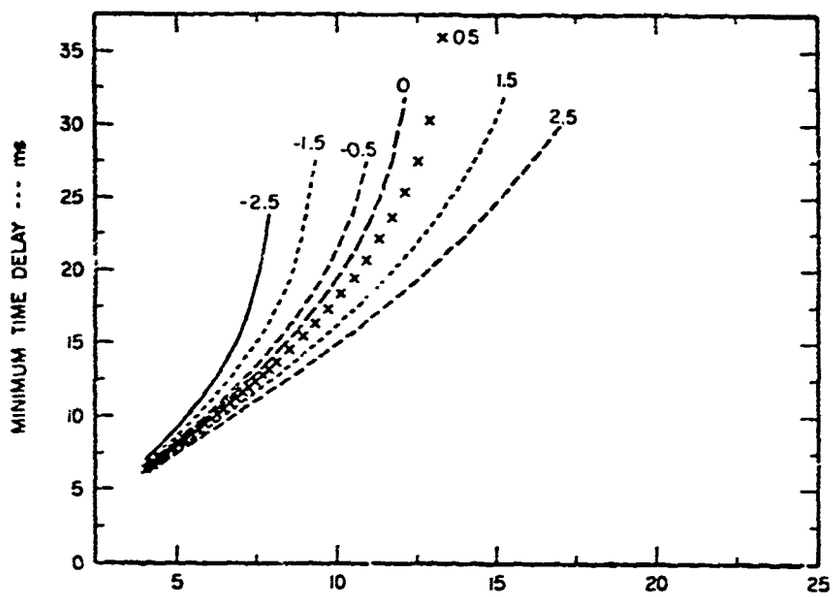

Figure 3-21 Calculated Backscatter Ionograms for a Linear Horizontal Gradient in foF2.

Overhead cirtical frequency = 3.5 MHz, height hmF2 = 350 km, gradients range from -2.5 to +2.5 MHz/300 km. (after Bartholomew et al., 1968).

and peak altitude (350 km) we reproduce one of their examples in Figure 3-21.

What is clearly seen, and is expected, is the leading edge of the backscatter is steeper than normal for negative gradients and flatter than normal for positive gradients. For a time delay of 20 msec, the "normal" maximum frequency is 10.4 MHz. If the maximum electron density decreases in the direction of propagation by 1.5 M[illegible] [illegible]00 km, then the m[illegible]imum frequency is reduced to 8.8 MHz; if it increases by the same amount, the maximum frequency increases to 12.0 MHz. Thus, it is quite obvious that the target illumination can be missed during times when such gradients exist, i.e., a frequency of say 9 MHz is selected to illuminate a ground target (based on the assumption of a uniform ionosphere with d(foF2/dD = 0), but in reality such a frequency never illuminates the ground even out to 25 msec because d(foF2)/dB is negative. If on the other hand d(foF2)/dB is strongly positive, the target may be far away from skip focusing region. Similar cases like Figure 3-21 can be found in Croft's report (1965) to which we refer for further investigations.

As the observations of foF2 (Figure 3-4) show, the gradients of d(foF2)/dD will not be as uniform over the entire path as in the above example; and, therefore, it will be hard to predict the leading edge of the backscatter. It seems, therefore, essential to record the actual backscatter ionogram using a wideband backscatter sounder. Such measurements should be made perhaps four times per hour during dawn and dusk over the

propagation path during routine surveillance observations. During day or night conditions, one per hour may be sufficient. Comparing the obtained backscatter ionogram with that for the last three days at the same local time will give clear indications if the ionospheric conditions during operating times will be similar to those for the last few days or not. If the wideband backscatter curve differs markedly from those for the same time period obtained during the last few days, then the narrowband surveillance frequencies have to be changed accordingly.

3.5.2 Sunset

During sunset the ionosphere is not uniform; in our test period, the electron density increased westward. Of course, the gradient d(foF2)/dD is not constant and, as shown by the vertical ionograms from Ava and U.I., even at some times negative (Figure 3-4). Thus, the general electron-density distribution over the path shows irregularities of scale size $<$ 1000 km. The electron-density distribution along the path for sunset leads to the leading edge with a less steep gradient Γ than for a uniform ionosphere (Figure 3-21). In our test period, d(foF2)/dD $<$ 0.6 MHz/300 km ($\lesssim$ 2 MHz/1000 km), so that the change is small (compare curves labelled 0 with those labelled + 0.5).

The backscatter curves in Figure 3-10 indicate that in this time period the gradient Γ of the leading edge for large time delays is steeper than normal around 2111 UT (Table III-3). At the same time, Figure 3 4 reveals that the horizontal gradient in electron density along the path is

negative (foF2 (U. I.) < foF2 (Ava)). Thus, this period of an unusual leading edge can be explained.

The second unusual period occurs from 2130 to 2200 UT (Figure 3-9). The explanation offered here is a change in Γ along the path. Over the path the horizontal gradient in foF2 is strongly positive for a first 600 km (midpoint to D≈ 1200 km); beyond that distance foF2 is either constant or even negative.

We assume the gradient d(foF2)/dD to be positive (+ 2 MHz/1000 km) up to about 600 km and zero beyond. Using the data from Figure 3-21 we can construct the resulting backscatter record in Figure 3-22. The leading edge has a sharp change in gradient dp'/df when the ionospheric gradients change. The computed backscatter curves for gradients 0 and +2 MHz/1000 km are shown by dashed-solid lines. Assuming the sudden change in the horizontal gradient at about 12 msec will result in the solid curve. This curve shows a gradient Γ of 200 km/MHz below 12 msec and about 900 km/MHz above 15 msec with a strong inflection between 12 and 15 msec. Such cases seem to happen in our sunset records. Since the SRI data are based on foF2 = 3.5 MHz, whereas Ava records about 8.5 MHz actual values of Γ cannot be compared, unless new ray tracing computations are carried out. Nevertheless, such a model could explain sunset conditions such as shown in Figure 3-9.

3.5.3 Sunrise

At sunrise, the increase in electron density is more drastic than at sunset. The tilts are large and consequently the backscatter can become complicated.

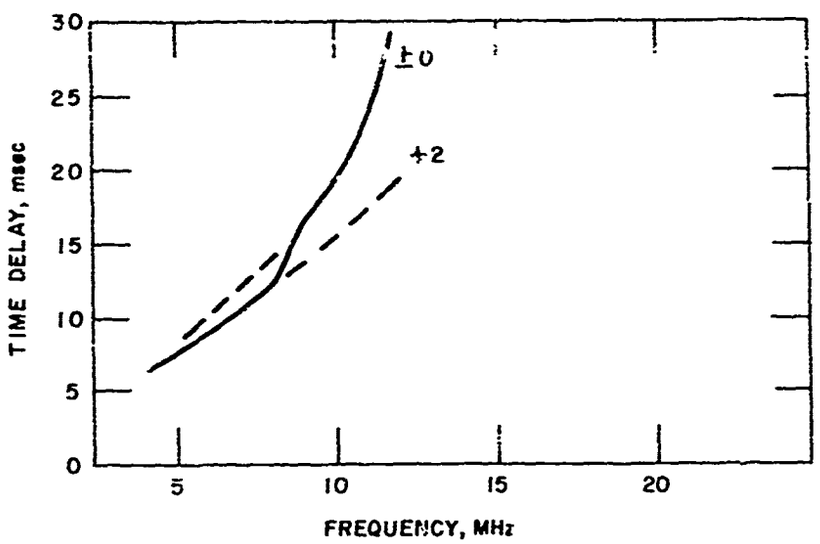

Figure 3-22 Calculated Backscatter Ionograms for Changes in Horizontal Gradient in foF2.

A gradient of 2 MHz/1000 km is assumed for path midpoints from 0 to 600 km, and zero gradient beyond that distance. These two ionograms are indicated by dashed line. The resulting composite backscatter ionogram is indicated by a solid line.

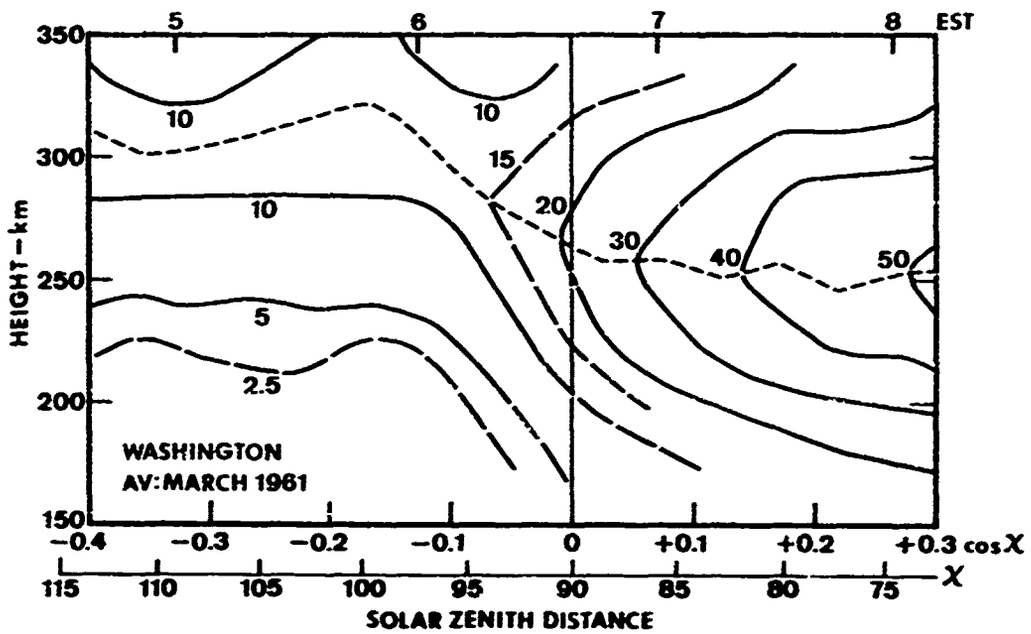

Figure 3-23 True Height Electron Density Profile During a Sunrise Period for Washington, D. C.

Average of three days for March 1961. Abscissa is solar zenith distance. Ordinate is true height in km. Isoionics are drawn for every 5×10^{10} el/m^3. Dashed line is height of maximum of F2 layer. Isoionics above maximum of layer are assumed.

Let us first look at some examples of electron density. In Figure 3-23, for Washington, D.C., the abscissa is linear in $\cos\chi$, the zenith distance of the sun, and the corresponding local time is at the top. The ordinate is height in km. The dashed line is the height of the maximum electron density of the F2 layer, the solid lines represent lines of equal electron density in units of 10^{10} el/m^3. The average for March (3 days) shows smooth contours, the other case for 14 December shows small scale irregularities, because we used data every 5 minutes.

Assuming such changes with time above one station to be representative of an east-west cross section, one can convert such diagrams, as shown in Figures 3-23 and 3-24, into electron density distributions along the propagation path. A proper coordinate system is required with height and distance on equal scale. The time difference of 1 hour in Figure 3-23 corresponds to about 1300 km and a replotting reduced the tilts to their proper value of 5° or less. A propagation path from the right side of Figure 3-23 towards the left will find rays with some take-off angles to become parallel to the tilts and not return to the ground. Such a situation could explain the unusual backscatter after 1211 UT (Figure 3-18a).

The sample given above is not an extreme case because the 55 sunrise profiles published by Penndorf (1969) contain some which are even more extreme. Since we do not have a true height profile series for the same day we investigated, it is not possible to correlate the backscatter records with an actual ray tracing program. At the present time, we can

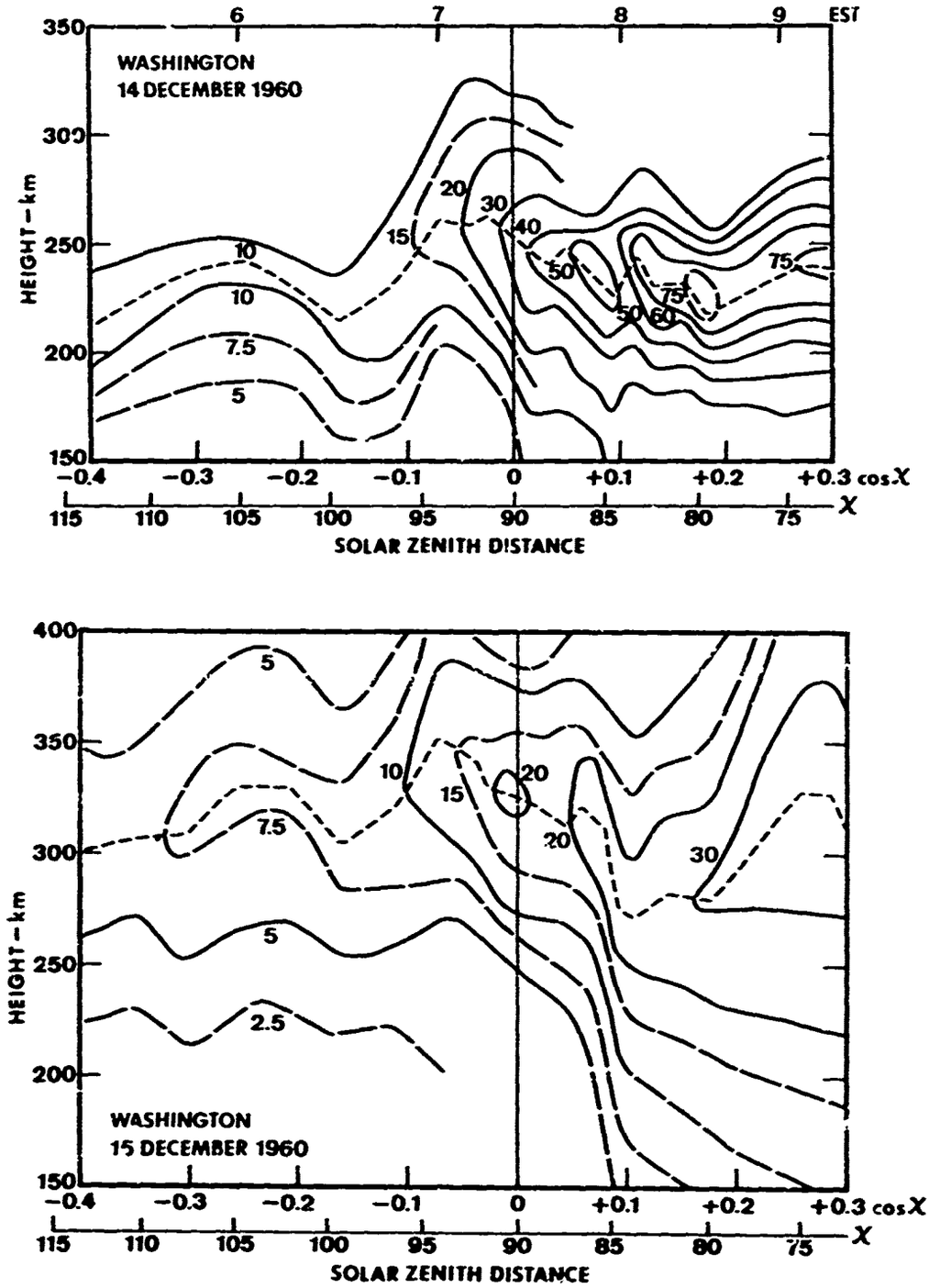

Figure 3-24 True Height Electron Density Profile During Sunrise for Washington, D. C., 14 and 15 December 1960.

Abscissa and ordinate as in Figure 3-23. Data in 5 min intervals lead to small scale irregularities even for such quiet d s.

only point out that the backscatter records can be explained using existing ionospheric profiles. It is suggested to carry out ray path calculations through such ionospheres to simulate sunrise conditions. One can also make a complete analysis using ionograms, true height calculations, and ray path calculations for the same day backscatter is measured during a sunrise period.

3.5.4 Prediction

3.5.4.1 Method

To evaluate the advantage of real time wideband backscatter soundings for predicting the proper surveillance frequency, we select a few samples from the sunset period of 30 November 1970. As stated in Section 2.3, we possess information about the ionospheric parameters along the path:

(1) Vertical soundings at the transmitter site (Ava)

(2) Vertical soundings at U.I. (D = 1120 km)

(3) Transponder at U.I. giving ionospheric data for the midpoint (D = 560 km)

(4) Forward propagation Ava to U.I. giving also information about ionospheric structure at midpoint.

Thus, we have information at two points along the path plus that over the transmitter and can evaluate the importance of taking vertical soundings at the transmitter site.

These ionospheric data can be used to construct backscatter ionograms in a simplified way by assuming a homogeneous ionosphere. That means we take the ionospheric structure for each of the four foregoing measurements, assume it to be homogeneous over a 3000 km path, and compute the resulting leading edge of a backscatter ionogram every 500 km (5 points). This is done for all four measurements and will give, in general, four different leading edges. The method is explained in Appendix B.

A leading edge can also be computed using the ionospheric prediction method by NOAA. We utilize the published maps for November 1970 (the December 1970 predictions are practically identical for the path) (ESSA, ionospheric predictions, 1970). For 20, 22, and 24 UT we read off MUF (zero)F2* and MUF (4000)F2 for the midpoints of a 1000, 2000, and 3000 km path starting in Ava and going westward. Then the values MUF (zero)F2 and MUF (4000)F2 have been interpolated in time to correspond to the selected UT times of our samples for 30 November 1970. A reflection height of 300 km was assumed which corresponds best with the actual cases. The leading edge of the backscatter was then computed in the same way as for the actual ionospheric structure (see Appendix B for the method used).

---

* MUF (zero)F2 is identical with (fxF2) which has to be used in the simple ESSA prediction method as described by Davies (1965).

3.5.4.2 Comparison of Results

Figures 3-25 a to d contain the observed leading edges from the wideband backscatter soundings, the leading edge computed from the four ionospheric observations, and a computation based on ESSA predictions.

1. At 2031 UT (1531 EST) the whole path is illuminated by the sun; at Ava the zenith distance of the sun is 82.3°. The ionosphere is fairly homogeneous at that time; Δf_1 between Ava and U.I. is only 0.1 MHz and the various synthetic backscatter curves all fall within a range of about 1 MHz, which is a very good agreement. These synthetic backscatter curves also agree with the observed backscatter curve within 1 MHz as shown on the right. The difference between the observed leading edge and the ESSA predictions are larger and of the order of 1 to 2 MHz.

From a practical point of view one looks at the deviation in time delay $\Delta\tau$ between observed and synthetic or predicted leading edges for selected operating narrowband frequencies. The deviations $\Delta\tau$ are shown at the top (+ $\Delta\tau$ means computed leading edge appears for that frequency at a longer time delay than the actual observed leading edge). For the four synthetic leading edges $\Delta\tau$ is about 0-1 msec, with average deviations of 0.15 to 0.6 msec, for the NOAA prediction $\Delta\tau$ = + 1.0 msec on the average, increasing from 0 msec at 12 MHz to + 1.9 msec at 30 MHz. For FOT = 0.85 MUF, recommended by NOAA, the deviations increase from + 1.3 msec at 12 MHz to + 4.8 msec at 24 MHz with an average deviation of + 2.3 msec, which is unacceptably large.

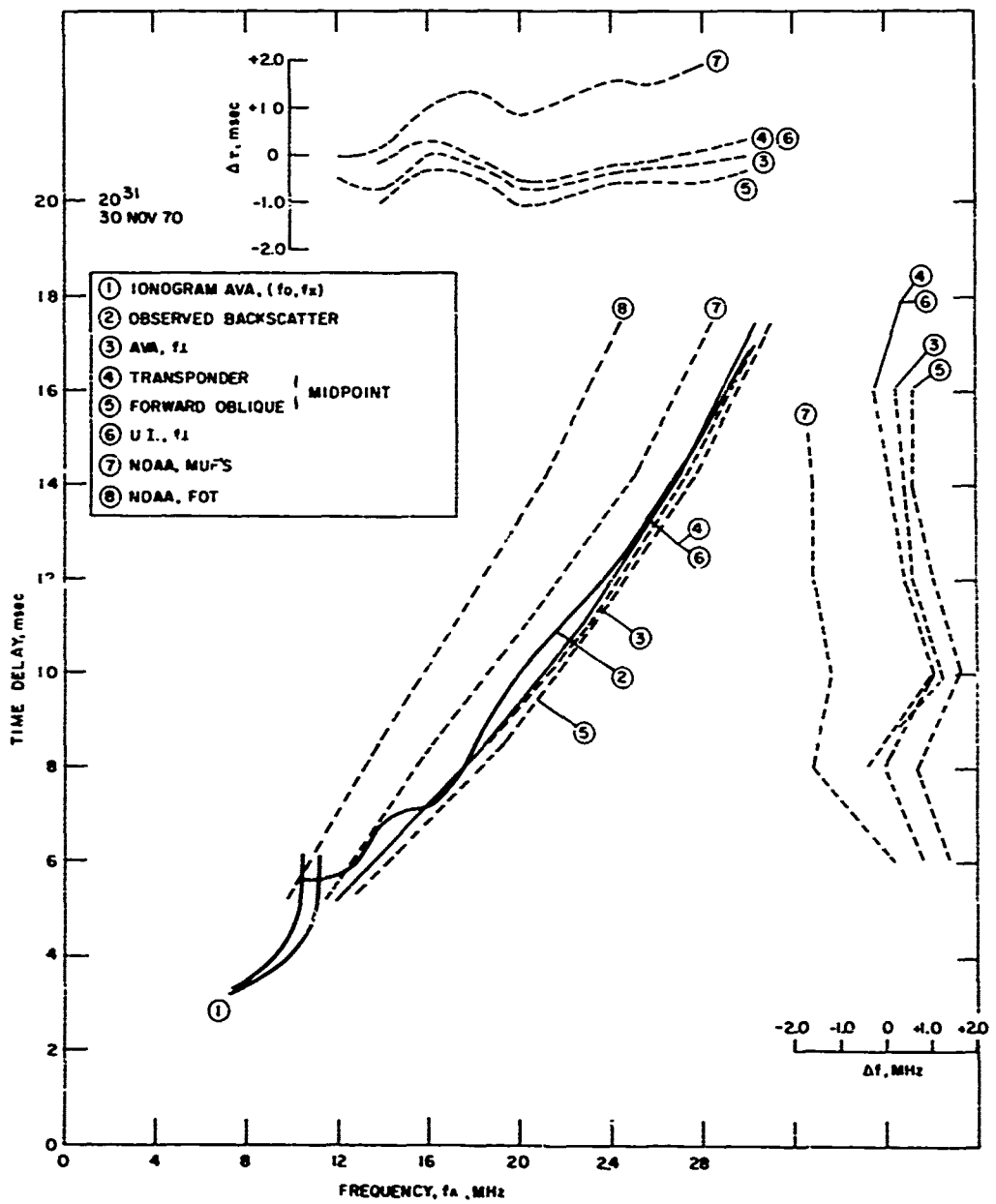

Figure 3-25 Comparison Between Observed and Predicted Backscatter Ionograms.

Selected are four particular times during the sunset test period. Construction of predicted ionograms is explained in the text.

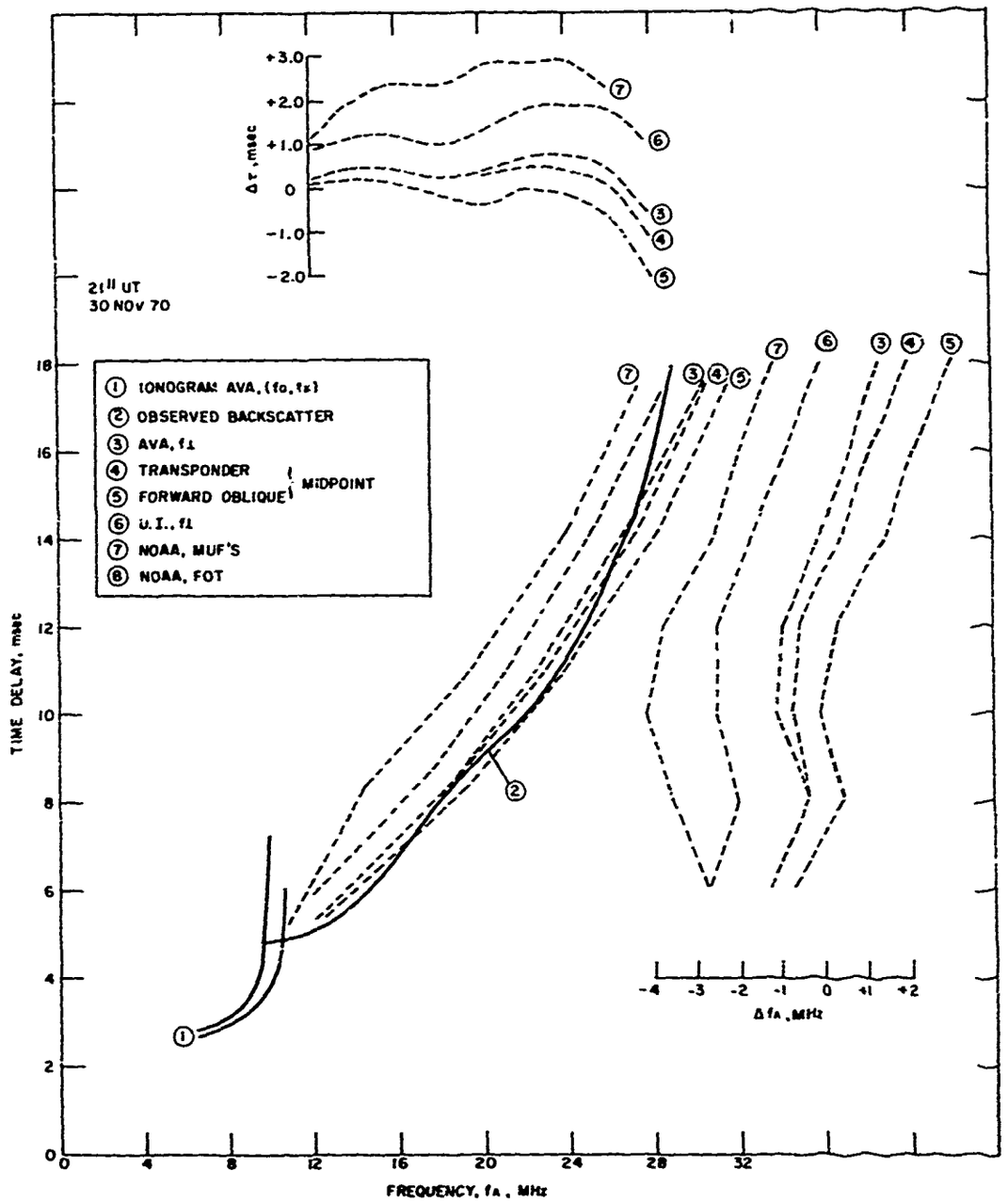

Figure 3-25 Continued.

2. At 2111 UT (1611 EST) we reach nearly sunset over Ava with a zenith distance of the sun of 87.9°. At that time, U.I. has a lower $(foF2)_{\perp}$ than Ava (about 0.3 MHz) and a higher peak altitude than at Ava or midpoint Ava-U.I. Therefore, the leading edge of the backscatter for U.I. gives much lower frequencies (for the same time delay) than the other synthetic ionospheres. The observed backscatter curve fits the Ava and midpoint synthetic backscatter curves below about 14 msec time delay ($D \lesssim 2000$ km). At $\tau = 18$ msec ($D \approx 2600$ km) it fits best the (U.I.) synthetic backscatter curve.

The strong bending backwards of the observed backscatter after $\tau = 12$ msec can well be explained as a change in the ionospheric structure with lower peak electron density further west than at Ava (and, in addition, a small rise in layer height).

Looking at the deviations between the observed and computed backscatter curves (right hand side) we find that the agreement is very good, about 1 MHz out to $\tau = 13$ msec for Ava and midpoint, but then it becomes larger (2 MHz) and poor; for U.I. out to about $\tau = 16$ msec the agreement is poor, but very good at $\tau = 16$-20 msec ($<$ 1 MHz).

Looking at the deviations in time delay for fixed frequencies (top figure), $\Delta\tau$ is small up to 26 MHz (on the average -0.1 tc $+ 0.4$ msec) but large above 28 MHz. The NOAA prediction, as an hour earlier, leads to the lowest synthetic backscatter curve. NOAA predictions are 2-4 MHz too low, which is unacceptable. The $\Delta\tau$ is 2.0 msec all the time, 2.3 msec

on the average. Using FOT instead of MUF, the deviations increase even further. This case, although probably unusual for sunset, can be well explained by a negative gradient in electron density.

3. At 2221 UT (1721 EST) the path is no longer sunlit for the first 1100 km. The zenith distance of the sun is 99.5° at Ava and 90° at U.I. The gradient of maximum electron density is about zero between Ava and midpoint and large between midpoint and U.I. (2.1 to 2.4 MHz) over a distance of 560 km.

The three synthetic ionospheres, Ava and midpoint, agree, within about 1 MHz, but $(U.I.)_{\perp}$ is showing much higher frequencies for the same time delay than the others. The observed backscatter curve fits the first three to about τ = 10 msec (D < 1300 km) but not beyond and it fits the $(U.I.)_{\perp}$ backscatter from 12 msec to 15 msec (D ≈ 2000 km). Again, the observed ionosphere over the transmitter leads to good agreement with the observed backscatter for a ground range up to 1000 km from the transmitter, and the midpoint ionosphere (U.I.) gives good agreement for the ground range 1500 to 2200 km. No backscatter beyond that range is recorded. The deviations between the observed and synthetic backscatter (right hand side) are such that Ava and midpoint deviate by ± 1 MHz up to about 10 msec, but are -4 MHz off at 16 msec. The $(U.I.)_{\perp}$ ionosphere is about 2 MHz too high for small distances, but in excellent agreement from 12-16 msec. This is also obvious for the deviations (-0.4 to + 0.2 msec on the average), but increasing to > + 3.0 msec at 28 MHz. U.I. data deviate by 1.0 msec up to 22 MHz, but not from 24 to 28 MHz.

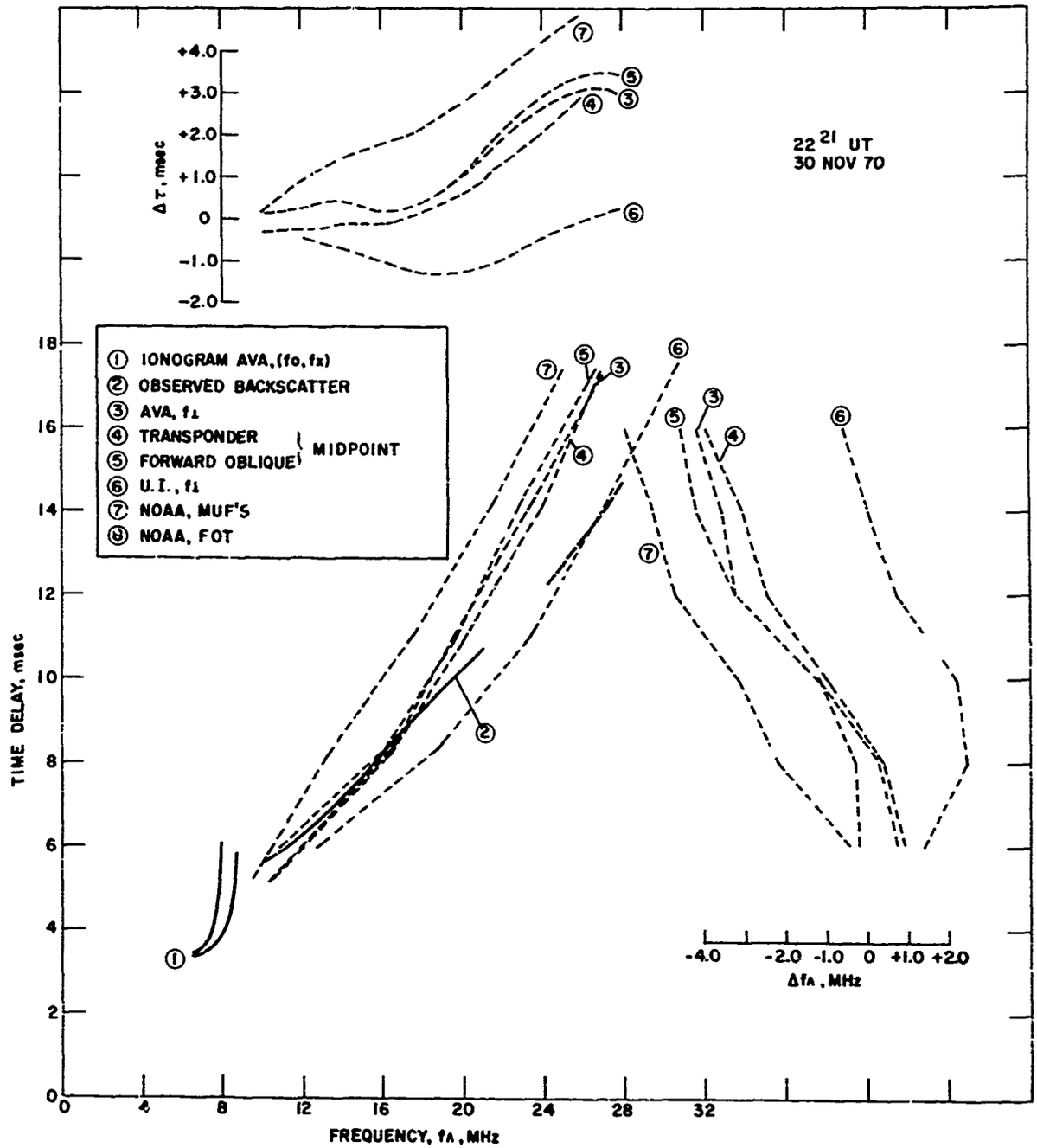

Figure 3-25 Continued.

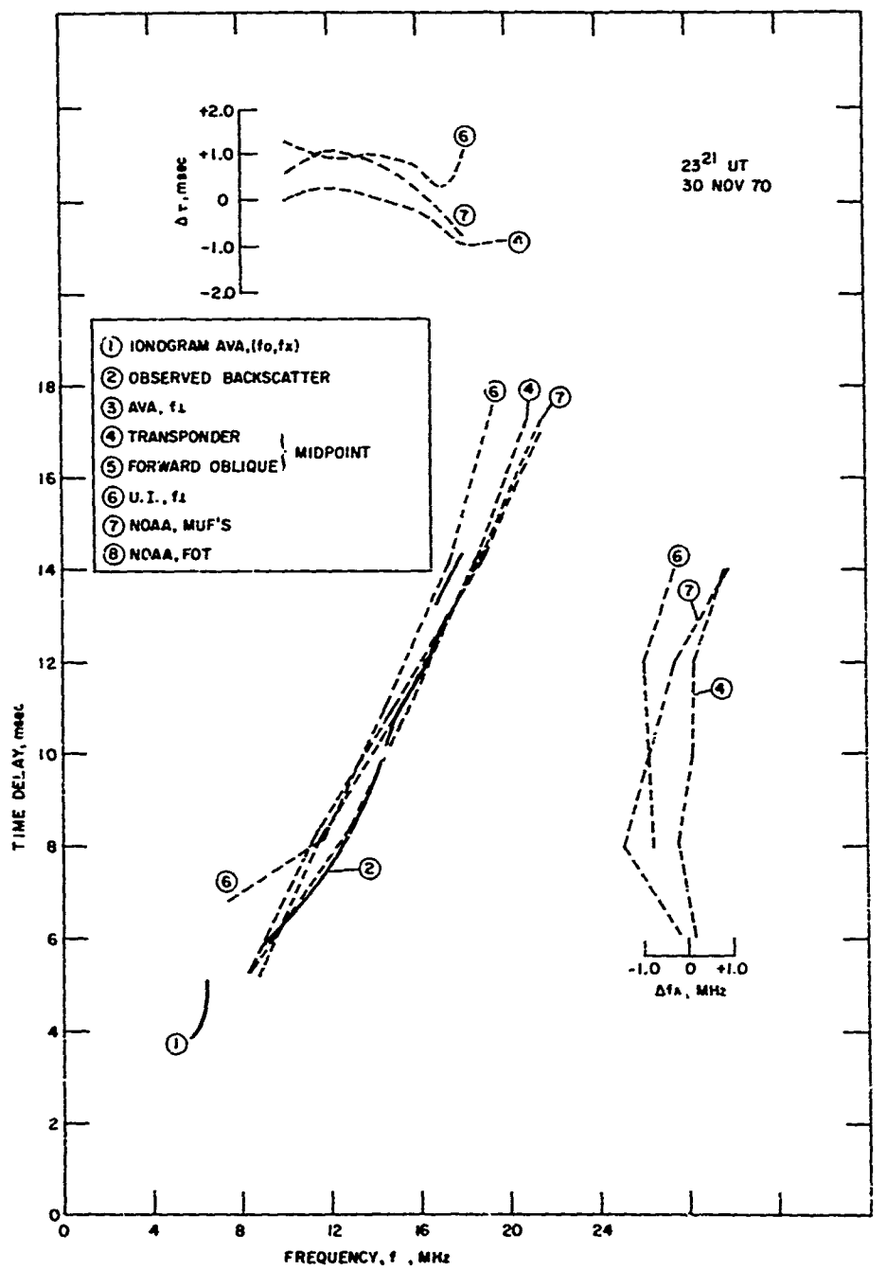

Figure 3-25 Continued.

The NOAA predictions give a backscatter curve which is much too low in frequency. The difference between the NOAA prediction and the observed backscatter curve is about zero at Ava and increases steadily to -6 MHz at 16 msec. ($\Delta\tau$ increases from zero to 5.0 msec at 26 MHz.) Hence, the use of NOAA predictions would lead to erroneous surveillance frequencies.

4. At 2321 UT (1821 EST) the path is now in darkness out to a distance of 2500 km. The solar zenith angle at Ava is 109.8°. We lost information at Ava and the forward oblique path, but not at U.I. and the transponder. There exists some difference between $(U.I.)_{\perp}$ and midpoint (transponder data). The observed backscatter curve agrees remarkably well with the midpoint data out to 13 msec ($D \leq 1800$ km). The observed backscatter curve jumps backwards at 13 msec and is then close to the synthetic backscatter curve for $(U.I.)_{\perp}$, out to about D = 2000 km just where both should fit. At this time, the NOAA predictions lead to good agreement ($\Delta f = \pm \lesssim 1$ MHz and $\Delta\tau = +0.3$ msec). This is the only time we find the NOAA predictions to lead to good results for predicting the proper surveillance frequency.

3.5.4.3 Summary

The observed backscatter curves during a sunset period have been found in agreement with the ionospheric structure along the path. During this time the maximum electron density at times decreases, but generally

increases westward and, therefore, the observed backscatter deviates from that obtained for a homogeneous ionospheric structure. The deviations between the observed and synthetic leading edges of backscatter are always small if the ionospheric structure measured at path midpoint is used for comparison with a corresponding range or time delay. The NOAA predictions have not led to good agreement except in one case.

Although we have selected only a few cases, each one was chosen for a particular reason to represent the various ionospheric structures which occur and thus they are typical for that day. The greatest deviations between observed and synthesized backscatter in this operating period lasted for about 1.5 hours. The use of a wideband backscatter sounder correctly determines the best surveillance frequencies for a specific ground range.

3.6 REFERENCES

Air Force Cambridge Research Lab., Geophysics and Space Data Bulletin, 8, No. 1, 1971.

Bartholomew, R. R., V. E. Hatfield, J. B. Lomax and G. H. Smith, Some Further Results of Backscatter Data Analysis, Stanford Research Institute, SRI Project 6315; 1968.

Bernstein, M. R., D. G. Detert and C. M. Rush, Ionospheric Effects on HFDF. Final Report, Contract N00014-68-C-0332, Avco/SSD, Wilmington, Massachusetts, 1968.

Coffey, M. E., D. G. Detert and S. M. Bennett, Backscatter Parameter Investigation, RADC-TR-71-71, Avco Corp./SD, Lowell, Mass. 1971. AD882 795L

Croft, T. A., The Synthesis of Sweep Frequency Ground Backscatter by Digital Computer, Stanford Electronics Lab., Stanford University, SU-SEL-65-002, Stanford, California, 1965.

Davies, K., Ionospheric Radio Propagation, U. S. Printing Office, 1965.

Katz, A. H., Auroral Backscatter Study (Phase I), RADC-TR-70-265, Avco Corporation/SD, Lowell, Massachusetts, 1970. AD513 322

Katz, A. H., Auroral Backscatter Study (Phase II), AVSD-0378-71-RR, Avco Corporation/SD, Wilmington, Massachusetts, 1971.

Kobayashi, T., Transmission Curves for the Curved Ionosphere, J. Radio Res. Lab. (Japan), 8. 395, 1961.

Moeller, H. G., Impulsuebertragungsversuche mit schraeger Inzidenz, Forschungsber. Nordrhein-Westfalen No. 1149, 1963.

Penndorf, R. and A. H. Katz, Ionospheric Morphology (Phase II), RADC-TR-69-360, Avco Corp./SSD, Lowell, Mass., 1969. AD864 892

Stephenson, J. and T. M. George, Computer Routines for Synthetic Ground Backscatter from Three Dimensional Raysets, ESSA Technical Report, ERL-120-ITS-84, Boulder, Colorado, 1969.

APPENDIX A

Determination of Absolute Time Delay

The processed backscatter data contain time delay markers every 2 msec (see, for example, Figure 3-11), but the information is given in relative time delay. Absolute time delay is not known but can be established. The corrections are small and for some practical applications not important.

The best way to establish zero time delay in relation to the time delay markers is based on the vertical ionosonde traces, especially on the time difference between multiple reflections between ground and ionosphere. We define zero time as the time the signal leaves the transmitting antenna. Figure A-1 shows such traces (f_o). In such an ionogram

$$\tau_3 - \tau_2 = \tau_2 - \tau_1 = \tau_1$$

or

$$\tau_2 = 2\tau_1 \; ; \; \tau_3 = 3\tau_1$$

In this way, we establish the zero time delay line. At the right, we indicate the position of the 2 msec time delay markers and there remains a difference between the absolute and relative zero time delay, called τ_s.

In this case

$$\tau_2 - \tau_1 \neq \tau_1$$

but

$$\tau_3 - \tau_2 = \tau_2 - \tau_1 + \tau_s = \tau_1 + \tau_s$$

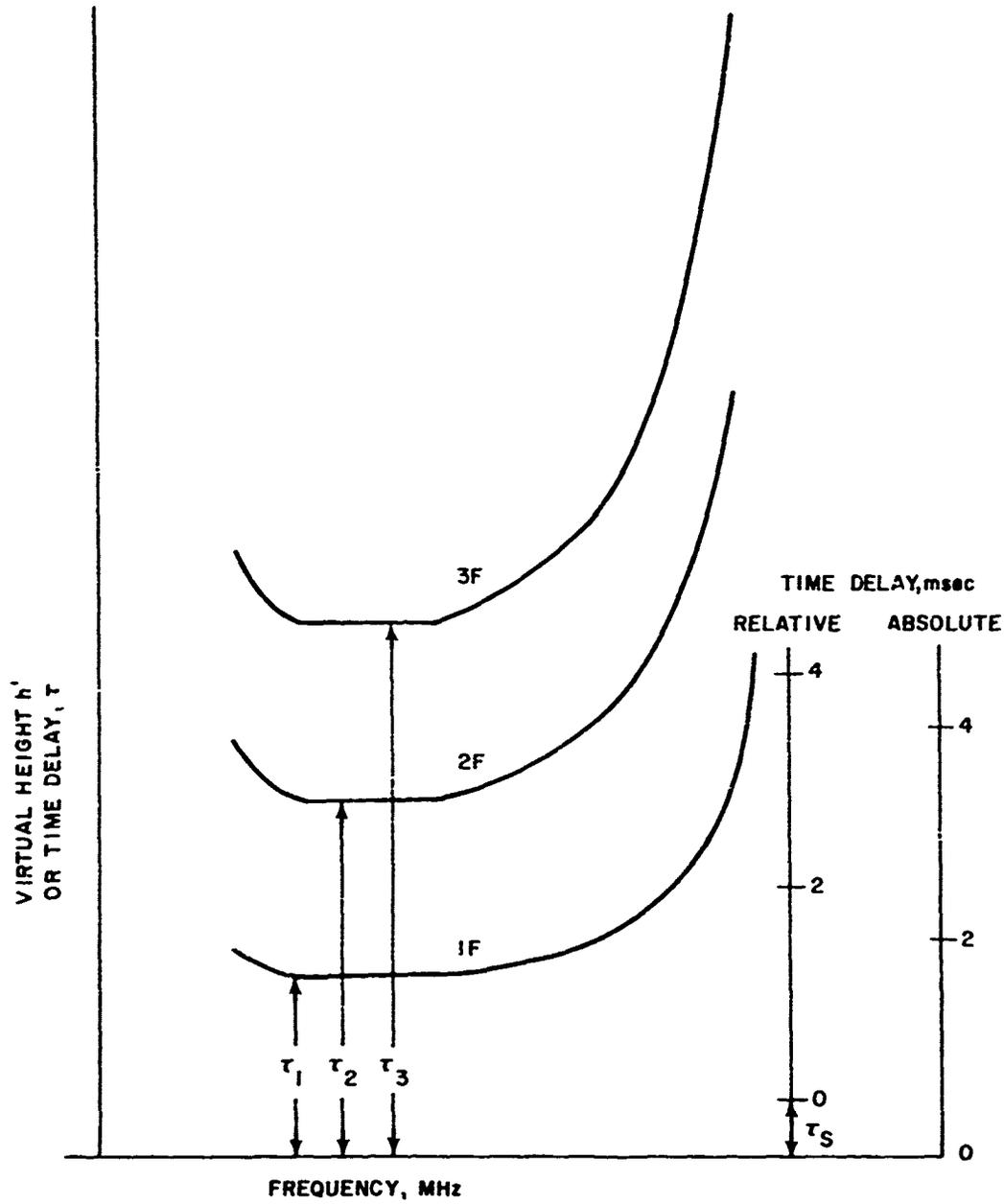

Figure A-1 Determination of Time Delay From Traces of Vertical Incidence Ionosonde.

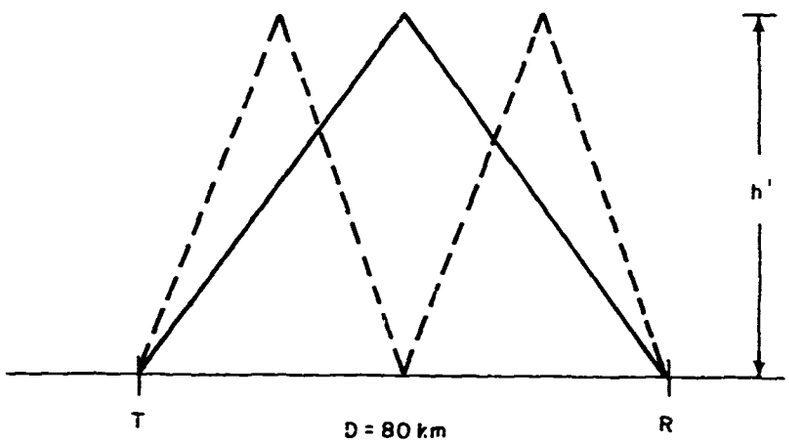

Figure A-2. Geometry of Ray Paths for 1F and 2F to Determine Time Delay Between Ava-Dexter.

thus τ_s can be determined easily at several frequencies and the absolute time delay is shown on the right hand scale.

In backscatter systems, transmitter and receiver are separated; the distance between Ava and Dexter being 80 km. The time delay for such a geometry is now computed. For simplicity, a flat earth and flat ionosphere is assumed and this is a fairly good approximation for such short distances. Figure A-2 shows the geometry. One has to keep in mind that for a transmitter/receiver separation, the 2-hop path is somewhat larger than twice the 1 hop. Therefore, the time delay is

$$\tau_2 = 2\tau_1 + \tau_c$$

and the correlation τ_c can be computed. The path length p' for 1 hop and 2 hop (dashed line) is computed for h' = 110 km (E layer) and h' = 200 to 500 km (F layer). The path length is converted into time delay ($p' = c.\tau$) and listed in Table A-1. In the first column is the virtual reflection height h' and in the second, the time delay $\tau_\perp$ for D = 0, i. e, vertical transmission (transmitter and receiver at same location). The next columns list τ_1, τ_2, $2(\tau_2 - \tau_1)$, and τ_c for an 80 km separation between transmitter and receiver. Using the 2 msec time delay markers, we can measure accurately

$$\tau_2 - \tau_1 = \Delta\tau$$

with

$$\tau_1 = \Delta\tau + \tau_c$$

and

$$\tau_2 = 2\Delta\tau + \tau_c$$

TABLE A-1

TIME DELAY FOR AVA-DEXTER FACILITIES AND VARIOUS REFLECTION HEIGHTS

Time Delay in msec, Altitude h in km.

h'	$\tau_{\perp}$ for D = 0	τ_1 for 1 Hop	τ_2 for 2 Hop	$2(\tau_2 - \tau_1)$	τ_c
110	0.73333	0.78031	1.4907	1.4200	0.071
200	1.3333	1.3598	2.6800	2.6404	0.040
225	1.5000	1.5235	3.0118	2.9766	0.035
250	1.6667	1.6880	3.3442	3.3124	0.032
275	1.8333	1.8527	3.6766	3.6478	0.029
300	2.0000	2.0178	4.0090	3.9824	0.027
325	2.1667	2.1831	4.3418	4.3174	0.024
350	2.3333	2.3486	4.6743	4.6514	0.023
400	2.6667	2.6800	5.3400	5.3200	0.020
500	3.3333	3.3440	6.6720	6.656	0.016

where τ_c is taken from Table A-1, the absolute time delay is established.

The additional correction τ_c is largest for the E layer trace and smallest for the F layer trace. For the E layer, the correction is 0.071 msec and about 0.030 msec for normal F region heights, namely the flat part of the trace. This correction is, in general, so small that other inaccuracies due to trace thickness and scaling errors make such a correction unnecessary. However, there may be cases where it becomes important. The correction due to the arbitrary position of the markers, called τ_s before, has to be taken into account. Thus,

$$\tau_2 = 2(\tau_2 - \tau_1) + \tau_c + \tau_s$$

The 2 msec time delay marker is finally corrected to read 2.20 msec on 1 December (sunrise) and 2.18 msec on 30 November (sunset).

The transponder signal was offset by 500 Hz = 2 msec and, therefore, seen at about 6 and 10 msec. The correction to absolute time was τ_s = 0.25 msec using the E layer trace during daytime.

The forward oblique transmissions from Ava to U.I. are also obtained in relative time delay. By scaling the E layer trace and assuming a height of 110 km, we obtain a time delay of 3.835 msec. This determines the base and the F layer traces are determined from this base line. In this way, all recorded data have been converted to absolute time delays.

APPENDIX B

Methods to Obtain Leading Edge of Backscatter

A simplified method to obtain the leading edge in a backscatter ionogram.

(1) NOAA Prediction

The NOAA predictions for November 1970 map F2(0)MUF and F2(4000)MUF which correctly interpolated in time and geographic location give $(fxF2)_{\perp}$ and fxF2 for a 4000 km path. The data can be read to perhaps $\pm$ 0.2 MHz for MUF(0)F2 and $\pm$ 0.5 MHz for MUF(4000)F2. MUF(D)F2 for distances D = 500(500), 2500 km is obtained from the mapped data by using a nomogram (see Davies, p. 292). In general, FOT = 0.85 MUF is recommended as optimum working frequency. To convert distances into time delay, we assumed a reflection height of 300 km; slight height changes do not alter the backscatter leading edge curve very much.

(2) Vertical Ionograms

The vertical ionograms obtained at Ava and U. I. can be converted into oblique ionograms using transmission curves based on N. Smith's method for selected distances 500 (500), 3000 km. The method is based on a curved earth and curved ionosphere. The abscissa is a linear frequency scale (MUF) and the ordinate is virtual height, the foF2's are computed and are curving to the right. This "inverted" transmission curve, introduced by Möller, is found more advantageous than the usual transmission curves. For this system the high ray is parallel to the foF2 lines and permits to determine the nose frequency very accurately.

The oblique ionogram was constructed for each vertical incidence ionogram. The nose frequency and the peak altitude were read off. To correct for the extraordinary component, we added $\Delta f = JF(x) - JF(0)$ from Figure 4.21 from Davies' book. The correction is small.

Next, we convert altitude of MUF into time delay. Thus, we obtain MUF(D)F2 and time delay for each selected distance and enter it into Figure 3.25.

(3) Transponder Data

For the transponder and forward oblique transmissions, the time delay has been converted to altitude of reflection, again for the ordinary component. Plotting the data into a transmission curve for D = 1120 km allows us to read the frequencies $fo_{\perp}$ and virtual height h' of the corresponding, but hypothetical, vertical incidence ionogram. Such data ($f_{\perp}$, h') are then used for other distances to obtain MUF's for 500(500) 3000 km. We read off the $fo_{\wedge}$ and h' and correct $fo_{\wedge}$ to $fx_{\wedge}$ and h' into time delay as described above for vertical ionograms. The resulting values for MUF(D)F2 are entered in Figure 3.25.

4.0 AZIMUTHAL DISTRIBUTION OF RADIO NOISE

4.1 INTRODUCTION

This chapter presents the preliminary results of an experiment which utilized a Wullenweber antenna array to study the directional properties of received ionospherically propagated radio noise in the HF band. The most notable work on HF radio noise, by W. Crichlow and R. Disney is summarized in CCIR. 322, which is the standard method of predicting radio noise levels. But this work, as most other since, has been conducted with omnidirectional receiving antennas; the asymmetrical azimuthal distribution of terrestrial sources of broadband radio noise (primarily thunderstorm centers) and of the ionospheric propagation medium are, however, likely to result in a variation of received noise power as a function of azimuth, and diurnally on a fixed azimuth. The experiment was intended to verify this hypothesis, and although the data sample is quite limited, illustrate the usefulness of a circular antenna array for gathering the data required to develop a model of the azimuthal properties of radio noise.

4.2 DATA ACQUISITION

The WWV transmissions from Ft. Collins, Colorado on 5, 10, 15, and 20 MHz had, until recently, a silent (off) period of 4 minutes each hour, commencing at 45:15 after the hour. Radio noise measurements were made in the internationally protected guard frequency bands during

the silent period. Twelve discrete azimuths spaced 30° apart were sampled each for 16 consecutive seconds. The width of the azimuthal sector is determined by the Wullenweber antenna 3 dB azimuthal beam-width, which was, for the frequency discussed in this chapter, 6-8 degrees. The envelope detected receiver output was digitized and stored on digital tape for the processing operations described herein. The data acquisition system is shown in Figure 4-1.

The observations presented were made on a frequency of 10.004 MHz between 2245 UT, 11 December 1970, and 1345 UT, 13 December, 1970.

4.3 DATA ANALYSIS

The average noise amplitude was determined from the data collected for each hour. Following the lines of previous investigators of omnidirectional radio noise, the data were grouped into six time blocks per diurnal period and a composite average over two diurnal periods for each block was obtained. The results are given in Figure 4-2. The azimuthal distribution as seen in the Figure does tend to be asymmetrical. This asymmetry is seen to occur primarily in the early evening hours with the greatest noise levels experienced in the direction of South-Southeast. From Figure 4-3, it can be seen that thunderstorm centers in South America and Africa could be the source of the noise received at Illinois. Also, from Figure 4-3, there are no principal thunderstorm centers to the West and the noise levels to be expected from this direction should be below that of the South-Southeast providing that propagation conditions are nearly the same. Figures 4a and 4b present the hourly distribution of noise

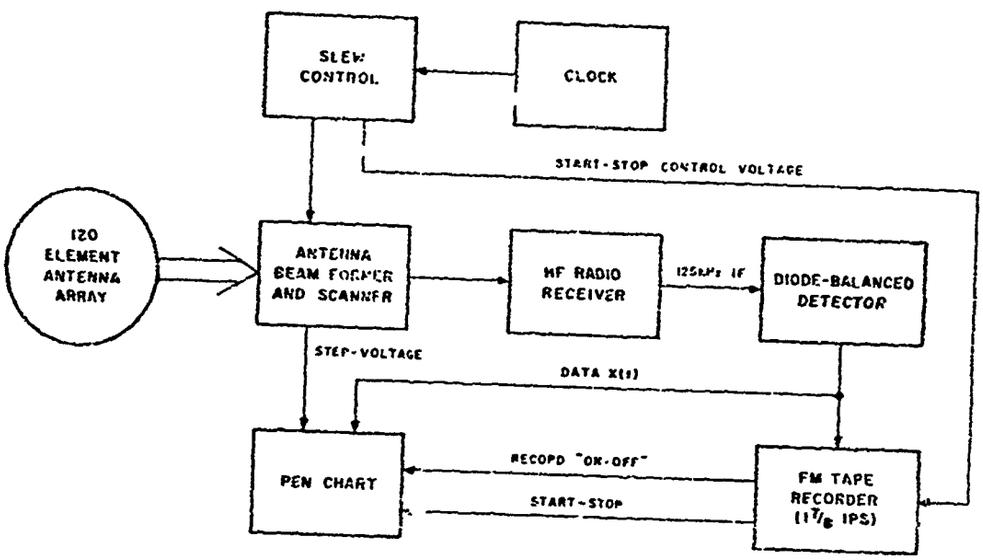

Figure 4-1. Data Collection System.

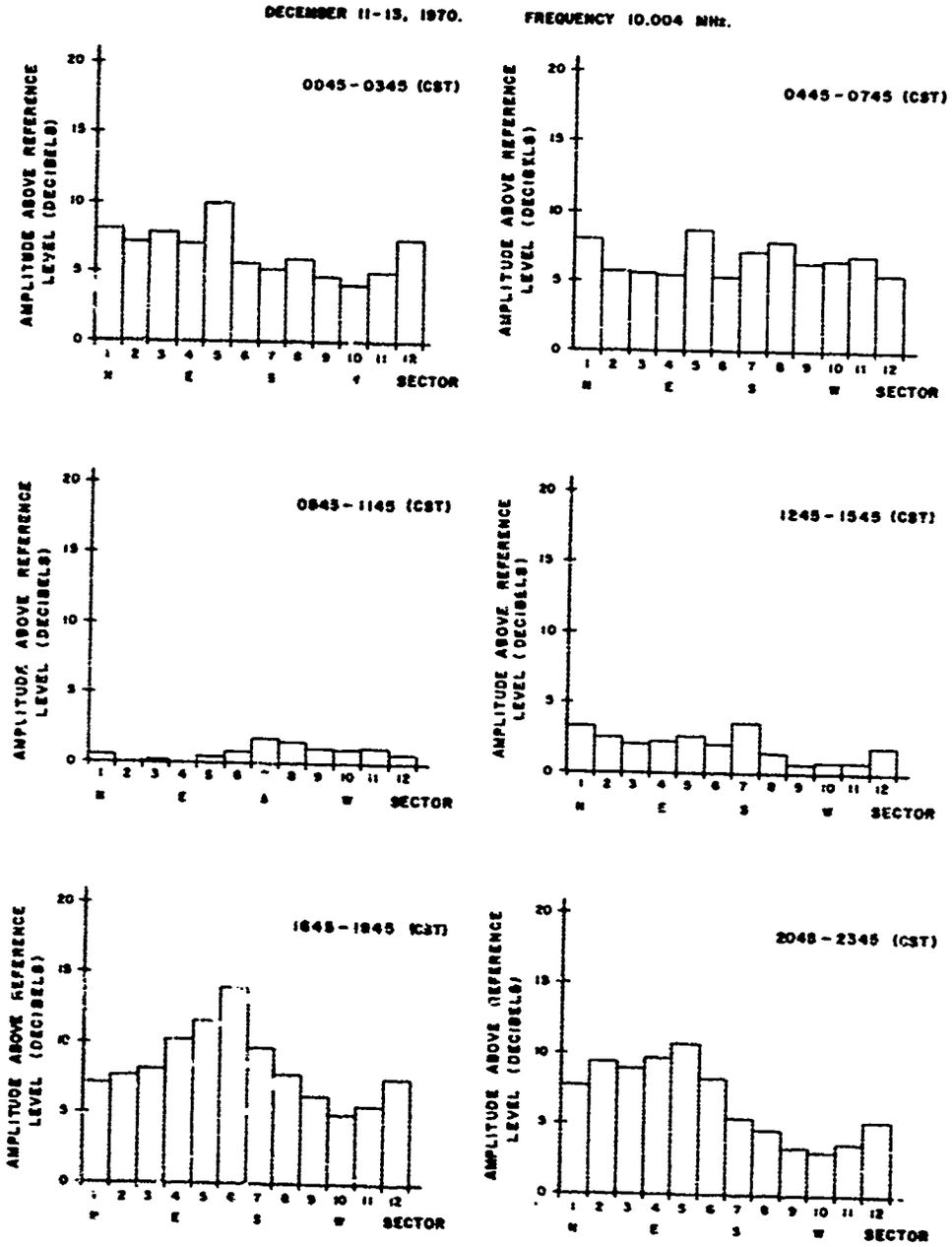

Figure 4-2. Sector Average Amplitude.

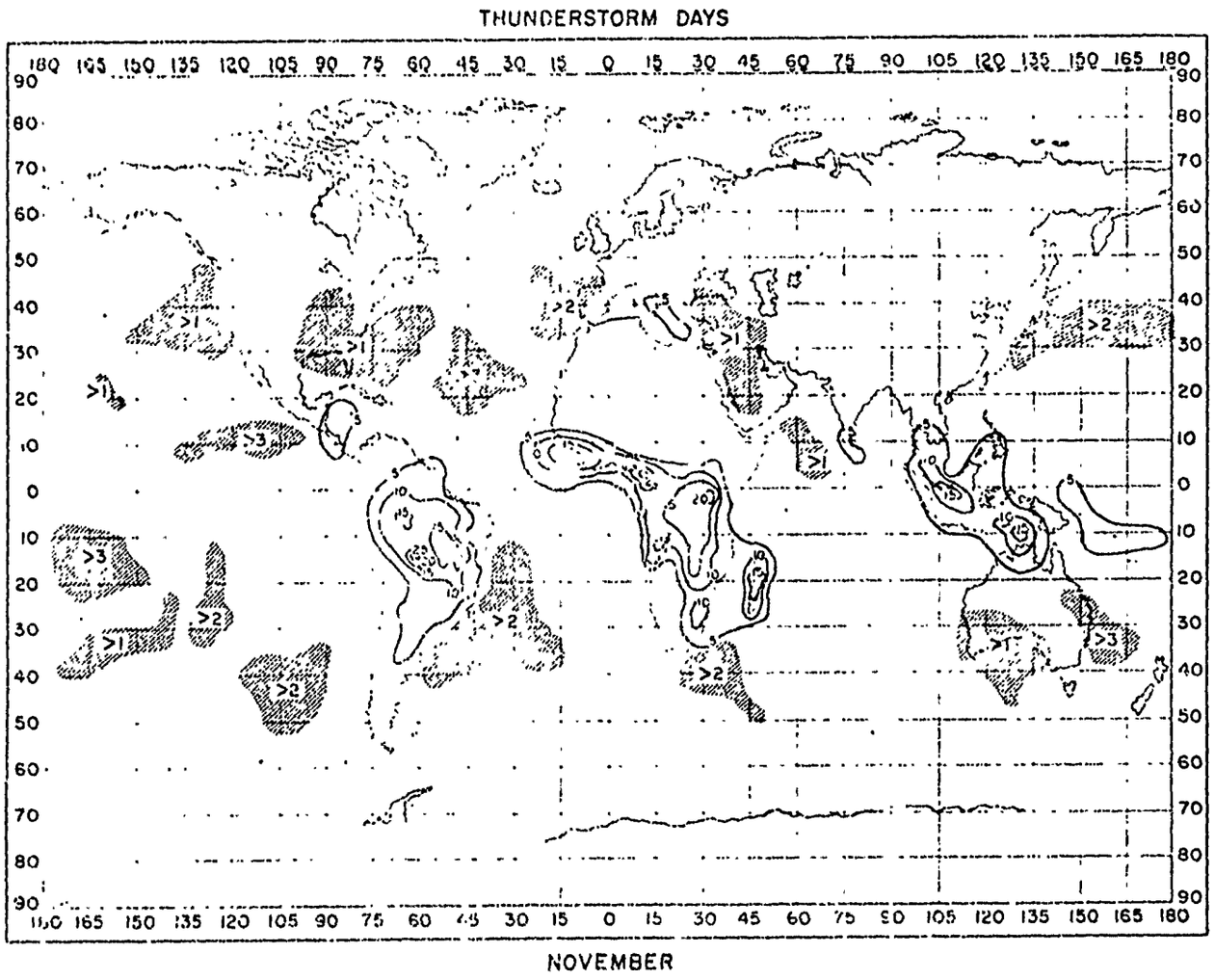

Figure 4-3. Frequency of Occurrence of Thunderstorms Throughout the World for November.

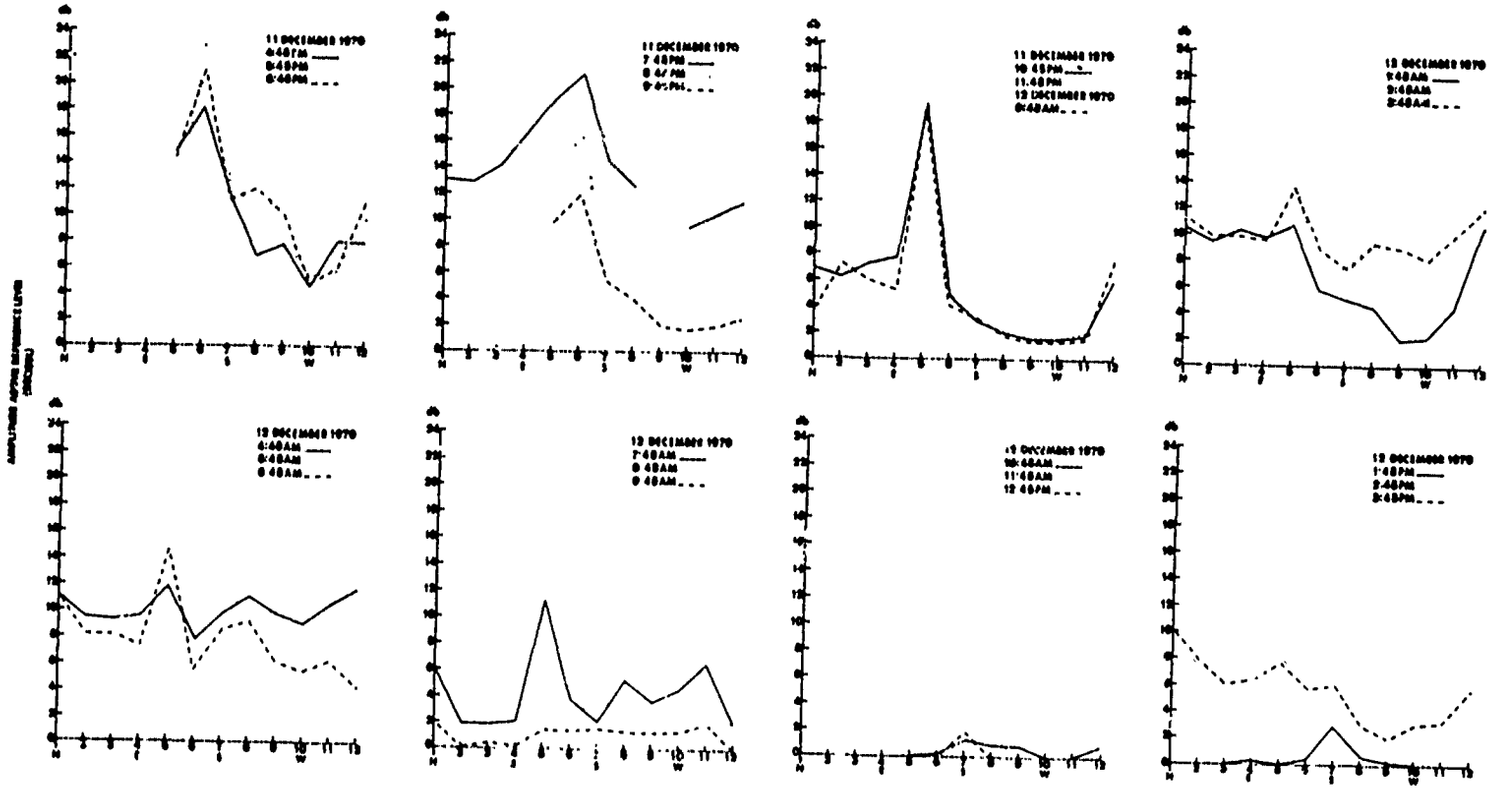

Figure 4-4a. Hourly Distribution
1645 11 December 1970 -
1545 12 December 1970.

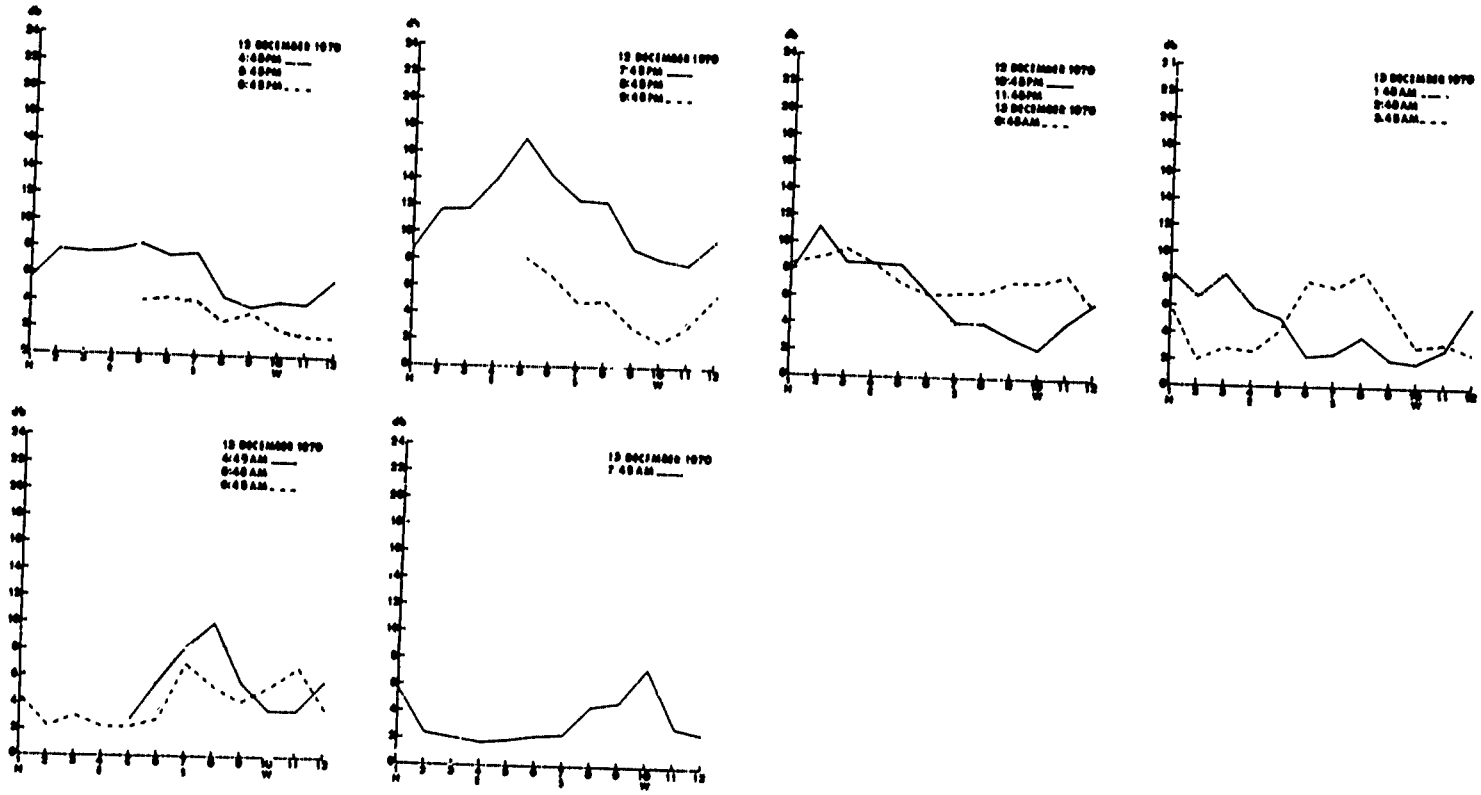

Figure 4. 4b. Hourly Distribution
1645 12 December 1970 -
0745 13 December 1970.

where the average hourly value for each sector has been plotted versus the corresponding sector.

Figure 4-5 is a plot of the average amplitude versus time. Variations in the hourly amplitudes require a departure from the usual averaging techniques and to consider the amplitude on an instantaneous basis to explain the characteristic seen in Figure 4-5. In the analysis, the noise sources were assumed to be distributed throughout each of the sectors. If the noise sources are uncorrelated, the noise power observed will be the sum of the powers of the individual sources. Therefore, a decrease in the measured noise amplitude in a sector may be the result of a decrease in sources (thunderstorms) or the result of the ionosphere no longer supporting propagation from areas of the sector. The question of which of the two choices is correct is a fundamental one if a predictive model of expected noise for a sector is to be developed. The latter choice was pursued in further analysis of the data. Skip distance, MUF, and absorption effects were considered and efforts made to correlate the time variation of these phenomena with characteristics of the data.

The analysis considered each sector as encompassing an area determined by the beamwidth mentioned above and having an 8000 km two-hop length. Using the ESSA predicted mean value of MUF for a 4000 km path during December, 1970, the minimum MUF for each sector was determined at two-hour intervals and plotted on the same time scale as the average hourly noise amplitude. Also, using vertical incidence

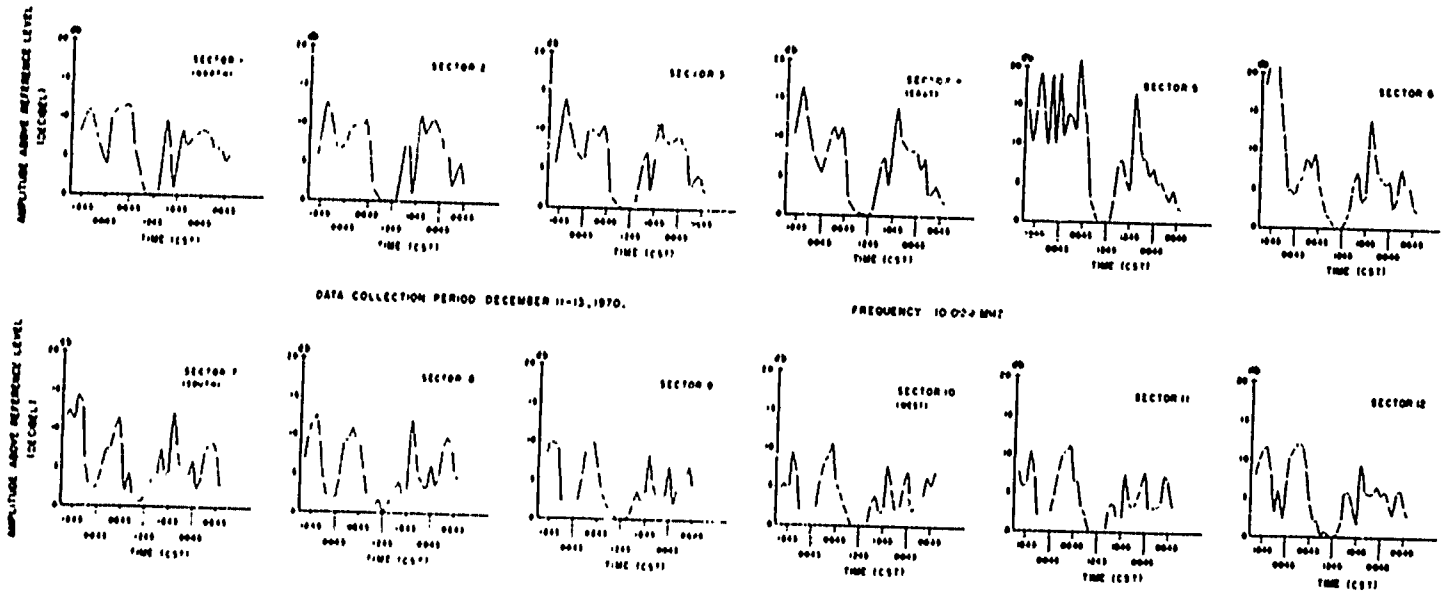

Figure 4-5. Sector Hourly Amplitude

ionograms made at the receiver site during the time of the experiment and assuming a plane-earth-plane ionosphere approximation, the skip distance was determined as a function of time and plotted on the same time scale as the average amplitude and minimum MUF. Figure 4-6 gives the results for four of the twelve sectors. The decrease in noise amplitude at approximately 2300 is seen to correspond to periods when the maximum MUF is at or below 10 MHz. That the curves do not match exactly may be the result of using median values rather than actual values of the minimum MUF. This decrease in amplitude is characteristic of all twelve sectors as shown in Figure 4-5. The skip distance effect can be seen in Figure 4-6 as a continued decrease in noise amplitude after the minimum MUF has increased above 10 MHz near 0300, 13 December in sectors 1 and 4. Sectors 7 and 10 indicate that an increase in skip distance does not cause a corresponding decrease in amplitude, possibly due to the major sources being located outside of the skip distance. None of the sectors indicate a relationship between skip distance and amplitude on December 12. This may be the result of a local disturbance. The significant decrease in noise during the day can be attributed to non-deviative absorption in the D layer. Careful analysis of Figure 4-5 indicates a more rapid decrease in amplitude for sectors to the sunrise side of the receiving site than for sectors 180 degrees away. Recombination in the D region is rapid and, therefore, the ionization density and the resulting absorption varies in synchronism with the elevation of the sun.

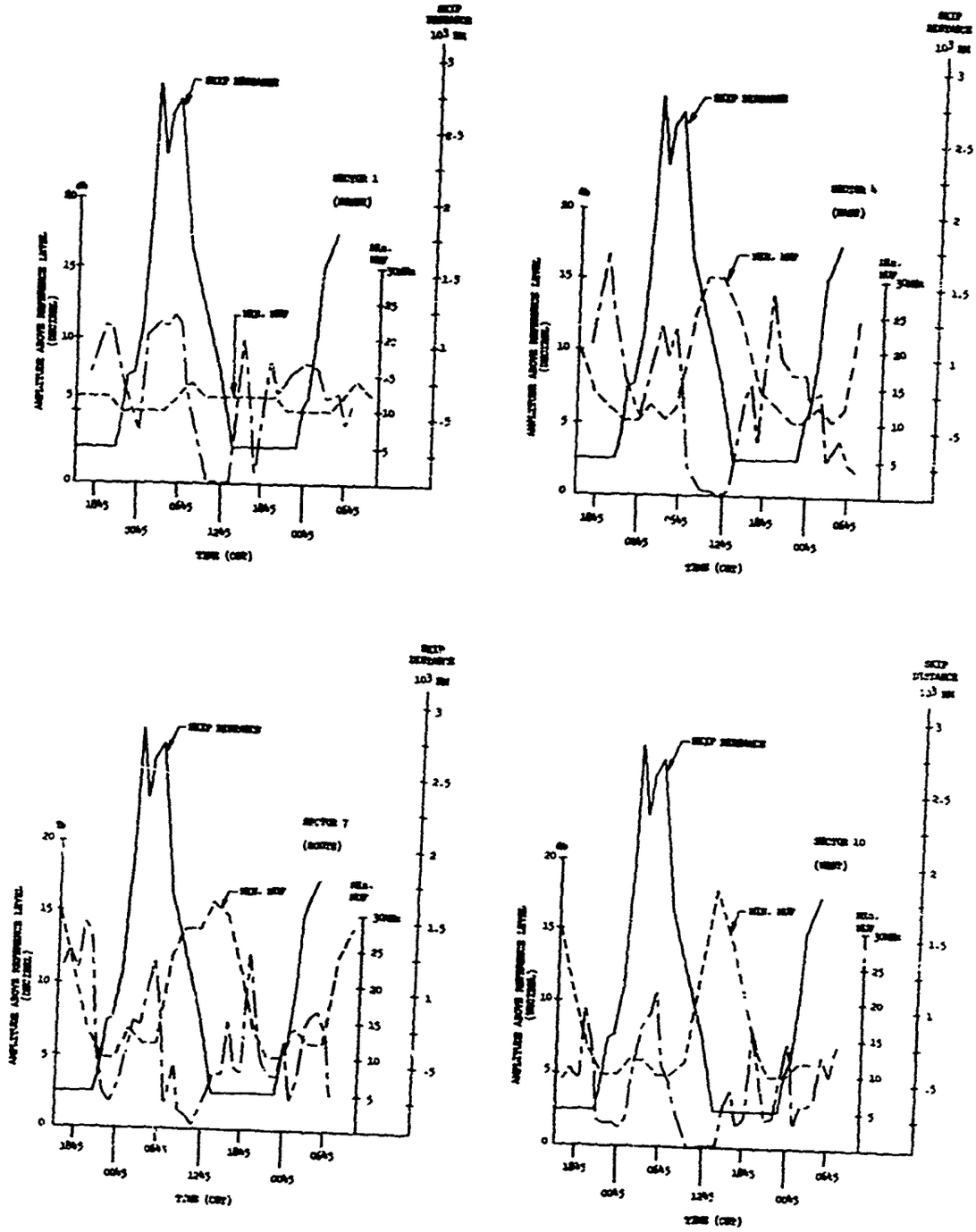

Figure 4-6.
Comparison of Radio Noise Levels and Propagation Factors.

4.4 SUMMARY

From the data presented here, there does appear to be an asymmetrical distribution of noise in the HF band. When considered on an instantaneous basis, the difference in peak and minimum levels may be as large as 10-15 dB. Averaging the small amount of data used in this investigation tends to underemphasize the extreme differences in distribution, but the general characteristics of the noise level characteristic are retained and follow what would be expected from propagation conditions and source locations. In the preceding analysis, ionospheric effects were primarily considered in explaining the variation in noise level as a function of time. A complete analysis of the noise data would require a more comprehensive knowledge of source variation with time and direction.

5.0 Further Aspects of the Backscatter Illumination Control Problem

There are still a number of unknowns in the problem of optimally illuminating OTH ground targets with an hf backscatter radar system. If one considers as optimum the placing of maximum possible energy on the target at the range of interest, then the usual algorithm is to select that frequency whose minimum time delay echo shows an apparent ground range slightly shorter (or closer) than that of the suspected target. This may ultimately turn out to be the recommended approach for all but the most sophisticated field operations, but there are some uncertainties which should be investigated to insure that the above procedure can be used with the requisite degree of confidence.

5.1 Conversion of Time Delay to Ground Range

The first problem arises in the conversion of time delay measurements into ground ranges, or, more typically, "calibration" of the leading edge of a wideband backscatter sounding in terms of ground range. The simple, straight line ray path geometry technique is well understood, and has been illustrated in detail in a recent Avco report.[1] The basic tool is a graph of the type shown in Figure 5.1. Time delay values scaled from the backscatter sounding are entered into the graph on the ordinate, and the appropriate ground ranges are determined by using the proper parametric virtual reflection height curve.

The problem lies in selecting the "proper" virtual height value. When using a graph of this type, one typically selects a single

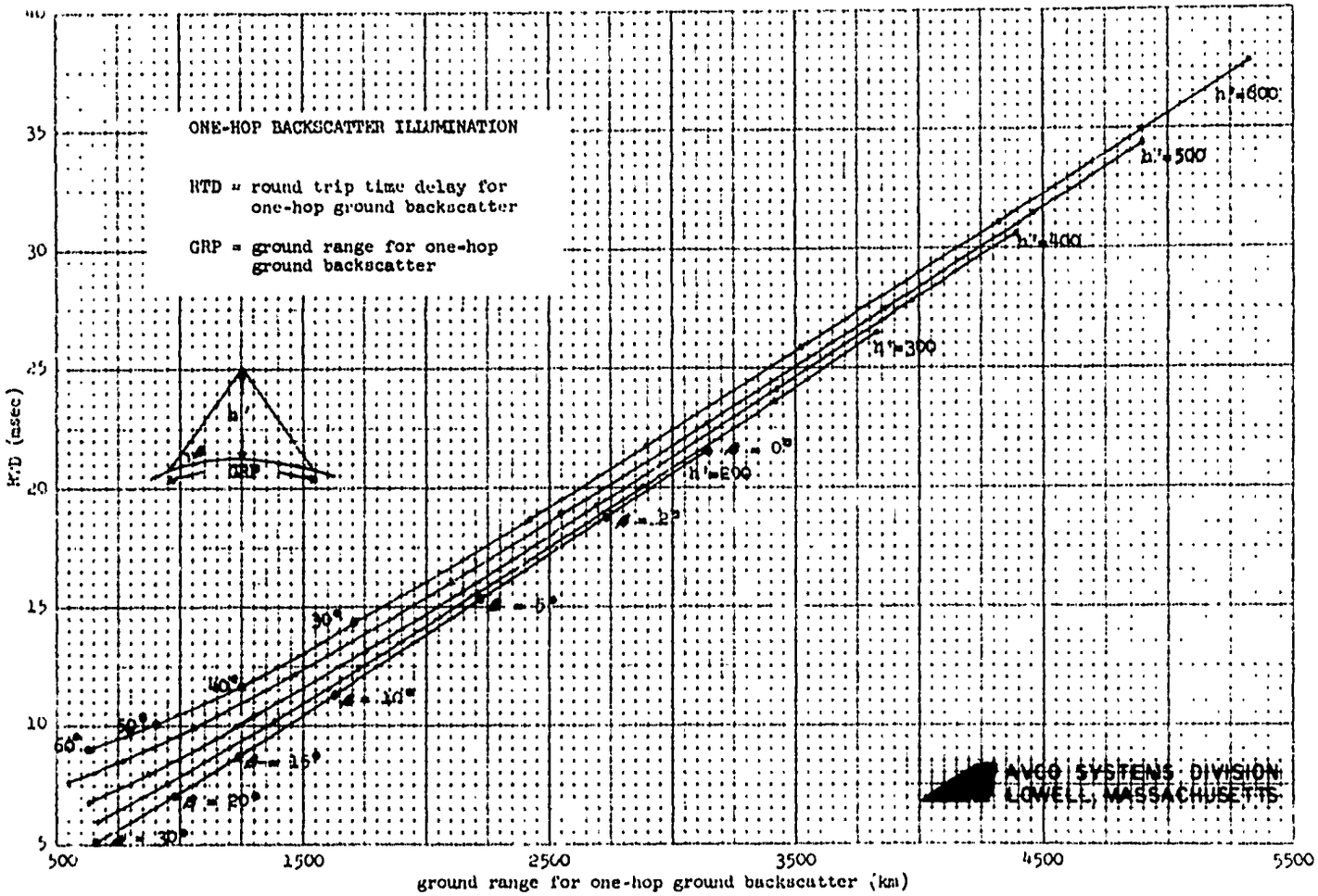

Figure 5-1. Ground Range vs. Time Delay for One-Hop Ground Backscatter

characteristic virtual reflection height for all propagation paths. This is a reasonably good assumption when the vertical electron density profile shows a high vertical gradient of increasing density with height (i. e., the profile exhibits a flat bottom shape), but the question remains as to the degree of uncertainty introduced by this approach. Clearly, also, the assumption of a single value is not warranted at times when the ionosphere cannot be assumed to be spherically concentric to at least a first order of approximation.

If no real-time vertical incidence sounding data is available, then one must simply postulate a reasonable virtual height value (e. g., 200 km during the day) and perform the conversion in faith. An idea of the uncertainties this introduces can be gained by examining the spread of ground ranges for any given time delay value in Figure 5. 1, as a function of reflection height. At 19 msec, for example, ground ranges between 2480 and 2770 km obtain for virtual heights between 200 and 600 km. Thus, for a fixed time delay value, a 50% uncertainty in reflection height (about 400 km) produces a 15. 5% uncertainty in associated ground range. Clearly, the conversion is relatively insensitive to height uncertainties for situations not involving focusing. We will see later that this is not the case for the time delay focused leading edge of the backscatter, however. Note in the graph, also, that ground range uncertainty decreases with increasing distance.

If a local (overhead) vertical incidence ionogram is available, then one may select a virtual height value from the lower portion of the F-region trace. In this case, a further improvement may be made by using the

entire vertical incidence trace in a computerized reflectrix ray-tracing program, if this is available to the user. Even then, however, the calculation of ground ranges from time delay observations is still approximate to the extent that the local vertical incidence ionogram may not be representative of the intervening ionosphere cut at the one-hop reflection region where the analysis is actually appropriate.

5.1.1 Analysis of the Backscatter Ionogram Leading Edge

When conducting an analysis of wideband backscatter soundings, the most common test of the appropriateness of the ionospheric model being employed (to relate time delay to ground range) is whether or not the skip-focusing return observed on the ionogram can be reproduced by minimum time delay calculations through the model over the range of observed frequencies. This frequently turns out to be difficult to achieve particularly at the longer delay times. The purpose of this section is to show that the shape of the backscatter leading edge (variation of time delay with frequency) is strongly dependent on the spatial variation of foF2, and the height of the layer peak, along the sounding path. It is suggested that time delays to ground ranges interior to the skip zone are relatively independent of reflection height, as was demonstrated in the previous section in conjunction with Figure 5.1

Croft has shown[2] that if the height and maximum density of a spherically concentric model ionosphere are kept constant, the leading edge of the simulated backscatter ionogram will remain virtually unaffected by a

wide range of variations in the underlying ionization structure below the F peak. Increases in the height of the layer peak produce increases in the delay time to the leading edge at the higher frequencies, however.

Hatfield[3] has demonstrated that foF2 values at remote points in the illuminated backscatter region may be estimated with considerable accuracy by a sophisticated analysis of the backscatter leading edge. He assumes a fixed height and semi-thickness for a parabolic F layer model, and iteratively derived foF2 values (for the midpoint of the one-hop executed to the skip zone) from the time delay at each frequency.

These results suggest the spatial variation of the F region peak density and its height are the determinants of the shape of the time-focused return at the leading edge of the ionogram. We decided to investigate more thoroughly the influence of the height of the ionosphere peak density on the backscatter ionogram leading edge, since heights seem to be the most difficult parameter to estimate for model purposes or to derive from the observed data.

5.1.2 The Effects of Ionospheric Model Heights on Leading Edge Simulations

A simple analysis of this problem was carried out with quasi-parabolic[4] models of the ionosphere, which allow the pertinent propagation parameters to be written as closed form, analytic equations. Typical propagation conditions were simulated, and the effects of uncertainties in the height of the F layer maximum on the calculations of minimum ground range and the range at minimum time delay, as a function of frequency, were investigated.

Figure 5.2 shows the basic plot of minimum ground range versus layer maximum height, for an operating frequency 2.25 times that of the vertical incidence critical frequency. (The quasi-parabolic formulation allows the frequency dependencies to be expressed parametrically in terms of this ratio). The base of the quasi-parabolic ionospheric layer is set at 100 km height, and the maximum at 200 km; variations of $\pm$ 10% in the latter parameter are considered. Each point on the curve represents an independent re-determination of the minimum ground range for that height value. Note that the variation of minimum ground range with layer maximum height is linear over the 200 km range of variation shown here.

Figure 5.3 shows a similar plot of the variation of minimum group path (time delay), and ground range of the minimum group path ray, over a $\pm$ 10% range of layer maximum height values. Here again, each point represents an independent re-determination of the minimum group path value for the particular height value, and the two curves are basically linear. Note that the ground distance pertinent to the minimum time delay (skip-focused) ray is some 70 km greater than the actual minimum ground distance illuminated for these propagation conditions. This is a well-known phenomenon explained by Peterson in his early backscatter investigations[5], and should not be ignored in backscatter illumination control analysis.

Figure 5.4 shows the results of the two previous graphs replotted in terms of percentage variations. Again, over a $\pm$ 10% range of variation in the layer maximum height, the variations of minimum ground distance,

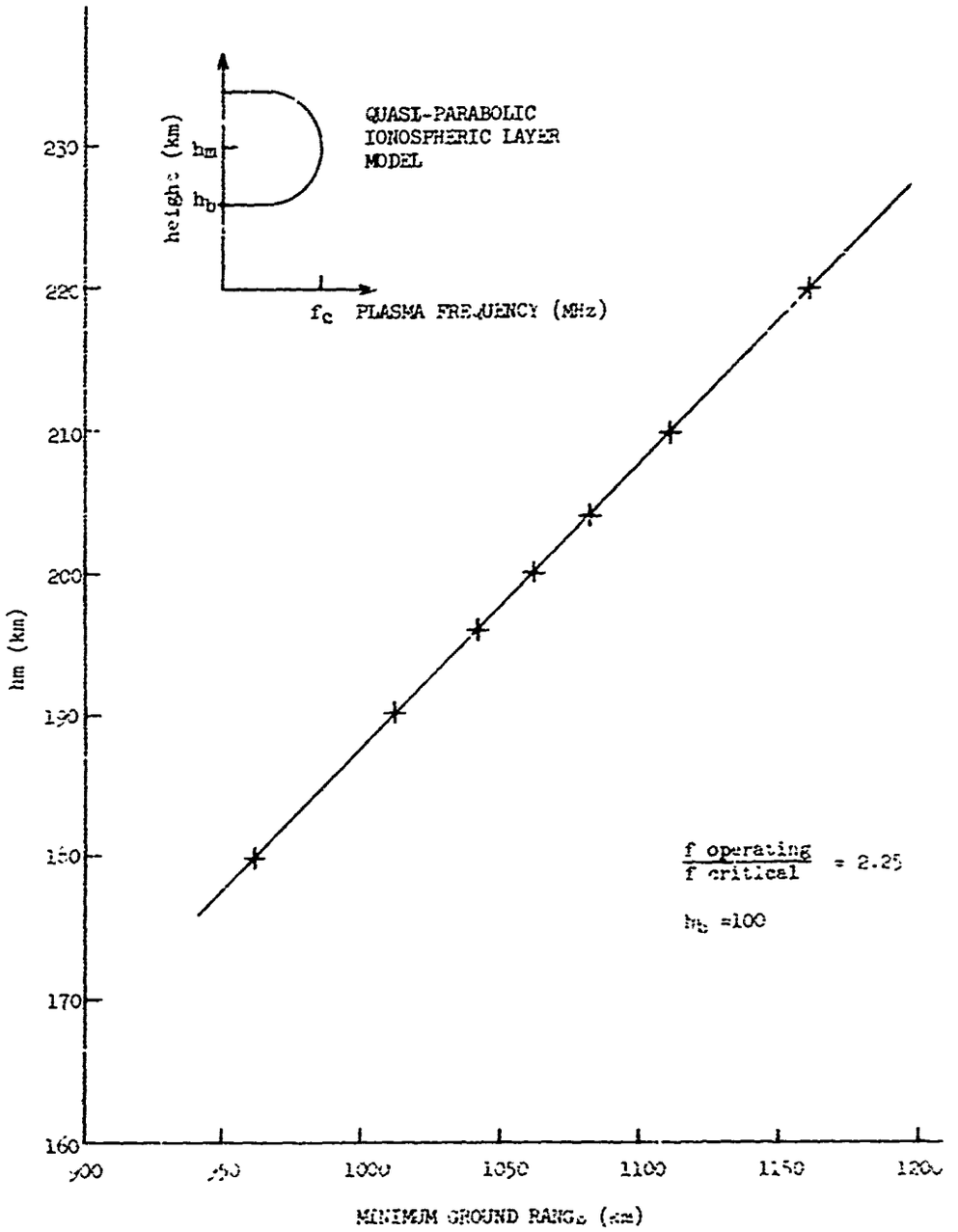

Figure 5-2. Calculated Minimum Ground Range as a Function of Layer Maximum Height

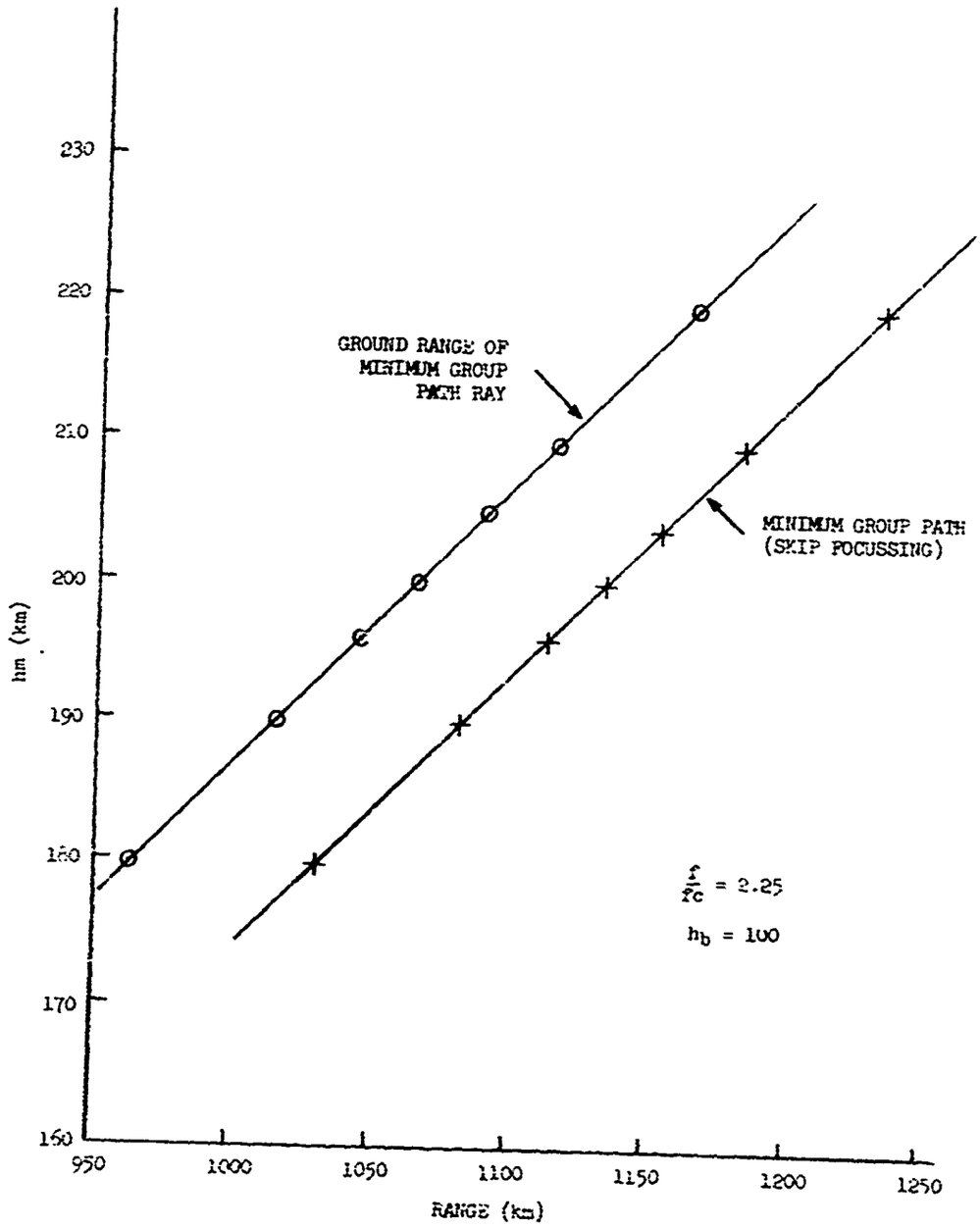

Figure 5-3. Calculated Minimum Group Path (and Associated Ground Range) as a Function of Layer Maximum Height.

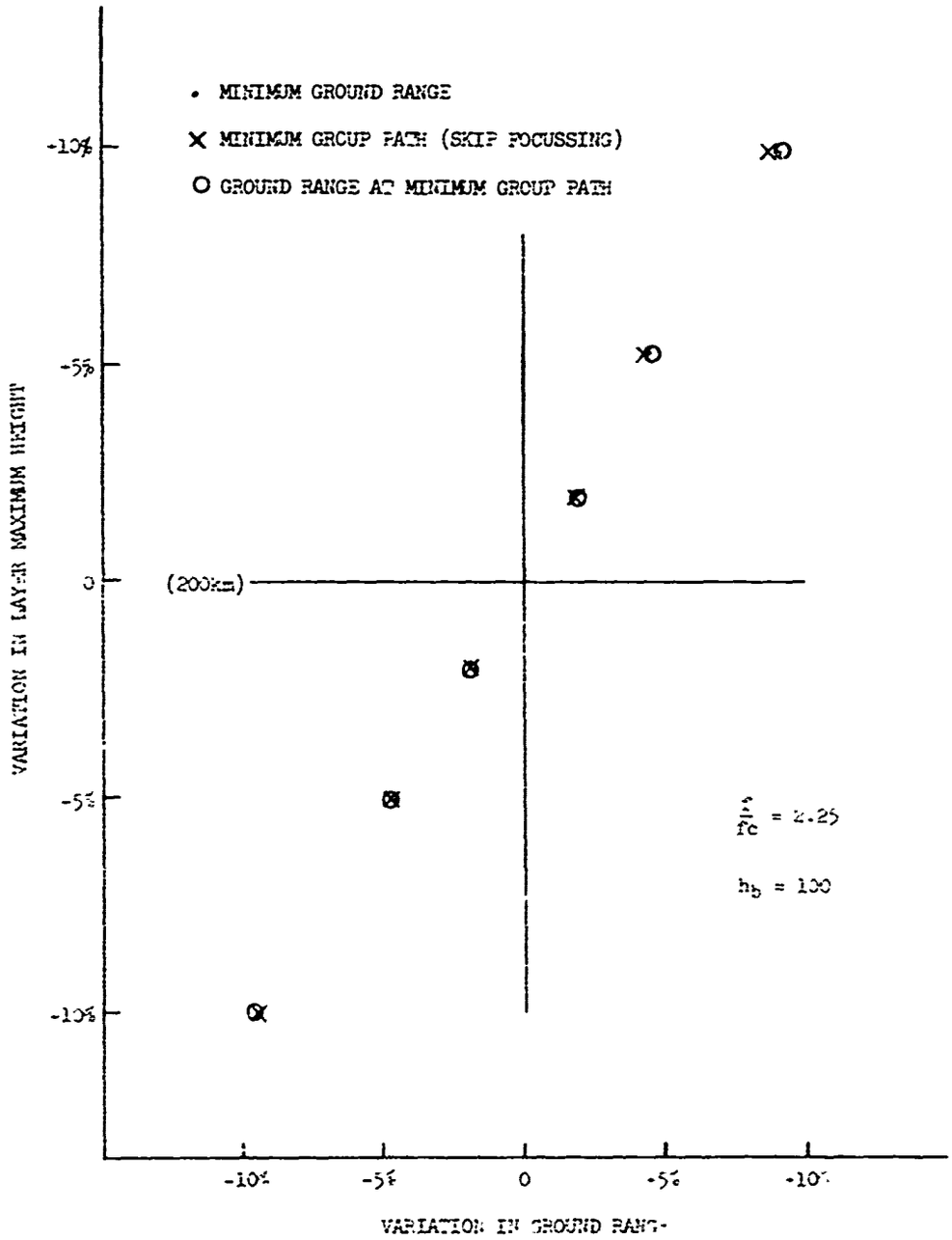

Figure 5-4. Uncertainty in Ground Range and Group Path as a Function of Uncertainty in Layer Maximum Height.

minimum group path, and ground range at minimum group path, are essentially linear. Note that they all have the same slope, and that an X% uncertainty in the height parameter produces approximately an X% uncertainty in the distance parameters. It should be pointed out that this result was derived with an operating frequency 2.25 times the vertical incidence critical frequency, and for an essentially thin ionosphere at relatively low heights.

Similar calculations were done for all of the following ratios of operating frequency to critical frequency: 1.25, 1.50, 1.75, 2.00, 2.25, and 2.50. The percentage uncertainty graphs were remarkably similar for all these cases, with the lower frequencies showing slightly more disparity between the individual slopes of the three curves, and with a distance percentage variation remaining related on a one-to-one basis with the height percentage variations.

The same analysis procedure was carried out for a thicker ionosphere layer, with unperturbed maximum height of 300 km and the base at 100 km. The results for this model are given in Table 5.1. Here it can be seen that the uncertainties in ground range are slightly less than those in maximum layer height, but still of the same order. Note that the difference between the minimum ground range, and the ground range at the skip focusing point (minimum time delay) becomes negligible for the longer ranges and higher frequencies.

TABLE V.1 - Calculation of Uncertainties in Range Introduced by Uncertainties in Layer Maximum Height

$\frac{f}{f_c}$ *	Minimum Range (km = 300)	Minimum Group Path (km = 300)	Range at Minimum Group Path (km = 300)	(% Δ D) =
1.25	662 km	784 km	685 km	.95(%Δh_m)
1.50	887	963	877	.90(%Δh_m)
1.75	1071	1157	1077	.85(%Δh_m)
2.00	1290	1369	1294	.80(%Δh_m)
2.25	1532	1609	1535	.80(%Δh_m)
2.50	1811	1888	1812	.85(%Δh_m)

* Quasi-parabolic ionosphere model

h_b = 100 km, h_m = 300 km $\pm$ Δh_m

The implication of these simulation results is that uncertainties in the estimation of reflection heights at path midpoints produce equivalent uncertainties in the estimation of ground range for the skip focusing region at all frequencies of interest. This supports quantitatively the implications drawn from the limited findings of Croft cited earlier. Thus, the difference between 200 and 300 km virtual height can be very significant in predicting the location of the skip focusing region on the ground, even though it may be of little consequence in deriving the ground range for time delay points at delays beyond the minimum at any particular frequency of operation.

5.1.3 Range/Time-Delay Calculations for a Particular Backscatter Ionogram

This point is illustrated by the analysis of an RADC Ava-Stockbridge FM/CW backscatter ionogram presented in a previous Avco report on this program.[1] A tracing of the record, taken at 2137 UT looking west on 19 January 1970, is reproduced here in Figure 5.5. The solid lines represent the actual observed returns, with the nearly-constant-range returns from a number of the large single scatterers identified as to suspected city of origin. The local vertical incidence x-trace was scaled and entered into a reflectrix ray-tracing program employing straight-line raypath geometry. The program utilized the reflectrix model to calculate the return trace for a scatterer located at the nominal range of Chicago, and the result is shown as the round dots, clearly matching the observed return.

Being confident of the identification of this return (which is consistently seen on west-looking ionograms taken from Ava-Stockbridge), its

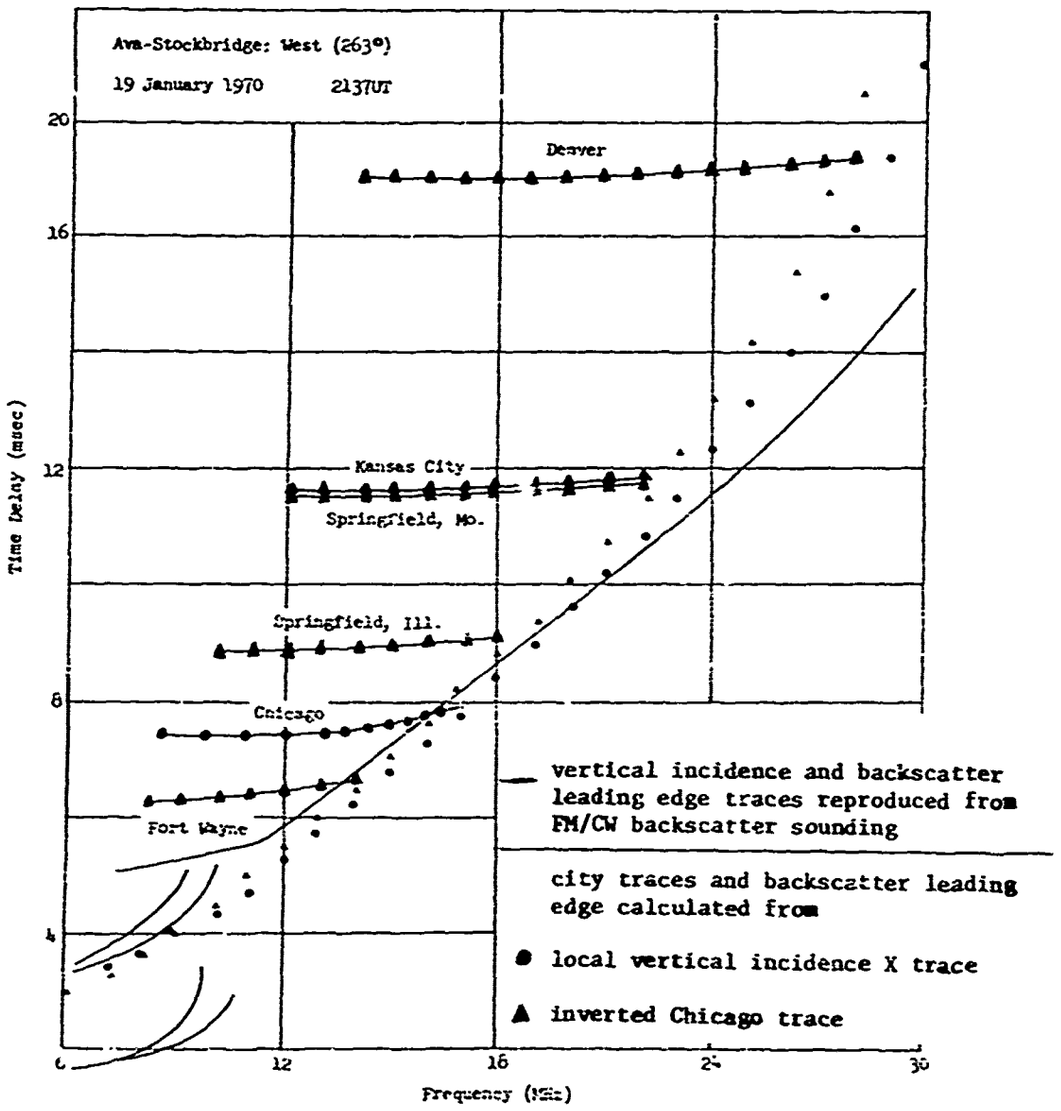

Figure 5-5. Reflectrix Analysis of FM/CW Backscatter Ionogram Constant Range Traces and Leading Edge.

time delay vs. frequency was scaled and entered into the reflectrix program in the oblique ionogram mode. The oblique return was inverted into a model of the effective intervening vertical incidence ionosphere, and the time delay vs. frequency shape of returns from ranges equivalent to the cities listed in the figure was calculated. The results are shown as solid triangles, and clearly match observed traces extremely well.

In order to further test this procedure, the reflectrices derived from both the local vertical incidence trace and the inversion of the Chicago echo were used to calculate the minimum time delay versus frequency leading edge for backscatter propagation through the two representations of the ionosphere. The results of this exercise are shown as the solid dots and triangles along the actual leading edge trace. The two derived leading edges do not match the observed trace except in the 8 to 10 millisecond delay region.

The point of this exercise is to note that even the crude propagation model employed in this analysis provided excellent conversions between time delay and ground range for ground points located interior to the skip zone, but provided only a poor representation of the time delay to the skip zone itself. It has been previously suggested that this discrepancy could be explained at the longer ranges by the fact that an uncorrected Secant Law was employed in the reflectrix manipulations, but this does not seem to have adversely affected the calculations of time delay for the Denver echo. A more likely suggestion is that neither the local vertical incidence ionogram nor the inverted Chicago echo provide an adequate vertical incidence

representation of the ionosphere at the longer ranges. And since the Denver return is matched so closely, it is most likely the ionospheric features near the peak of the layer which are different at the longer ranges, producing the leading edge mismatch.

5.2 Skip Region Measurements

A second problem in optimally illuminating a specified range of interest concerns the actual character of the energy distribution over the ground in the skip zone, as a function of range, frequency, ionospheric conditions, etc. Although this can be calculated theoretically,[6,7] there remain a number of questions concerning what physically occurs.

1. What is the nature of the build-up of energy with increasing range, as one approaches the skip zone from shorter ranges? What is the rate of decrease of incident energy with increasing range as one moves through the skip zone to longer ranges?

2. To what extent is energy actually focused in the skip zone? What is the range depth of the skip region?

3. Can you actually see the low ray, high ray interference effects in the skip zone, and how severe is the destructive interference?

If the width of the focusing region is narrower than the uncertainty of range estimation inherent in the conversion of time delay to range, then its focusing cannot be depended on to enhance illumination on the target with any degree of reliability. If the interference fringing in the focused region is severe, then it is also unacceptable to use this region for enhancing target illumination.

Any investigation of these problems requires an empirical approach, but making adequate measurements to answer these questions is difficult, and the results are further complicated by polarization phenomena. One approach is to make a fixed-frequency, time sequence of incident signal energy measurements at one location in the backscatter region during a period when the range of the skip zone is decreasing or increasing with time. The variation of energy with time is then related to the passage of the skip region over the local fixed receiving site.

Such an effort was conducted at the University of Illinois' Thomasboro site, during local sunrise, so that no signal was received in the beginning of the period, followed by the incidence of the focusing region. The signal strength variations were monitored on two cross-polarized log periodic antennas pointed toward RADC, where a 20 kw unmodulated cw signal at 15.043 MHz was being transmitted on the west-looking rhombic of RADC's Ava field site. The results are shown in Figures 5.6 and 5.7 along with a block diagram representing the instrumentation utilized to monitor the fixed frequency signal strengths*.

The initial onset occurring between 1224 and 1225 UT is seen to possess an increase in incident signal level of some 60 db over the background noise-plus-interference level previously existent. Classical Airy interference fringes appear simultaneously and in phase on the signals from the two cross polarized antennas until 1227, at which time the signal appears

*We would like to thank David Casavan, Raytheon Company, for these measurements.

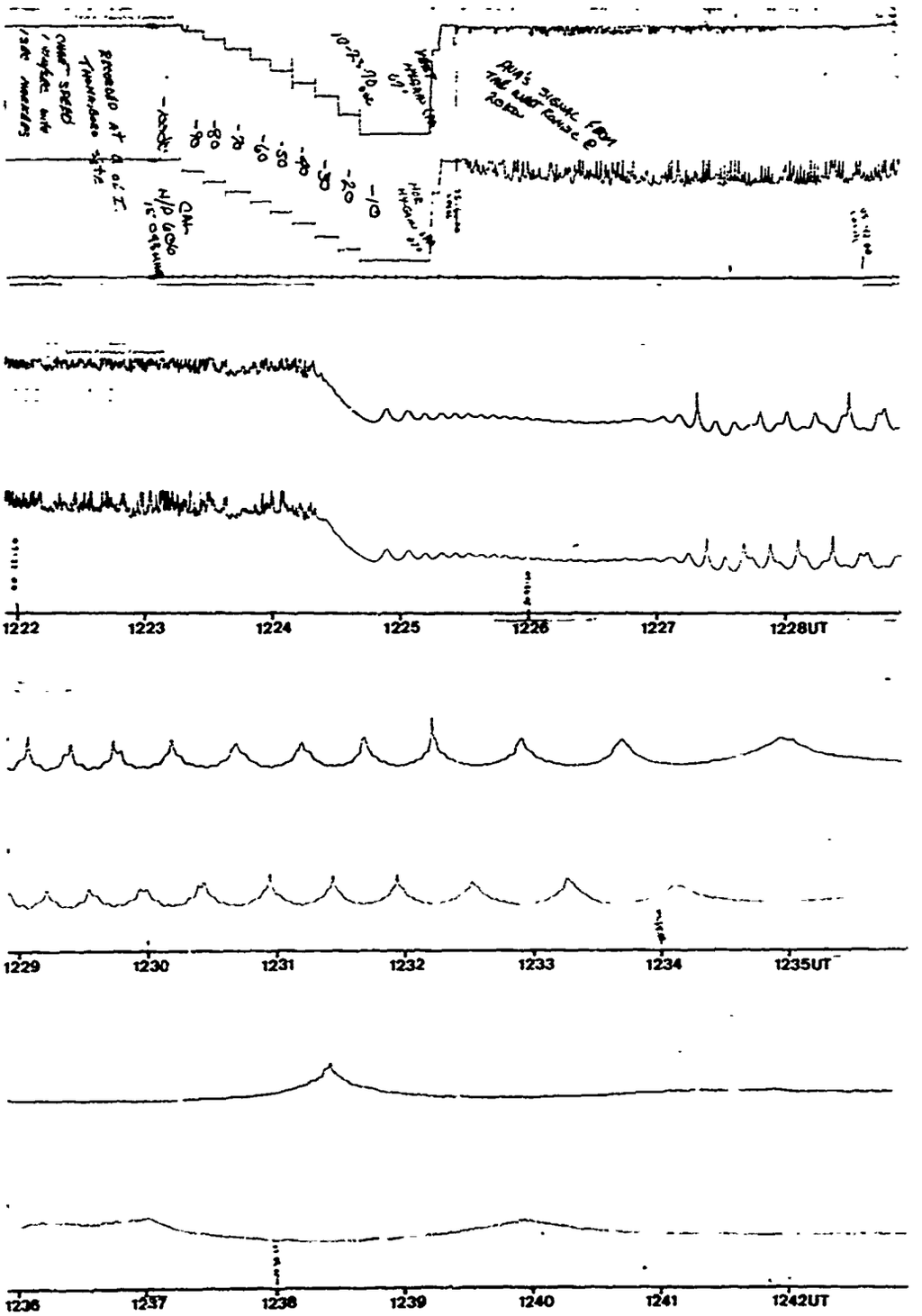

Figure 5-6. Signal Strength Levels in the Skip Zone, Received on Cross-Polarized Antennas.

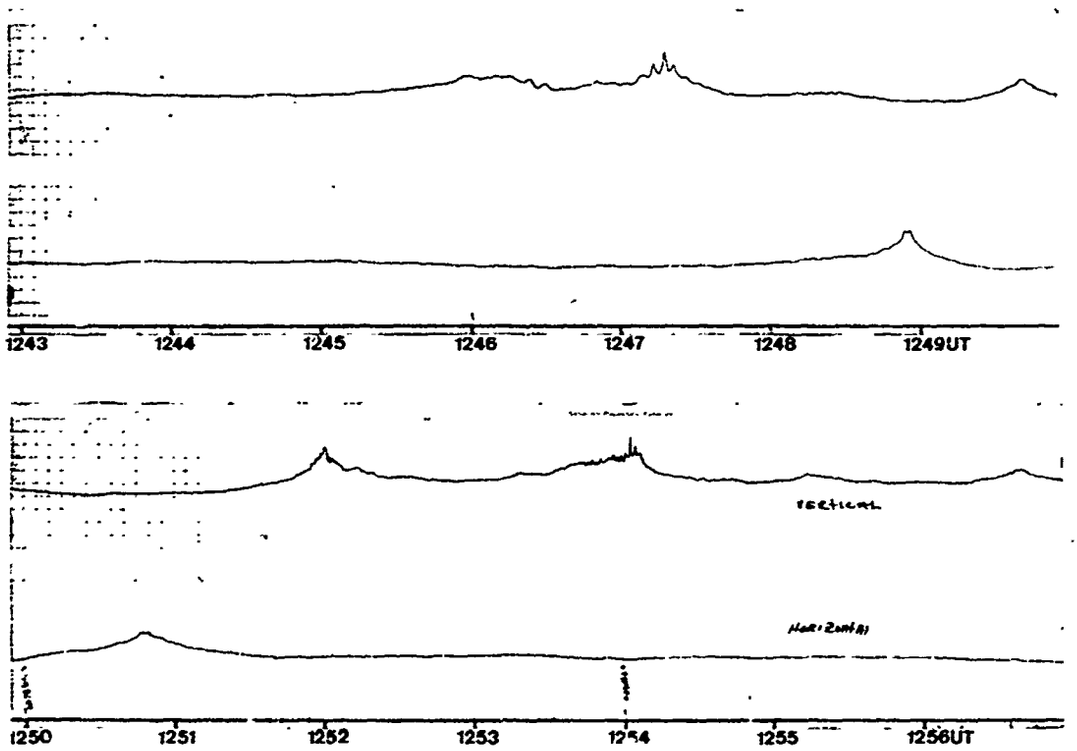

TUI EQUIPMENT FOR SKIP TEST

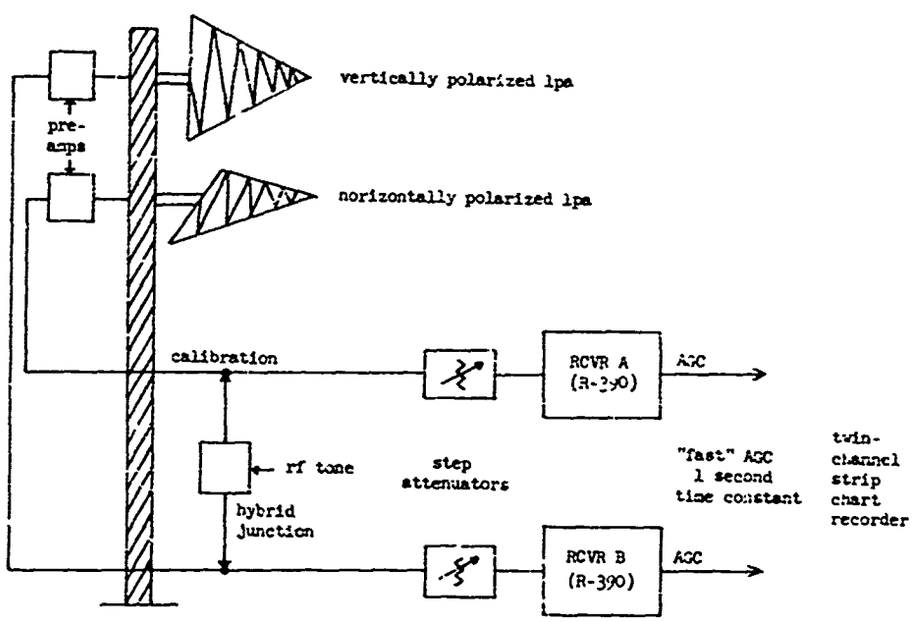

Figure 5-7. Signal Strength Levels Received in the Skip Zone with Cross-Polarized Antenna System.

to separate into low ray and high ray components, and polarization fading (clearly identified, because of the 180 degrees out of phase character of the two fading patterns) sets in. The peak signal level received on both antennas does not appear to diminish with increasing time.

What one would like to do is interpret this record in terms of the instantaneous distribution of signal energy over an extended range of ground distances from the transmitter, but this is extremely difficult during the sunrise period, since the ionospheric changes occurring as the sun illuminates the upper atmosphere appear earlier at higher altitudes and later at lower, etc. The resultant dynamic ionosphere of the sunrise situation is difficult to model and cannot be treated as a rotating "frozen" pattern. Thus, an effective range scale replacing the time abscissa of Figures 5.6 and 5.7 would be highly non-linear, and virtually impossible to determine.

The fade depth prior to the onset of the polarization fading after 1227 is less than 10 db in the Airy interference fringe region. During the high ray, low ray polarization fading period, the fade nulls are typically about 20 db below the signal peaks, but the null regions are quite brief in time separated by broad, slowly varying maxima. It should be pointed out that the character of these polarization effects must be qualified by the (here unknown) polarization resolution of the particular antenna pair utilized to make these measurements. This data sample does not provide a definitive answer to the third question posed at the outset of this section, but it does give some indication of the magnitude and character of the problem.

The answers to the rest of the questions posed at the beginning of this section remain to be answered by some alternative to this approach such as flying a high-speed aircraft across the skip focusing region during midday when ionospheric conditions are fairly stable, and recording the strength of fixed-frequency cw signals received at the plane. The time scale of this measurement process would be sufficiently rapid during the stable part of the day to describe fairly accurately the instantaneous state of the incident energy distribution over the ground.

5.3 Backscatter and HF Repeater Echoes in the Skip Region

In Section 5.2, one approach to the investigation of the energy distribution over the ground in the skip region was taken by utilizing a fixed frequency point to point, forward oblique path. In this section, an expansion of the technique is made by utilizing fixed frequency backscatter and a fixed location modulated repeater. The data collection was made between 9 a.m. and noon local time during February. The Ava-Dexter system was operated in the narrowband mode and during part of the experiment MTI clutter cancellation was utilized. The sweep rate was 1 MHz/sec and the bandwidth 100 kHz resulting in a PRF of 10 Hz and a time delay resolution of 10 μs. The University of Illinois HF repeater at Thomasboro was operated with an odd integral multiple of 1/2 the PRF, specifically 1005 Hz in order to place the repeater at the peak of the visibility function and translate its apparent range by $\pm$ 1 ms.

The transmitted frequency was chosen so as to place the ground range to U. I. on the edge of the skip zone. Thus, when the repeater was

illuminated, one of its translated echoes fell in the clear and the other within the ground backscatter echo region. Figure 5.8 shows a photo of three facsimile records. The two records on the left are identical except that the left most record shows MTI cancellation at the near end.

The purpose of this figure is to give a fairly long time history view of the illumination energy distribution near the leading edge of the backscatter--the MUF region. The right most record from 19 February 1971 shows a time history from 1320 UT at the far end until 1610 UT at the near end. The range window (right to left) is 5 ms. Several oscillations in the time delay of the apparent leading edge with an amplitude of about $\pm$ 0.5 ms are clearly discernible. Three periods of repeater illumination and four periods of non-illumination are evident. The turning on and turning off of the repeater illumination gives characteristic nose type traces where the high rays and low rays join together. But, the noses are of two types as will be examined further in more detailed records.

In the two left records (identical day and data) from 18 February 1971, the passage of at least two phase fronts of a traveling ionospheric disturbance (TID) is evident from the two sweeps from top left to lower right. About half way through the time sequence, a frequency change was made to bring the U. I. repeater closer to the leading edge and MUF failure is experienced in the foreground.

What is obvious from the outset is the complicated nature, even during the Winter Day, of the propagation to the leading edge of the

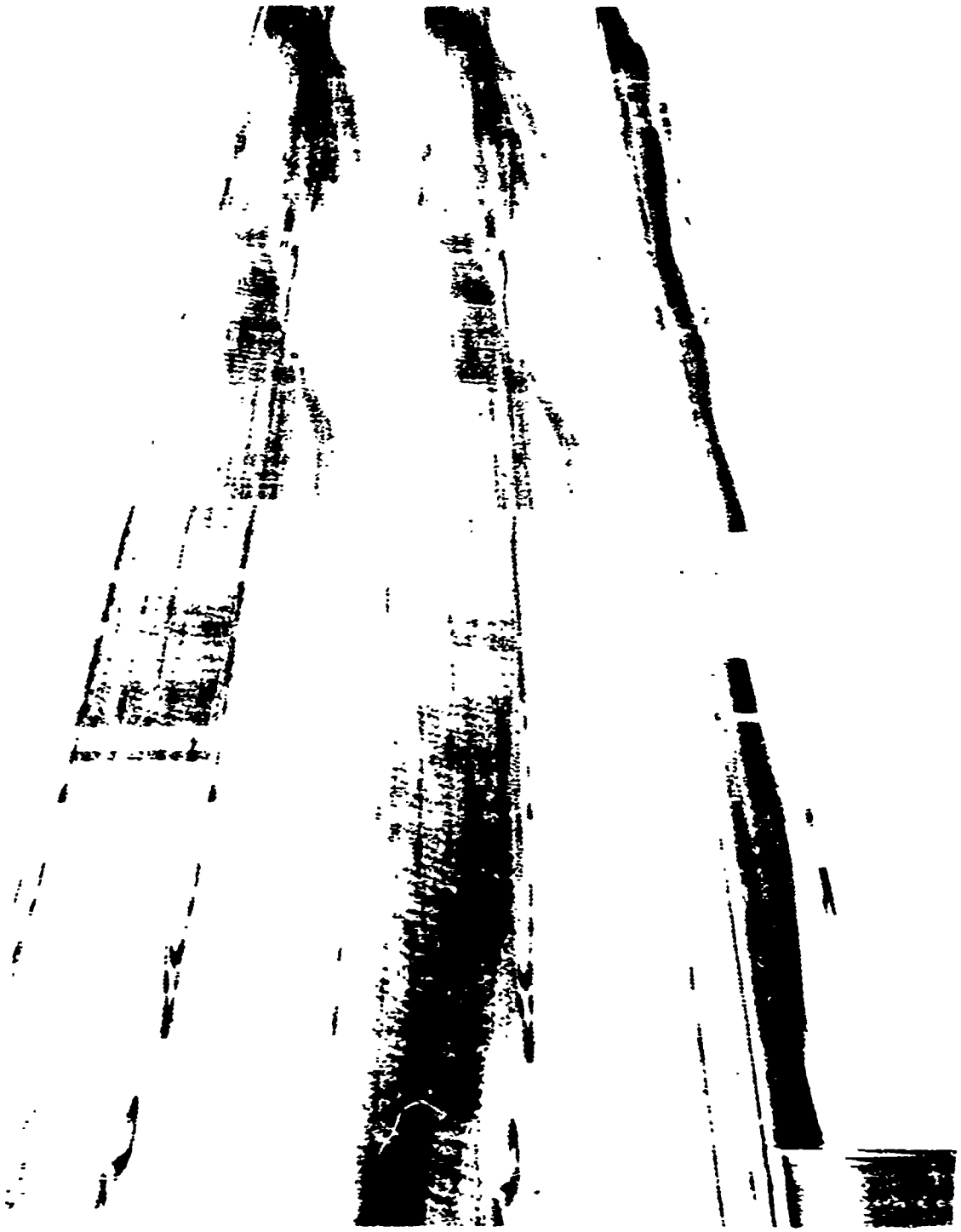

Figure 5-8. Range-Time-Intensity Records of University of Illinois HF Repeater Echo for 18 (left two) and 19 February 1971 (right) during Late Morning Local Time.

Reproduced from best available copy.

backscatter and how susceptible such propagation is to MUF failure and the effects of TID's. Such movement introduces Doppler shifts which make the use of MTI cancellation tenuous at best. Even from the large scale view given in Figure 5.8, the conclusion is manifest that the use of the skip region for target surveillance should be avoided if the resulting sacrifice of its focusing gain can at all be tolerated.

However, from a phenomenonological point of view, it is interesting to look in more detail at the mode structure and variation thereof in the skip zone. Figure 5.9 shows a portion of the 19 February facsimile record of Figure 5.8. The time extent is from 1442-1533 UT and the time delay window shown is 6-10 ms. The range to the University of Illinois HF repeater is approximately 8 ms, but because of the 1 ms time delay translation resulting from the 1005 Hz modulation, the repeater echo shows up at 7 and 9 ms. The amplitude of the calibration tone at 9.5 ms is 3μv and is clearly visible in the MTI'd data from 1517 to 1531 UT. During this same period also, the leading edge of the backscatter increased its range from 7.3 ms to 8.3 ms, as indicated by the broken line; and when it crossed the range to U. I. the repeater echo shows the characteristic MUF failure--first, the ordinary rays then the extraordinary rays. Note the noses are at approximately the same time delay but different epoch times. The turning on of the repeater echo at 1443 UT is quite different. The onset for what appears to be three noses is nearly simultaneous although the time delays are all different. The high rays diffuse quite rapidly in each case.

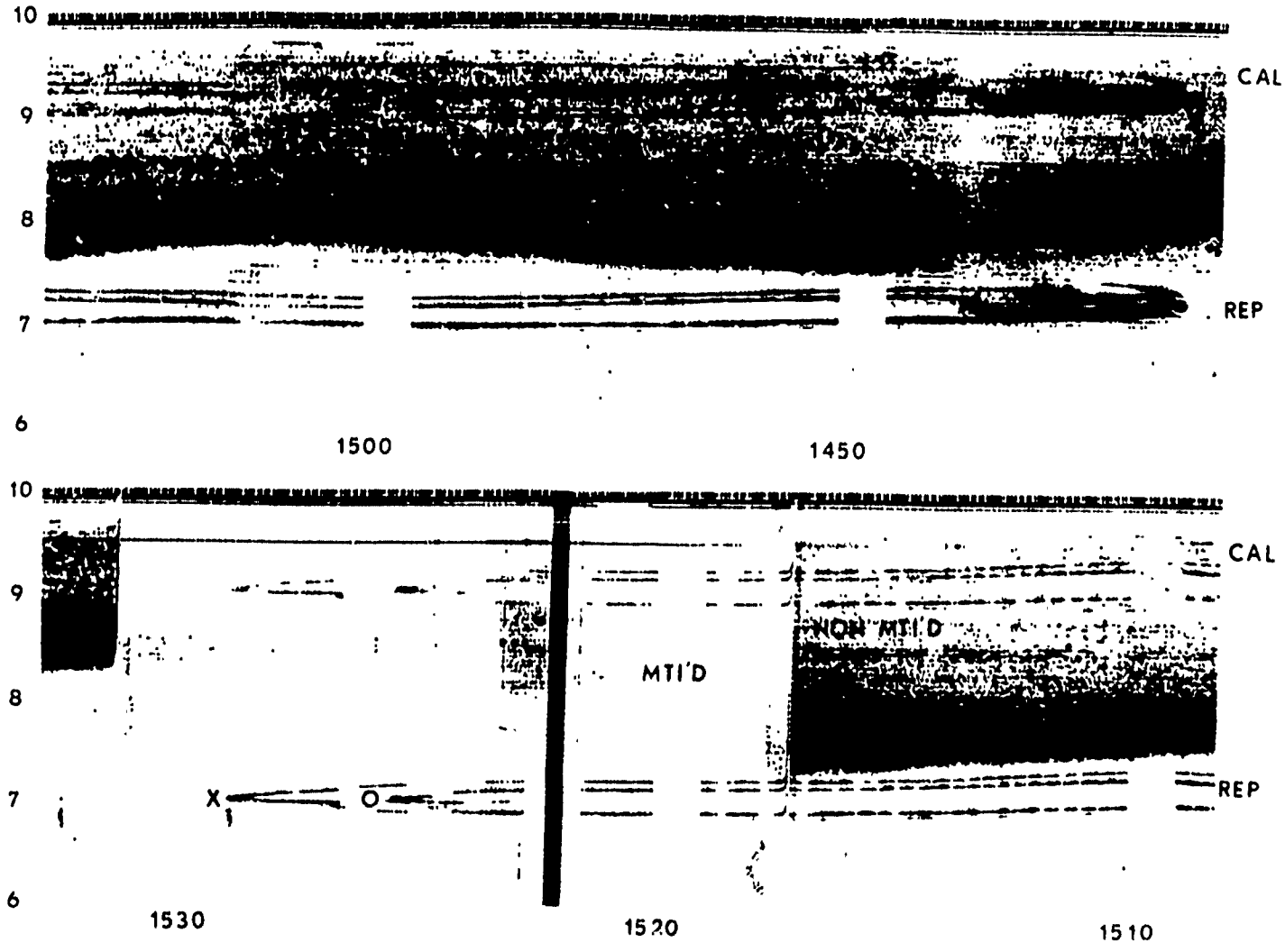

Figure 5-9. Range-Time-Intensity Record of U. I. HF Repeater Echo 1442-1533 UT, 19 February 1971 Showing TID and MUF Failure Effects.

Reproduced from best available copy.

The ground illumination terminator is not traversing the range to U. I. The "Z" trace indicative of a TID is quite obvious on two of the three traces.

Notice the considerable amount of characteristic Faraday rotation beading evident when the various modes illuminating the target are unresolved such as between 1450 and 1520 UT. But, when the o and x modes are resolved after 1520 this mode interference is not evident.

The mode structure around 1445 is quite interesting but too complicated to unpack from this vantage point without recourse to rapid vertical incidence soundings taken at the path midpoint. However, the implication is clear that operation of a surveillance system in this same propagation regime will also produce records whose meaning it will be impossible to unpack. The focusing advantage of the leading edge region may be far outweighed by its disadvantage of multimoding and time variability.

5.4 Conclusions

The results of this chapter suggest that ground-range/time-delay conversions for backscatter propagation to ranges beyond the skip zone at any given frequency will be relatively independent of the peak density and height of the intervening ionosphere. In the skip zone, however, any uncertainties in the height of the model ionosphere will be directly reproduced as equivalent uncertainties in the estimation of ground range for the focused region.

It has been shown by Croft[2] that the incident signal amplitudes for ranges beyond the skip zone are highly dependent on the lower ionosphere structure however. Thus, having accurately identified the ground range associated with a particular time delay beyond the skip zone for any operating frequency, (using simple ionospheric model and propagation concepts), the estimation of incident signal energy at that range and frequency is still a complex problem.

There is a focusing advantage to operation near the skip zone. However, because of the variability of the position of this zone for any operating frequency over short periods of time and because of the susceptibility of this region to the effects of TID's, its use may unduly complicate the identification and tracking problems of any surveillance radar and perhaps should be avoided.

5.5 REFERENCES

1. Coffey, M. E., D. G. Deter, and S. M. Bennett. Backscatter Parameter Investigation, RADC-TR-71-71, April 1971 AD 882 795L

2. Croft, T. A., Skywave Backscatter: A Means for Observing our Environment at Great Distances, Reviews of Geophysics (1972)

3. Hatfield, V. E., Derivation of Ionospheric Parameters from Backscatter Data, AGARD Conference Proceedings No. 49, "Ionospheric Forecasting", January, 1970.

4. Croft, T. A., and H. Hoogasian, Exact Ray Calculations in a Quasi-Parabolic Ionosphere with no Magnetic Field, Radio Science, 3, 69 (1968).

5. Peterson, A. M., The Mechanism of F-Layer Propagated Backscatter Echoes, JGR 56, 221 (1951).

6. Bremmer, H., Terrestrial Radio Waves, American Elsevier, New York (1949).

7. Poeverlein, H., Field Strength Near the Skip Distance, AFCRL Propagation Laboratory, TR 54-104 (1955).

8. Althouse, E. L., J. R. Davis, and P. E. V. Shannon, Computer Simulation of Structural Details of High-Frequency, Over-The-Horizon Earth Backscatter, NRL Report 6960 (1969).